Wiretapping the Brain: Communication of Spatial Selectivity between Frontal and Parietal Cortices

by

Rebecca Jeanne Gerth

B.S., University of Pittsburgh, 2013

Submitted to the Graduate Faculty of

The Swanson School of Engineering in partial fulfillment

of the requirements for the degree of

Doctor of Philosophy

University of Pittsburgh

2019

UNIVERSITY OF PITTSBURGH

SWANSON SCHOOL OF ENGINEERING

This dissertation was presented

by

Rebecca Jeanne Gerth

It was defended on

March 28, 2019

and approved by

Aaron Batista, Ph.D., Associate Professor
Department of Bioengineering

Neeraj Gandhi, Ph.D., Professor
Department of Bioengineering

Carl Olson, Ph.D., Adjunct Professor
Department of Neuroscience

Matthew Smith, Ph.D., Associate Professor
Department of Ophthalmology

Dissertation Director: Carol Colby, Ph.D.: Professor
Department of Neuroscience

Wiretapping the Brain: Communication of Spatial Selectivity between Frontal and Parietal Cortices

Rebecca Jeanne Gerth, PhD

University of Pittsburgh, 2019

Our interactions with the world around us are often guided by vision. The ability to perceive a visual stimulus and plan an eye movement to it requires the coordination of many brain areas. Though we have identified many networks of brain areas that work together during these processes, the content of the information exchanged between them is still poorly understood. We sought to answer this question by analyzing the flow of spatial selectivity information in simultaneously recorded neural activity of two cortical areas, the frontal eye fields (FEF) and the lateral intraparietal area (LIP).

First, we found that the spatial selectivity of the location of the visual stimulus but not the saccade target is well encoded by the local field potential (LFP) induced power. We determined this by comparing the spatial selectivity of the multi-unit neuronal activity (MUA) to that of the LFP at the same recording site. Next, we explored the interactions between FEF and LIP for insight into the exchange of information between the two areas. We analyzed the low-frequency neural signals across areas and found that there is less coherence between signals around the saccade onset when the saccade is directed to the preferred target location of both recording sites compared to the nonpreferred location. For a more direct analysis of the interactions between the two areas, we analyzed the LFP of one area with the MUA of the other by calculating the spike-field coherence (SFC). We found that a small number of recording site pairs exhibited significant SFC, but that the SFC was not significant across the population of pairs.

In summary, we found that the LFP signals both encode the spatial preference of visual stimuli and indicate cortical processing related to saccade generation and execution in FEF and LIP. Both areas appear to conduct this cortical processing largely independent of one another, though they have long been assumed to be working in concert. These results indicate a much more nuanced view of the functional interactions across the frontoparietal network.

Table of Contents

List of Tables

List of Figures

Preface

Nothing exists in a vacuum, and this dissertation is no exception. Where we are in life is the product of where we've been, what we've done, and who we've met along the way. I would like to take this opportunity to thank some of the countless individuals who have helped me to make this dissertation a success. I would like to thank my advisor, Dr. Carol Colby, for giving me the scientific freedom to pursue a project outside the scope of what her lab has historically focused on and for supporting me throughout. I would like to thank my committee members for always being available to me when I had questions or needed a fresh perspective to decide how to best move forward. I would also like to thank my parents, extended family, and friends for their unconditional support, encouragement, and much-needed gifts of chocolate. Lastly, I would like to thank those who could not be here to see the completion of this dissertation: my grandfather, who always stressed the importance of educating yourself to your highest abilities, and my step-father, who nurtured my love of engineering and always made me believe that I could change the world.

1.0 General Introduction

We interact with the world through our behavior, which is often guided by vision. Visual perception and the planning/execution of behavior is governed by many brain areas working in concert. Decades of anatomical research have provided us with a map of how different brain areas are connected to one another. The rise of whole brain functional imaging has, likewise, provided evidence for which brain areas are active during the generation and execution of specific behaviors. Lastly, electrophysiology studies have served as the backbone of research that aims to understand how the brain works to product behavior. Through countless electrophysiology studies, we have evidence of what drives the activity in different brain areas. Combining these three foci of study together, we have a fairly thorough comprehension of the networks of interconnected brain areas and under what conditions they are active.

What we still lack is an understanding of the content of the information that is passed between brain areas. The historical approach to this largely consisted of comparing activity in separate brain areas to a given stimulus and evaluating the latencies and magnitude of the response. For example, you could imagine seeing a robust neural response to a visual stimulus in neurons located in one brain area and then, after a stereotyped delay, see a neural response in neurons in another area. If you know from anatomical studies that these two areas are connected, it is reasonable to conclude that the information about the visual stimulus was passed from the first area to the second. This approach, while providing valuable insight into network dynamics, still relies on conjecture when trying to decipher the content of the information passed between the two areas.

To tackle this lingering problem, simultaneous recording studies have seen a surge in popularity. These studies can employ methods used across many applications of signal processing to assess the content of the information. Contained within this thesis dissertation, you will see that as the overarching theme with a specific focus on the transmission of information between the Frontal Eye Fields (FEF) and the Lateral Intraparietal Area (LIP) during the perception of a visual stimulus as well as the generation/execution of a saccade.

With the main goal of these experiments in mind, we wanted to record from two areas that had a high probability of passing information between each other in a given context. We chose to target areas FEF and LIP for four main reasons: 1) they have numerous reciprocal anatomical connections, 2) neurons within these areas exhibit similar responses, 3) both areas are involved in the generation/execution of saccades, and 4) both areas are involved in higher-order cognitive processes. These reasons will be examined in further detail in the following sections.

1.1 Reciprocal Connections Between FEF and LIP

Frontal and parietal cortices have an extensive network of reciprocal connections that span several areas, including FEF and LIP (Cavada & Goldman-Rakic, 1989; Andersen et al., 1990; Stanton et al., 1995; Schall et al., 1995; Petrides et al., 1984; Selemon & Goldman-Rakic, 1988; Medalla & Barbas, 2006). The connections have been both defined through anatomical segmentation of the areas and functional segmentation of the areas. The majority of studies found that the different segments of neurons FEF all had targets in LIP. The laminar structure of these projections from FEF to LIP found that neurons in FEF tended to target pyramidal neurons in the middle layers of LIP (Anderson et al., 2011), which Medalla & Barbas (2006) interpreted as

evidence of a feedforward connection between the two areas. While LIP was found to have projections to nearly all of the rostral bank of the arcuate sulcus, the projections specifically to FEF were much stronger from LIPv compared to LIPd (Schall et al., 1995; Medalla & Barbas, 2006). In addition to the direct connections between FEF and LIP, there is evidence for indirect connections through other prefrontal and posterior parietal areas (Rozzi et al., 2006; Cavada & Goldman-Rakic, 1989; Andersen et al., 1990). Though all of these studies have found very detailed connections between prefrontal and posterior parietal cortices, there is still much we don't know about the functionality. The anatomical findings of Selemon & Goldman-Rakic (1988) suggest that there is parallel organization of the connections and that each controls a particular aspect of spatial perception and visually guided behavior. While various physiological studies have found that electrical stimulation of subdivisions of LIP can elicit contrasting types of saccades, which do not appear to align with the observed anatomical connections (Kurylo & Skavenski, 1991; Thier & Andersen, 1998; Blatt et al., 1990). Together, these previous studies suggest that the functional interactions between prefrontal and posterior parietal cortex are very complicated and poorly understood.

1.2 The Frontal Eye Fields

Another property that makes FEF and LIP appealing targets for analyzing simultaneously recorded neural activity is the similarity of their neural responses to visual stimuli and saccades. This section will highlight the activity of neurons in the frontal eye fields.

During purposive saccades (saccades made in the context of a task), neurons in FEF can generally be grouped into those that exhibit activity before the saccade (presaccadic neurons) and

those that exhibit activity after the saccade (postsaccadic neurons). The presaccadic neurons are further classified, based on their activity, as either visual cells, movement cells, or visuomovement cells (Bruce & Goldberg, 1985). Visual cells are defined as those that show enhanced firing in response to a visual stimulus in the receptive field (RF) of the neuron. Movement cells fire robustly before the onset of a purposive saccade, regardless of the presence of a visual stimulus at the target location. Visuomovement cells exhibit enhanced firing both following visual stimulation and preceding a purposive saccade. The relative magnitude of the visual or movement related activity in a given visuomovement cell is variable. This suggests that the neurons in FEF can fall anywhere on a spectrum between being purely visual and purely movement related. Both visual and movement related activity (across all three cell types) has a preferred direction and amplitude (Bruce & Goldberg, 1985).

Previous studies have provided evidence that FEF is not just involved in the generation of saccades, but plays a causal role. One of the defining features of FEF neurons is that low-threshold electrical stimulation can elicit saccades (Bruce et al., 1985). The low-threshold stimulation is only effective in visuomovement and movement type cells that exhibit presaccadic activity. Also, the direction and amplitude of the electrically elicited saccade typically aligns with the movement field of the neuron's presaccadic activity. In addition to the electrophysiological evidence, there have been several studied that show that lesioning (Schiller & Chou, 1998; Schiller et al., 1987; Schiller et al., 1980; Lynch 1992) or reversibly inactivating (Dias et al., 1995; Dias & Segraves, 1999; Sommer & Tehovnik, 1997) the FEF impairs the execution of saccades. Together, these findings suggest that FEF, specifically the visuomovement and movement cells, are necessary for the initiation of a saccade.

When analyzing FEF neurons in the context of the delayed saccade task (otherwise known as the memory-guided saccade task) another type of presaccadic activity has been observed – delay period activity. Lawrence et al. (2005) found that visual and visuomovement cells tended to carry similar amount of delay period information, while movement cells fell into two classes, which they termed "canonical" and "paradoxical". The "canonical" movement cells exhibited enhanced firing when the saccade was made in the preferred direction, which the "paradoxical" movement cells had an increased response when the saccade was made in the direction opposite of the preferred direction. Interestingly, they found that all of the "canonical" movement cells exhibited presaccadic activity while all of the "paradoxical" movement cells exhibited postsaccadic activity. During the double-step task, postsaccadic neurons in FEF have also been observed to be sharply suppressed during subsequent saccades (Goldberg & Bruce, 1990). The "paradoxical" delay period activity and the suppression of activity during subsequent saccades suggests that postsaccadic neurons in FEF might play a role in maintaining spatial information without triggering a saccade.

This maintenance of spatial information would contribute to a general stability of visual perception, which is also seen in other properties of FEF neurons. One example is FEF neurons responding to trans-saccadic changes in visual stimuli (Crapse & Sommer, 2012). Another is the presence of predictive remapping (Umeno & Goldberg, 1997; Umeno & Goldberg, 2001; Zirnsak et al., 2014). Predictive remapping refers to the shifting of a neuron's RF preceding a saccade to the location it would fall after the completion of the saccade. FEF is one of three notable areas where predictive remapping has been observed, with the other two areas being the superior colliculus and LIP (Walker et al., 1995; Duhamel et al., 1992). That this phenomenon is common to these areas, particularly areas FEF and LIP, suggest that these areas are functionally connected during the planning and generation of saccades.

In addition to the maintenance of visual stability, FEF has been shown to be involved in a number of higher order cognitive processes. This is the final property of FEF that makes it an area of interest for our investigation. Several studies that suggest FEF plays a role in visual attention. Findings include better performance during spatial attention tasks following subthreshold electrical stimulation of FEF (Moore & Fallah, 2004), impaired performance during visual search tasks following reversible inactivation of FEF (McPeek & Keller, 2004), and attention-like enhancement of activity in other areas of visual cortex following stimulation of FEF (Moore & Armstrong, 2003; Armstrong et al., 2006). Evidence also suggests that FEF plays a role in working memory, a process in which LIP has also been shown to be involved in. This has largely been demonstrated by activation of FEF neurons during the delay period of various tasks that require working memory (Fuster & Alexander, 1971; Chafee & Goldman-Rakic, 1998; Sommer & Wurtz, 2001). Another cognitive process that FEF plays a role and is tightly linked to visual attention is task switching. Task switching paradigms typically rely on features of a stimulus to denote its relevance in the task (i.e. a target or a distractor). The relevant feature will then change, either cued or un-cued, so that in one trial a stimulus that was a target is now a distractor and vice versa despite no change in the stimulus' features. Studies in monkeys where FEF was lesioned found that the monkeys' accuracy on trials where the target criterion changed was drastically reduced (Rossi et al., 2007). Following these studies, the same group carried out a functional imaging study characterizing cortical activation patterns in humans performing the same task (Pessoa et al., 2009). They found that prefrontal activation was enhanced during trials requiring a switch in the feature to which the subject attended. They also found that parietal cortex showed increased activation on those trials, suggesting that this process relies on frontoparietal communication.

As detailed above, FEF has many characteristics that made it an area of interest for our study including its causal involvement in the generation of saccades, the visual and motor properties of its neurons, and its involvement in higher order cognitive processes. Each of these properties indicate that FEF is a center of sensory and motor integration that influences behavior in many ways.

1.3 The Lateral Intraparietal Area

The lateral intraparietal area (LIP) is one of the most studied areas of the brain. One of the biggest reasons for recording from LIP and FEF is the similarity of their neural responses. Several examples of neural responses in FEF and their relation to those in LIP were detailed in the previous section. The following paragraphs will detail additional properties of LIP neurons and highlight their similarities to those recorded in FEF.

As in FEF, previous studies have found that neurons in LIP also exhibit visual and eye movement related responses (Gnadt & Andersen, 1988; Mazzoni et al., 1996) and that these responses fall on a visuomovement spectrum (Colby et al., 1996). One of the differences between LIP and FEF in this respect is that LIP neurons tend to respond more strongly to visual stimuli than movement, where FEF neurons tend be more tuned for saccadic eye movements (Colby et al., 1996; Bruce & Goldberg, 1985). In LIP neurons, both the receptive fields of visual stimuli and the movement fields of saccades tend to be located in the contralateral hemifield (Barash et al., 1991b). Additionally, the majority of LIP neurons tend to be excitatory (Barash et al., 1991a).

Neurons in LIP have been shown to be involved in the planning and execution of saccadic eye movements. Studies in which LIP has been inactivated, either through lesioning or a reversible

method, have also shown that saccades are impaired without the involvement of LIP. Though monkeys are still able to execute saccades following inactivation of LIP, the latency, peak velocities, and end point accuracy were affected (Li et al., 1999). Electrical stimulation of LIP can elicit saccades, though neurons in LIP require higher currents than those in FEF (Their & Andersen, 1998). Also, electrophysiology studies have found that LIP neurons that exhibit presaccadic and saccade-coincident firing tend to have higher levels of activity than neurons that exhibit postsaccadic activity (Barash et al., 1991a), suggesting that saccade planning is an important role that LIP plays. This presaccadic activity in response to a purposive saccade is present regardless of whether a visual stimulus was ever present in the RF (Barash et al., 1991b), which implies that LIP's role is one of transforming visual information to be used in the planning of an upcoming saccade.

LIP's role in preparing for an upcoming saccade is further defined by its involvement in visual stability. As mentioned in the previous section, LIP is one of three distinct areas where predictive remapping has been observed, the others being FEF and superior colliculus. It was also the first area in which predictive remapping was discovered (Duhamel et al., 1992). To expand on how remapping underlies visual stability, one recent theory suggests that predictive remapping in LIP acts as an attentional guidance system (Mirpour & Bisley, 2016). As the visual scene jumps with saccadic eye movements, this attentional guidance system predictively remaps before the new visual information reaches cortex in order for the attended locations to be perceived as stable (Cavanagh et al. 2010).

Modulations of activity in LIP are also apparent in a host of cognitive functions. One theory to explain previous widespread effects of attention on LIP is that neurons in LIP are involved in the encoding of a priority map. The priority map is thought to encode objects or locations or

behavioral importance, which the neural firing activity in LIP being directly related to the level of priority (Bisley & Goldberg, 2010). The priority map combines both visually salient features and top-down, attentional influence. The salient features are hypothesized to come from areas in visual cortex (Koch & Ullman, 1985; Itti & Koch, 2000; Walther & Koch, 2006), while the top-down influence is thought to arise from areas in prefrontal cortex, notably FEF (Ibos et al., 2013), providing another example of interaction between FEF and LIP. The construct of a priority map could also account for similar activity in LIP and FEF in other cognitive processes, such as working memory and task switching, which were discussed in the previous section. It is also possible that not all networks of neurons in LIP are involved in the construction of this priority map. Activity in LIP also appears to represent decision making processes (Gold & Shadlen, 2007), anticipation (Colby et al., 1996), categorization (Freedman & Assad, 2006), confidence (Kiani & Shadlen, 2009), as well as other stimulus features (Sereno & Maunsell, 1998; Fanini & Assad, 2009; Toth & Assad, 2002). Each of these properties, however, are likely subject to modulation by attention or task relevance, further highlighting the wide net of cognitive processes that LIP is involved in.

Neural activity in LIP can represent many different things, making the areas still somewhat of an enigma. Regardless of the study, LIP appears to be a center of integration between sensory, motor, and attentional influences. As highlighted in this and the previous section, we see that many of its neural properties overlap with or compliment those of FEF. The foremost of these similar functional properties being neural responses to visual stimuli and saccadic eye movements, the involvement in the planning and execution of saccades, and the involvement in higher-order cognitive processes. These similarities have led to an abundance of studies that aim to document and decipher the interactions between FEF and LIP. A brief overview of their findings will be detailed in the following section.

1.4 Fronto-Parietal Interactions

Finally, exploring the interactions between these two areas is not a new endeavor. There is a wealth of studies that seek to document how prefrontal cortex (PFC) and posterior parietal cortex (PPC) functionally connect. This is no surprise considering the anatomical connections and functional similarities that have been highlighted in the previous sections.

One method of exploring how these two areas interact is through lesioning or reversibly inactivating one area and recording from the other. During memory-guided saccades, Chafee and Goldman-Rakic (2000) found that reversibly inactivating parietal cortex resulted in 71% of prefrontal neurons to exhibit a significant change in firing rate. The firing rate changes consisted of both increases and decreases in approximately equal frequency. Similar results were seen in the reverse experiment with 76% of parietal neurons exhibiting significant changes in firing rate. One conclusion from this experiment is that parietal and prefrontal neurons exchange symmetrical neuronal signal during a memory-guided saccade, which then accounts for the similar functional responses in both areas during this task. While this method of experimentation shows a reliant relationship between neural activity in prefrontal cortex and neural activity in parietal cortex, it does not necessarily show the way in which these two areas interact. The same results could be obtained if both areas exchange information indirectly. Another interpretation of these findings could be that the combined output of prefrontal and posterior parietal neurons is necessary in a downstream area. And so, reversibly inactivating one area requires compensation in activity in the other.

The inverse of approaching the problem through inactivation is, of course, approaching it with electrical stimulation. The intuition behind this approach is that electrical stimulation mimics natural activation of an area in a controlled way. Premereur and colleagues (2012) found that sub-

threshold electrical stimulation of FEF resulted in enhanced gamma power in retinotopically corresponding sites in LIP but had no effect on spike rate or behavior. These enhanced gamma oscillations, however, appeared to be dependent on the task that the monkey was performing. The increases in gamma power due to electrical stimulation were only seen during visually guided saccades, not during memory guided saccades or passive fixation. This is consistent with the idea that FEF modulates LIP through spatial attention. In follow-up experimentation, it was found that microstimulation of FEF can modulate the spiking activity of LIP when spatial attention is already directed to the receptive field of the LIP neurons (Premereur et al., 2014). However, critics of electrical stimulation studies point out that it is still unknown where activated cells are located with respect to the stimulating electrode. Also, that stimulation likely activates local axons, which can result in distributed activation of neurons (Histed et al., 2009). Even without these criticisms, electrical stimulation studies still do not circumvent the issue of activating indirect pathways.

To try to disentangle the direct, functional relationship between prefrontal and posterior parietal cortex, many studies have begun to utilize simultaneous recording methods. One benefit that simultaneous recording offers is a more precise means of measuring timing differences in firing rate modulation across areas. With FEF and LIP encoding signals for much of the same information, determining which area has access to the information first is important for understanding its flow. Findings of simultaneous spike timing studies have provided evidence to support the top-down/bottom-up theory of information flow. In this theory higher order cognitive signals, such as attention, task relevance, and target selection, appear in FEF earlier than LIP (Sapountzis et al., 2018; Goodwin et al., 2012; Crowe et al., 2013; Ibos et al., 2013). Additionally, signals relating to the visual features of stimuli appear in LIP before they appear in FEF (Siegel at al., 2015). A recent study suggests that the top-down/bottom-up model of information flow is likely

distributed over multiple neural circuits. Sapountzis et al. (2018) found that a subpopulation of neurons in LIP discriminate between the target and distractors at the same latency as neurons in FEF. From this finding they conclude that the feature attention signals surrounding the identity of the target a processed concurrently by the two areas. These concurrent processing findings suggest that either a shared source or indirect connections are likely responsible for the similarity of information encoded in both FEF and LIP.

Another way to explore simultaneously recorded neural data is to do so in the frequency domain. Previous studies have done so by carrying out coherence, phase, and causality analysis (Engel et al., 2001). This approach involves determining how similar oscillatory activity in one area, measured at the level of the local field potential (LFP), multi-unit activity (MUA) or single-unit activity (SUA), is to oscillatory activity in another area. These oscillations can be evaluated for similarities in both magnitude (coherence) and phase (phase-locking). Following the philosophy that LFPs represent the summed synaptic input to an area and spiking activity represents the output, frequency domain studies can be used to compare the inputs across areas or the input of one area and the output of another. As such, measuring the coherence between the spiking in one area and the LFPs in another, known as spike-field coherence (SFC), appears to provide a more direct means of investigating information flow across areas. Studies between prefrontal and parietal areas that have been based on this approach have revealed significant coherence and/or phase-locking in the alpha, (7-13 Hz), beta (15-30 Hz), and gamma (30-80 Hz) bands. The particular frequency at which there is significant coherence/phase-locking is largely dependent on the areas of interest and the task (Buschman & Miller, 2007; Salazar et al., 2012; Fiebelkorn et al., 2018; Pesaran et al., 2008). Most previous findings report that stimulus and/or spatial preference plays a role in the magnitude of coherence modulations. Coherence appears to

be enhanced between recording sites that share a preferred stimulus when that stimulus is presented (Salazar et al., 2012). However, it has yet to be studied whether the same can be said of sites with shared spatial preferences when either a stimulus is presented at or a movement is made into that preferred area of visual space.

2.0 Spatial Selectivity Encoding of LFPs and Coherence Across Areas

2.1 Introduction

In August of 1875, Richard Caton reported the first electrical impulses to be recorded from the brains of animals (Caton, 1875). As the technology for electrophysiological recordings advanced, so has our understanding of the different electrical signals produced within the brain. One such electrical signals that can be recorded from the brain intracranially is the spiking of the neurons. The spiking activity is the high frequency, synaptic output of a neuron. Spiking activity has been widely used to study the functions of brain areas, information encoding of individual neurons, and much else. Another signal that can be recorded intracranially is the low frequency voltage oscillations, or local field potentials (LFPs). LFPs are thought to be the summed synaptic input to an area. Synchronous oscillations within the LFP have been implicated in many different functions, such as attention, working memory, and stimulus selectivity. These oscillations are also thought to play a role in long-range communication between brain areas and cortical processing. Though low frequency oscillations were the first electrical activity to be recorded in humans (Berger, 1929) they remain less well understood than spiking activity. Two major questions that remain about these electrical signals are how they relate to each other and how they each contribute to communication between brain areas.

Several studies have found that the power of the LFP is well correlated with the local multi-unit activity (MUA). Particularly at the gamma frequencies, these previous studies have found that LFPs have behavioral correlates and relate to stimulus selectivity of the spiking in monkey primary visual cortex, auditory cortex, middle temporal visual area, inferior temporal visual area, and

primary motor cortex (Jia et al., 2011; Berens et al., 2008; Brosch et al., 2002; Liu & Newsome, 2006; Kreiman et al., 2006; Perel et al., 2015). However, it is unclear whether this phenomenon is present across all brain areas.

Our approach to the questions of how spiking and LFP activity relate to each other and whether the relationship could be generalized across the brain was to examine the relationship between the LFP and the spiking in both the frontal eye fields (FEF) and lateral intraparietal area (LIP). FEF and LIP are both highly active during the perception of visual stimuli and the generation and execution of saccades. Neurons within FEF and LIP exhibit very similar responses to visual stimuli and saccades in various tasks, such as the memory-guided saccade (MGS) task. One characteristic that neurons in FEF and LIP share is spatially selective spiking to visual stimuli and/or the location of an upcoming saccade. We hypothesized that the spatial selectivity, which is prominent in the spiking, would also be present in the LFP. We tested this hypothesis by determining the spatial selectivity following the onset of the visual stimulus and the spatial selectivity around the onset of the saccade during the MGS for both the MUA and LFP power. Based on the findings in other cortical areas, we predicted that the spatial selectivity as determined by the LFP would be congruent with the spatial selectivity as determined by the MUA. This is important because with the LFP the input to an area and the spiking the output, findings of either congruence or incongruence between the LFP and the MUA spatial selectivity could provide new evidence of the local cortical processing as well as the organization of the underlying neural network.

To address the second major question of how spiking and LFP activity contribute to communication between brain areas, many studies analyze simultaneously recorded neural activity from two or more areas. There have been several investigations into the communication of

information between frontal and parietal cortices through analysis of both the spiking activity and LFP signals recorded in both areas (Engel et al., 2001). One such approach that uses the LFP signal involves determining whether oscillatory activity in one area exhibits shared power, or coherence, with the oscillatory activity in the other area. Studies based on this approach have found significant activity in the theta (4-8 Hz), alpha (7-13 Hz), beta (15-30 Hz) and gamma (30-80 Hz) bands across the frontal and parietal cortices, with the particular frequency dependent on the areas and the task. Findings from these studies show spatial selectivity and task dependence in the coherent oscillatory activity. We wanted to utilize this approach to study the communication of FEF and LIP during the MGS task. FEF and LIP are highly interconnected by strong topographically organized reciprocal pathways. In addition to the direct connections, these two areas are also linked through numerous indirect connections to other cortical areas and subcortical nuclei. With the abundance of anatomical connections and high similarity of neural responses it logically follows that FEF and LIP are in communication during tasks such as the MGS task. Previous work in our lab found that the spiking activity across the areas has a positive spike-count correlation coefficient during the MGS task, except for the time around the onset of the saccade. During approximately ±100 ms around saccade onset, we found a surprising decoupling of the spiking correlations when the neuron pair had similar spatial selectivity and the saccade was directed towards the shared preferred target location (Hall et al, in review). Our second hypothesis for this study was that this phenomenon of decoupled activity, present in the spiking, was also present in the LFPs. We tested this hypothesis by analyzing the magnitude-squared coherence (MSC) between LFPs recorded in FEF and LIP during the MGS task. We predicted that, as in the spiking, we would see a decoupling of the activity around the onset of the saccade for site pairs with congruent spatial selectivity. This would present as significantly lower MSC when the saccade is directed towards the preferred target

location compared to when it is directed to the non-preferred target location. This finding would indicate that the communication between FEF and LIP is more complex than previously thought.

2.2 Methods

Subjects

Electrophysiological recordings were conducted in two adult male rhesus monkeys (*macaca mulatta*). Prior to recording, each monkey was fitted with a surgically implanted cranial cap. The cap held the post for the head restraint and two cylindrical recording chambers, which were 2 cm in diameter. Magnetic resonance imaging guided the placement of the chambers. These were oriented normal to the cortical surface with the base of the frontal chamber centered over the genu of the arcuate sulcus and the base of the parietal chamber centered over the intraparietal sulcus. The chambers were positioned over the left hemisphere in monkey CY and the right hemisphere in monkey RY. Surgical, animal care, and experimental protocols were all in accordance with National Institutes of Health guidelines and approved in advance by the Institutional Animal Care and Use Committees of The University of Pittsburgh and Carnegie Mellon University.

Electrophysiology Recordings

The monkey sat in a primate chair with head fixed in a darkened room viewing a CRT monitor at a distance of 30 cm (19" ViewSonic® color CRT monitor at a refresh rate of 85 Hz using an 8 bit DAC with an ATI Radeon™ X600 SE graphics card). Stimulus presentation, monitoring of eye position and delivery of reward were under the control of NIMH Cortex software (provided by Dr. Robert Desimone). Eye position was monitored with an infrared eye tracker sampling at 240 Hz

(ISCAN Inc., Woburn, MA). Eye position voltage signals were continuously monitored and saved at a sampling rate of 1000 Hz for offline analysis on a separate computer running Plexon software (Plexon Inc., Dalls, TX). Data analysis was carried out offline using custom MATLAB® software (Mathworks, Natick, MA).

Neuronal spiking and local field potential activity was recorded using 8-channel linear array electrodes with recording sites distributed along the shaft at intervals of 150 μm (Alpha Omega Co. USA Inc., Alpharetta, GA) or tungsten microelectrodes (Frederick Haer, Bowdoinham, ME). All recording sessions in monkey RY (37) were conducted with a linear array placed in both frontal and parietal cortices. Recording sessions in monkey CY were conducted with either two linear arrays or a linear array in frontal cortex and two tungsten microelectrodes in parietal cortex (22 and 37 sessions, respectively). Microelectrodes were simultaneously inserted into the frontal and parietal cortices through stainless steel guide tubes stabilized in a nylon grid system at the beginning of each recording session (Crist Instrument Co. Inc., Hagerstown MD). Neuronal activity was thresholded at 2-3 standard deviations from the mean background noise as measured on the channel. Neural voltage signals were amplified, filtered, and saved at a sampling rate of 40 kHz using Plexon MAP system hardware and software. Spike waveforms were sorted online and offline using Plexon software. Multi-unit activity (MUA) is comprised of both well-isolated and small-amplitude waveforms.

Memory-Guided Saccade Task

The monkeys were trained to perform a memory guided saccade (MGS) task. To start each trial, the monkey was required to attain then maintain a fixation point (1°x1°) at the center of the screen for a randomly selected interval in the range of 300-500 ms. Then, as the monkey continued to

fixate, a white circle 0.5° in diameter appeared in the visual field periphery for 47 ms (four video frames at 85 Hz monitor refresh rate). The monkey continued to maintain central fixation during the delay period, with durations of 400-1200 ms. At the end of the delay period, the fixation point turned off, signaling the monkey to make a saccade to the remembered location of the target. The monkey was required to execute a saccade into a 3°x3° window centered on the target, exiting the central window within 500 ms and entering the target window within an additional 120 ms. The target reappeared when the gaze entered the window. The monkey was required to maintain gaze within the window for an additional 200-400 ms. Successful completion culminated in delivery of liquid reward.

2.2.1 D-prime Calculation

Spiking

To characterize the spatial preference of the MUA, we computed d-prime using the following formula:

$$d' = \frac{(M_1 - M_2)}{[(N_1 - 1) * V_1 + (N_2 - 1) * V_2] \,/\, (N_1 + N_2 - 2)} \qquad \text{Eq. 2-1}$$

where M and V are the mean and variance of the firing rate and N is the number of trials. The subscripts indicate the target location, resulting in a positive d-prime when target location 1 (upper quadrant) is preferred and a negative d-prime when target location 2 (lower quadrant) is

preferred. We used spiking activity during the window 50 to 200 ms following the onset of the visual stimulus to compute d-prime for the MUA. To determine spatial preference of the saccade related activity, we calculated the d-prime over the window -100 to 100 ms around the onset of the saccade.

Local Field Potentials

To characterize the spatial preference of an LFP site we computed d-prime following the same conventions described for spiking activity. In this case, however, M and V are the mean and variance of the power at a given frequency, rather than firing rate, during the time window of interest.

2.2.2 LFP Pre-processing

Elimination of trials with deviant voltage signals

Artifacts in the LFP signal obscure the neural activity and can be a result of various causes. We defined an artifact in the LFP of a single trial as an instance where the voltage fell outside of 3 STDV of the mean voltage for longer than 5 ms. Trials in which there was an artifact were not included in analysis.

Re-referencing

All LFP activity is measured relative to a reference signal. If activity is picked up by the reference it will appear in all LFPs that are measured relative to that reference, which could influence subsequent analyses. The reference for the LMAs is recorded at the tip of the electrode and is likely

to record neural activity. To remove the reference signal from the LFPs, we implemented a "nearest neighbors" re-referencing scheme (Shirhatti et al, 2016). For a given channel recorded on the LMA, we subtracted the mean signal of the channels directly above and below the channel of interest. This resulted in the first and last channel on the LMAs being excluded from analysis as they could not be re-referenced in a manner consistent with the other channels.

2.2.3 LFP Power

Spectral transformation of the LFPs was accomplished by convolving the signal, *S(t)*, with a complex Morlet wavelet, *w(t,f)* (Tallon-Baudry & Bertrand, 1999). The time-varying power spectrum, *P(t,f)*, of the signal around frequency *f* is the squared modulus of the convolution:

$$P(t,f) = |w(t,f) * S(t)|^2 \qquad \text{Eq. 2-2}$$

For each trial we computed the power around frequencies 1 – 100 Hz in 1 Hz steps. We normalized the power for each trial by dividing the spectrum by the average power at each frequency during the baseline window (-200 to 0 ms before onset of the visual stimulus). We then calculated the induced power of a site by averaging the power spectra for each trial to a target location. The induced power to each target location is the power measurement used in all subsequent analyses.

2.2.4 Coherence

Field-Field

The magnitude-squared coherence was calculated between the LFPs recorded on pairs of sites that met the following criteria: Pairs consisted of one site in frontal cortex and one site in parietal cortex. Each site in the pair had a spatial preference for one of the two target locations, as defined by the d-prime of the MUA recorded on that site. For each pair, we calculated the coherence using the following equation:

$$C_{xy}(f) = \left| \frac{S_{xy}(f)}{\sqrt{S_x(f) S_y(f)}} \right| \quad \text{Eq. 2-3}$$

where *Sx(f)* and *Sy(f)* are the autospectra of each site within the pair and *Sxy(f)* is the cross-spectrum of the two signals. We calculated the autospectra and cross-spectrum for each trial by multiplying the spectrum of the first signal by the complex conjugate of the spectrum of the second signal. The spectra used in these calculations were the convolution of the LFP signal and the complex Morlet wavelet described above. The autospectra and cross-spectrum were averaged across trials.

2.2.5 Cluster-Based Permutation Test

The statistical analysis of the magnitude-squared coherence analyses will be carried out using a cluster-based nonparametric test (Maris & Oostenveld, 2007). The nonparametric test solves the

multiple comparisons problem that occurs when comparing a large number of data points, such as each time-frequency point that makes up a spectrogram. The nonparametric test first uses an independent sample t-test to test for significant time-frequency points between the task conditions. Clusters are formed by grouping significant time-frequency points that are spectrally and temporally adjacent. The clusters are then treated as a single point and given a single significance metric (the sum of the p-values of all time-frequency points in the cluster). The largest significance metric of the clusters is then used as the test statistic during a Monte-Carlo analysis with 1000 permutations. The results from the Monte-Carlo analysis will be used to determine if there is a significant difference between the conditions being compared with $\alpha = 0.01$.

2.3 Results

We recorded multi-unit activity (MUA) and local field potentials (LFPs) from 216 sites in FEF and 215 sites in LIP in two macaque monkeys (90 FEF sites and 29 LIP sites in monkey C and 126 FEF sites and 186 LIP sites in monkey R). This resulted in 763 pairs of simultaneously recorded sites across areas that met our criteria (see Methods).

2.3.1 Spatial Preference of LFP Power

We asked how the LFP signal relates to the spiking activity in both frontal and parietal cortex. To do address this we compared the spiking of the MUA (defined as all sorted spikes recorded at a site) to the induced power of the LFP. Spiking activity in both FEF and LIP has been found to be highly selective for the spatial location of both visual stimuli as well as planned

saccades. We first wanted to examine whether the LFP power recorded at a given site carried the same information about the spatial preference that is present in the MUA. We used the memory-guided saccade task to temporally separate the neural response to the visual stimulus from the response to the saccade.

We found that the spatial preference present in the MUA was also present in the LFP power around the onset of the visual stimulus, but not around the onset of the saccade. Figure 2-1 shows an example site where the MUA and LFP power has an elevated response following the onset of the visual stimulus at target location 2, but not at target location 1. The increase in the induced power appears to coincide with an increase in firing rate. It also only occurs at frequencies below 60 Hz, suggesting that it is not due to contamination from spiking activity. Looking at the activity from the same site around the onset of the saccade in Figure 2-2, we see what appears to be slightly elevated LFP power following the saccade to location 2 compared to location 1. The LFP power, however, does not correspond to the activity of the MUA, as it does following the visual stimulus.

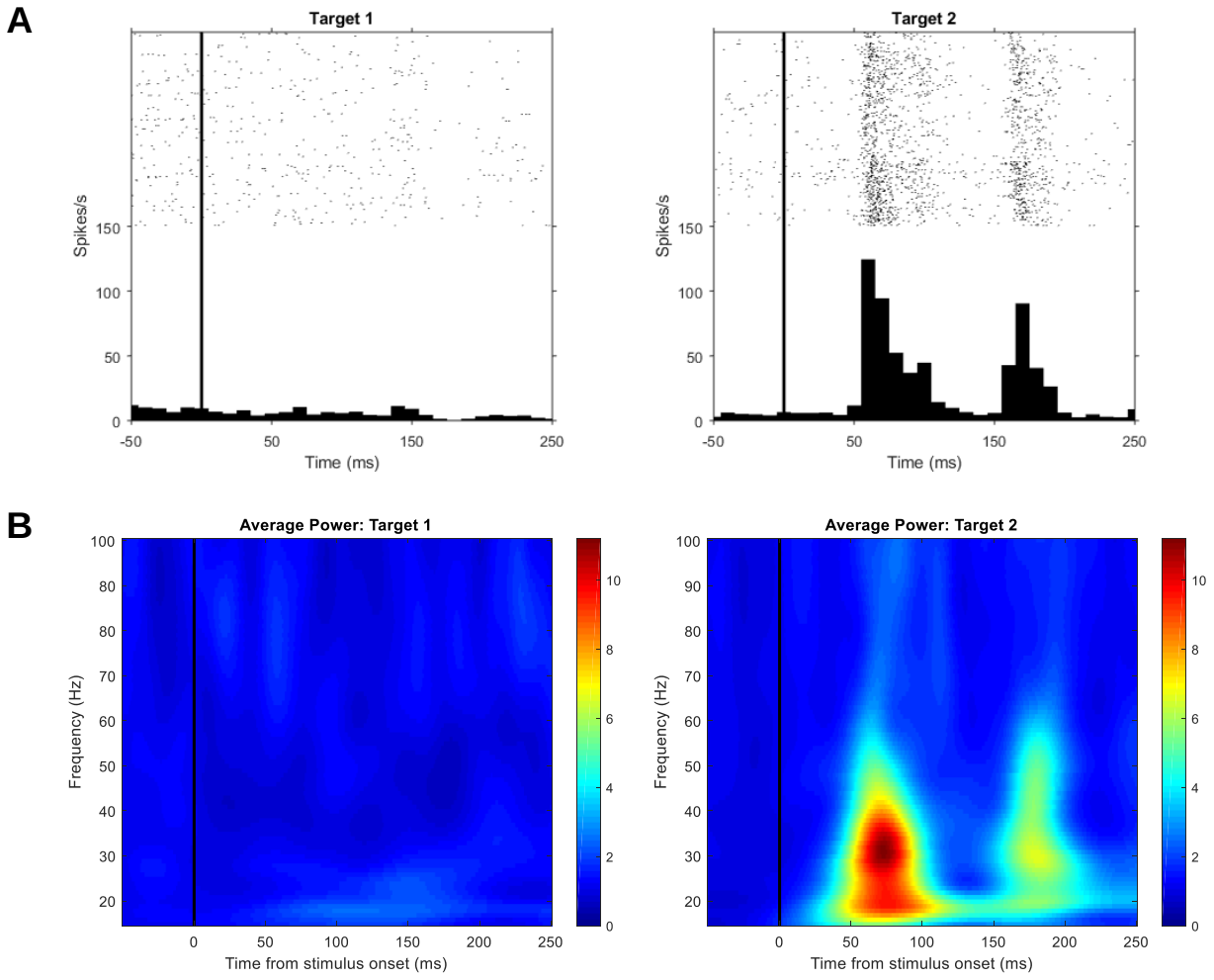

Figure 2-1. Example recording site activity aligned to stimulus onset.

A) Raster plot and PSTH of all sorted spikes (MUA) on the recording site. Spiking activity shows a response to the onset of the visual stimulus when presented at target location 2. B) Time-freqency plots of the normalized LFP power recorded at the site. Power is averaged over all successful trials to a given target location. The LFP activity shows a clear increase in induced power following the onset of the visual stimulus when presented at target location 2. The increase in power appears to temporally align with the MUA spiking response.

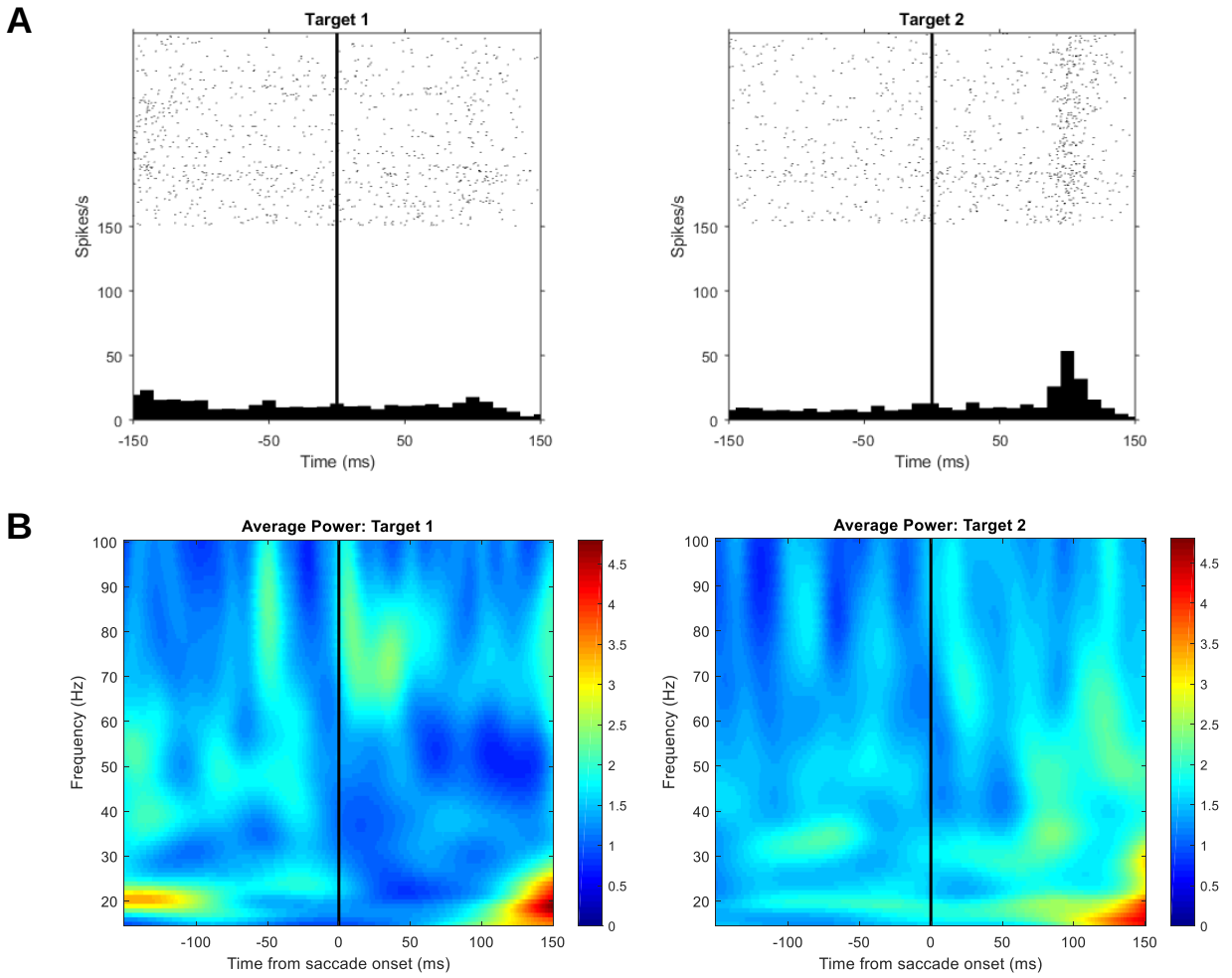

Figure 2-2. Example recording site activity aligned to saccade onset.

A) Raster plot and PSTH of all sorted spikes (MUA) on the recording site. Spiking activity shows a response following the onset of the saccade that is stronger when the target is presented at location 2. **B)** Time-frequency plots of the normalized LFP power recorded at the site. Power is averaged over all successful trials to a given target location. The LFP activity shows slightly higher LFP power following the saccade to target location 2 compared with location 1. Unlike the stimulus-aligned data, the activity of the LFP power aligned to the saccade onset does not appear to temporally correspond to the increase in MUA spiking.

To determine if this relationship between the LFP power and the MUA held for the population of recorded sites, we compared measures of spatial preference. For both types of neural activity, we used a signed d-prime metric (see Section 2.2.1). This resulted in two d-prime values for any given site. These two d-prime values could be congruent (have the same sign) or incongruent. Figure 2-3 is a cartoon depiction of a site with congruent d-prime values. As noted in the Methods, the d-prime of the LFP power can be calculated for any given frequency. We calculated the d-prime of the LFP power at frequencies of 1-100 Hz. This gave us the ability to explore whether there was a spectral component to the relationship between the MUA and the LFP power.

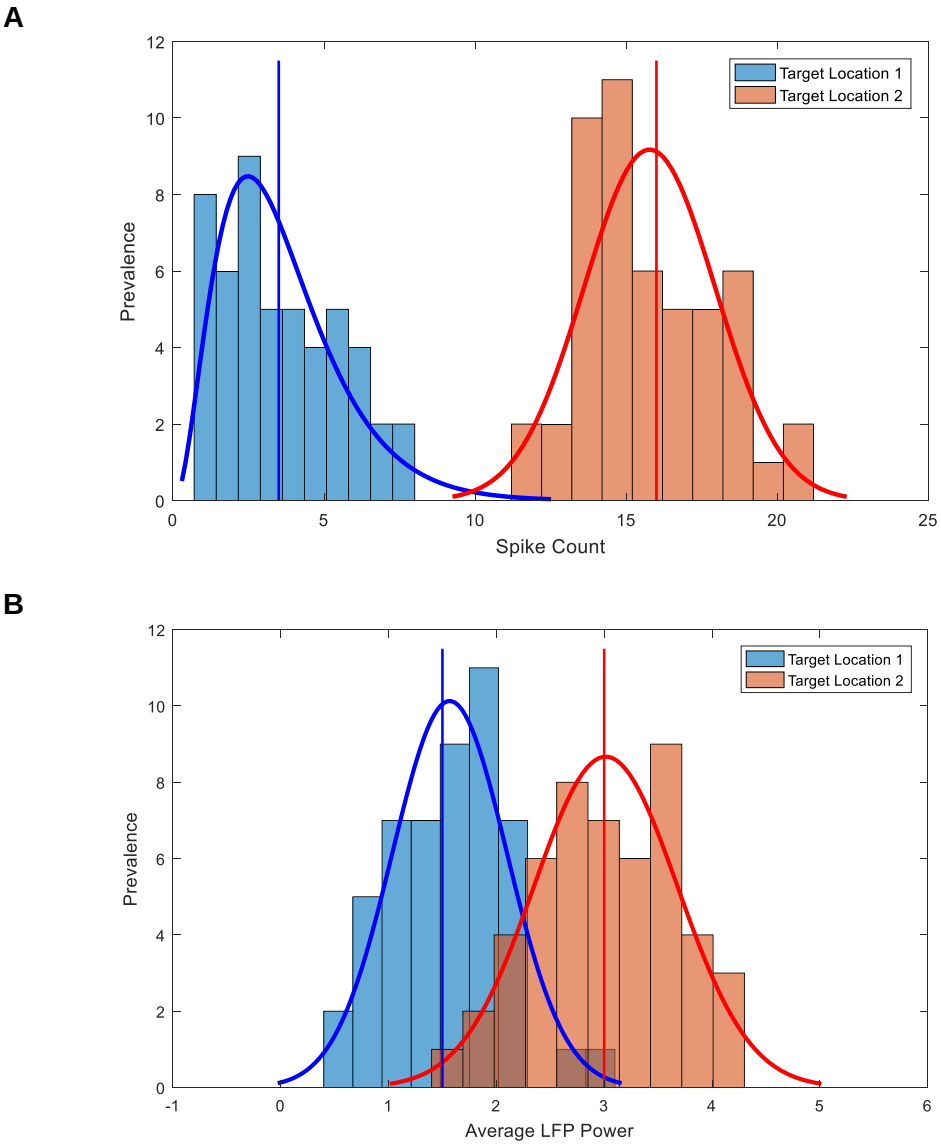

Figure 2-3. Illustration of d-prime cacluation methods

Illustration to demonstrate congruence between the d-prime value calculated using the MUA spiking and the d-prime value calculated using the LFP power. A) Shows a distribution of spikes during the epoch of interest for a given trial for trials to two target locations. B) Shows a distribution of the average LFP power, averaged across frequency and time, during the epoch of interest on a given trial for trials to two target locations. Though the resultant d-prime value from each distribution would be different, they would have the same sign (- or +). The convention we adopted in our d-prime calculations was to subtract location 2 from location 1 (blue – red). The illustration depicts a site that would have a negative (-) d-prime for both the MUA d-prime and the LFP power d-prime, and therefore be congruent.

We found that the d-prime values of the MUA and LFP power associated with the visual stimulus onset tended to have a positive, significant correlation ($p < 0.05$, Pearson's correlation coefficient). As shown in Figure 2-4, the correlation between the d-prime of the MUA and the LFP power differed by area. In LIP (solid blue line), correlations were significant at frequencies above 9 Hz with the highest correlation between the selectivity metrics occurring at 97 Hz ($r = 0.6760$). There is a sharp increase in the correlation coefficient from approximately 5 to 15 Hz. This can be largely explained by the loss of temporal resolution at low frequencies that occurs when using a wavelet-based spectral transformation. Above 15 Hz, all frequencies have a relatively high correlation coefficient, with a local maximum at 30 Hz ($r = 0.5764$). In FEF (solid red line), the correlation is much weaker with a significant correlation occurring at only certain frequencies. The correlation between the d-prime of the MUA and the LFP power has three local maxima. The highest correlation coefficient occurs at 100 Hz ($r = 0.2126$) and the other local maxima occur at 49 Hz ($r = 0.253$) and 16 Hz ($r = 0.1900$).

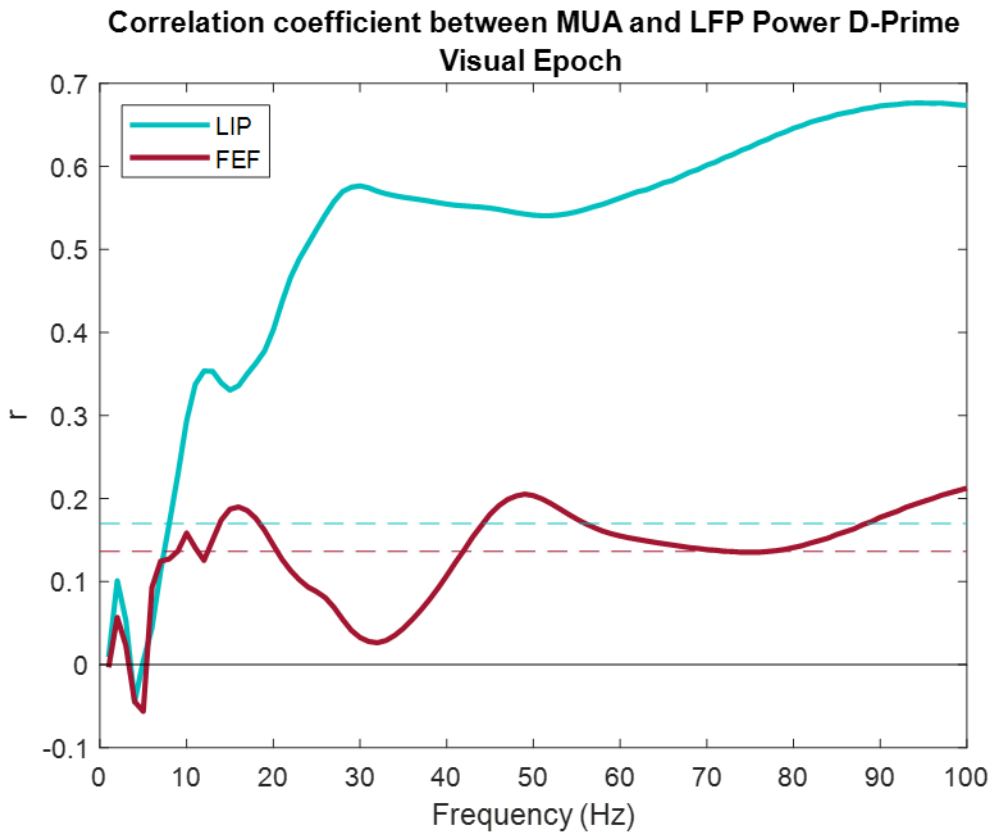

Figure 2-4. Visual epoch: Correlation between MUA d-prime and LFP power d-prime.

Pearson's correlation coefficient as a function of frequency between the d-prime of the MUA and the d-prime of the LFP power during the visual epoch. The correlation coefficient for parietal recording sites is represented by the solid blue line. The solid red line represents the correlation coefficient for frontal sites. The dashed lines indicate the significance threshold for $\alpha = 0.05$ for each area. Parietal sites had a significant correlation between the MUA and LFP power d-prime values for frequencies above 9 Hz. Frontal sites exhibited a significant correlation for only the following frequencies: 9-11 Hz, 13-20 Hz, 42-73 Hz, and 77 Hz and greater.

Figure 2-5A-D shows the comparison between the selectivity metrics for parietal and frontal sites at 22, 36, 45, and 53 Hz during the visual epoch. We see that at each example frequency there is a clear correlation at the parietal sites and a weak correlation at the frontal sites.

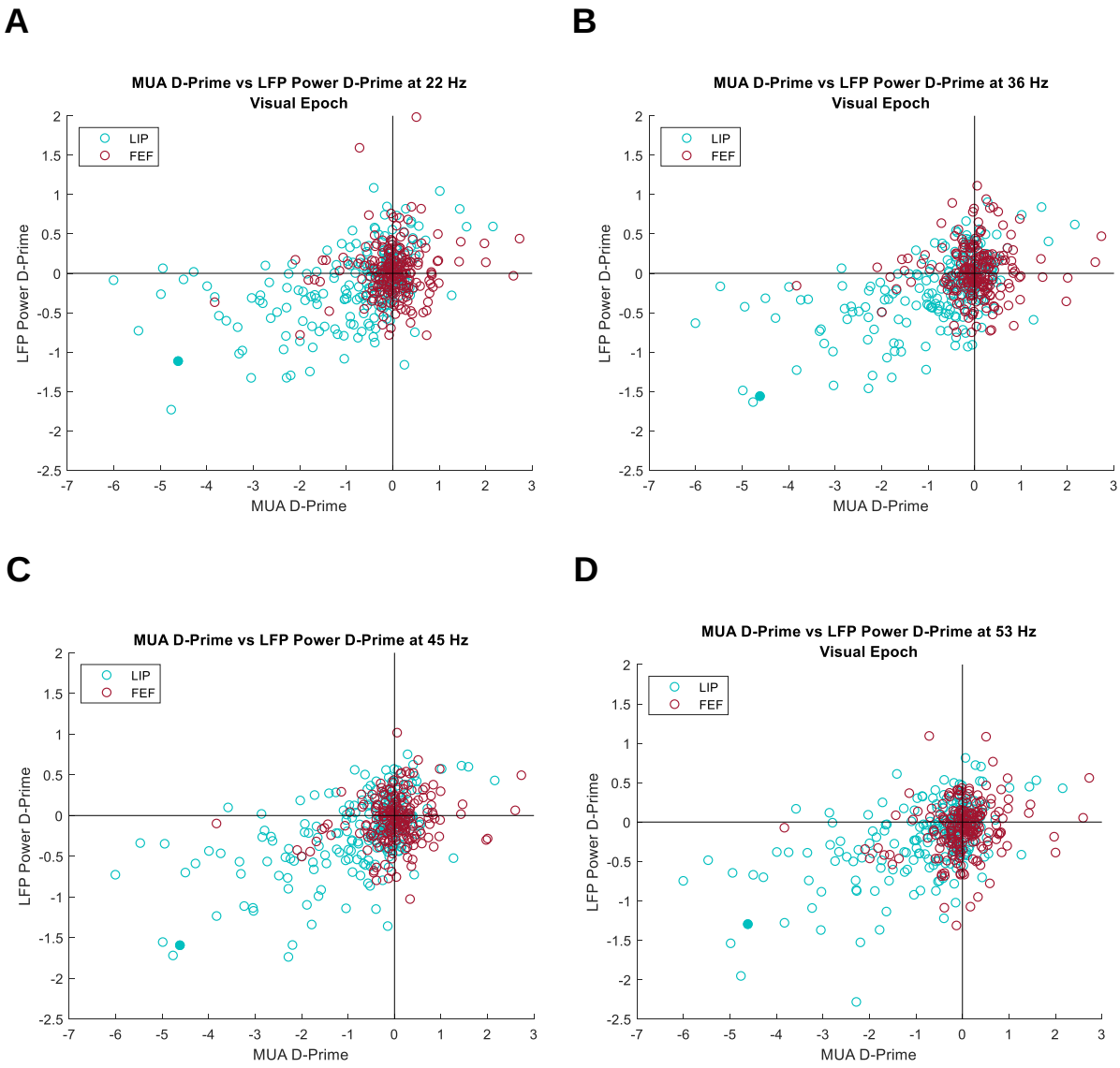

Figure 2-5. Visual epoch: Example frequencies of MUA d-prime vs. LFP power d-prime.

Relationship between the d-prime of the MUA stimulus response and the LFP power stimulus response at 22 Hz (A), 36 Hz (B), 45 Hz (C), and 53 Hz (D). Each circle corresponds to a recording site (n=431; 215 parietal & 216 frontal). Blue circles represent recording sites located in parietal cortex while red circles represent recording sites in frontal cortex. The filled blue circle is the example site depicted in Figs. 2.2-2.3.

We carried out the same analysis for the activity associated with the onset of the saccade for each area. We found that the correlation between the spatial preference of the MUA d-prime and the LFP power d-prime overall was weaker. As shown in Figure 2-6, the correlation coefficient between the MUA d-prime and the LFP power d-prime for parietal sites is positive and significant, though weak, at 12-13 Hz and frequencies above 20 Hz. Another peculiarity is the oscillatory nature of the correlation coefficient with respect to frequency. The correlation coefficient exhibits three local maxima, which occur at 31, 52, 99 Hz ($r = 0.2677$, 0.2570, and 0.3716, respectively). This might suggest that there is more than simply a spatial preference signal being represented in the LFP power around the onset of the saccade. The correlation coefficient between the d-prime values of the MUA and LFP power at the frontal recording sites was largely positive but non-significant. It was significant within the frequency range 33 – 57 Hz, with a maximum correlation coefficient at 52 Hz ($r = 0.1536$).

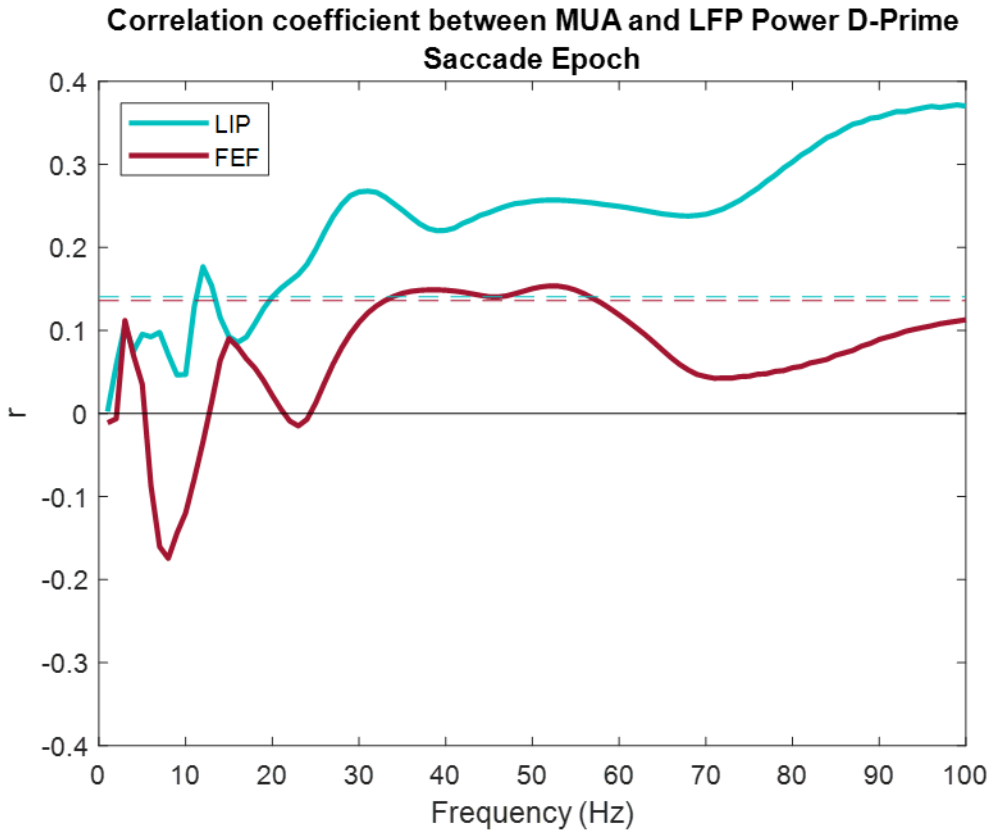

Figure 2-6. Saccade epoch: Correlation between MUA d-prime and LFP power d-prime.

Pearson's correlation coefficient as a function of frequency between the d-prime of the MUA and the d-prime of the LFP power during the saccade epoch. The correlation coefficient for parietal recording sites is represented by the solid blue line. The solid red line represents the correlation coefficient for frontal sites. The dashed lines indicate the significance threshold for $\alpha = 0.05$ for each area. Parietal sites had a significant correlation between the MUA and LFP power d-prime values for 12-13 Hz and frequencies above 20 Hz. Frontal sites exhibited a significant correlation for only 33-57 Hz.

Figure 2-7A-D shows the comparison between the selectivity metrics for parietal and frontal sites at 22, 36, 45, and 53 Hz during the saccade epoch. We see weak correlations at all frequencies for both parietal and frontal recording sites.

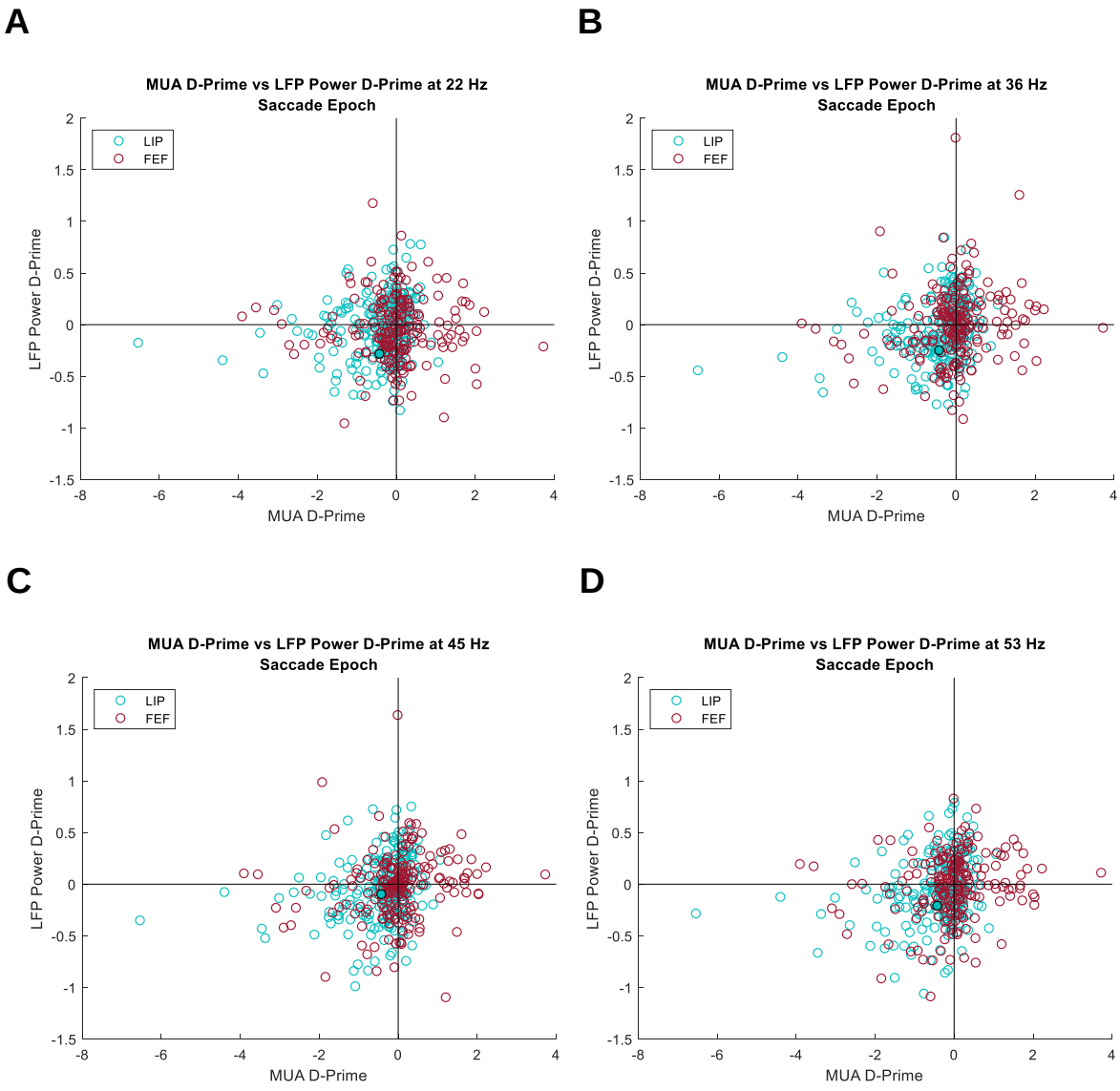

Figure 2-7. Saccade epoch: Example frequencies of MUA d-prime vs. LFP power d-prime.

Relationship between the d-prime of the MUA peri-saccade response and the LFP power stimulus response at 22 Hz (A), 36 Hz (B), 45 Hz (C), and 53 Hz (D). Each circle corresponds to a recording site (n=431; 215 parietal & 216 frontal). Blue circles represent recording sites located in parietal cortex while red circles represent recording sites in frontal cortex. The filled blue circle is the example site depicted in Figs. 2-3 and is outlined in black for visibility.

Though the majority of frequencies exhibited significant correlations the correlation coefficients tended to be low. We hypothesized that this was due to inherent variability of the signals. To confirm this, we conducted split-half reliability analysis for activity both following the stimulus onset and around the saccade onset. Trials recorded at a site were split into odd and even trials. New d-prime values were then calculated using only the odd or the even trials. In both time windows, the odd and even d-prime values calculated using the MUA were highly correlated, as shown in Figures 2-8 & 2-9 (stim: $r = 0.9397$; saccade: $r = 0.9293$). This suggested that if inherent variability of the signals was the reason behind the low correlation coefficients, it was in the LFP induced power.

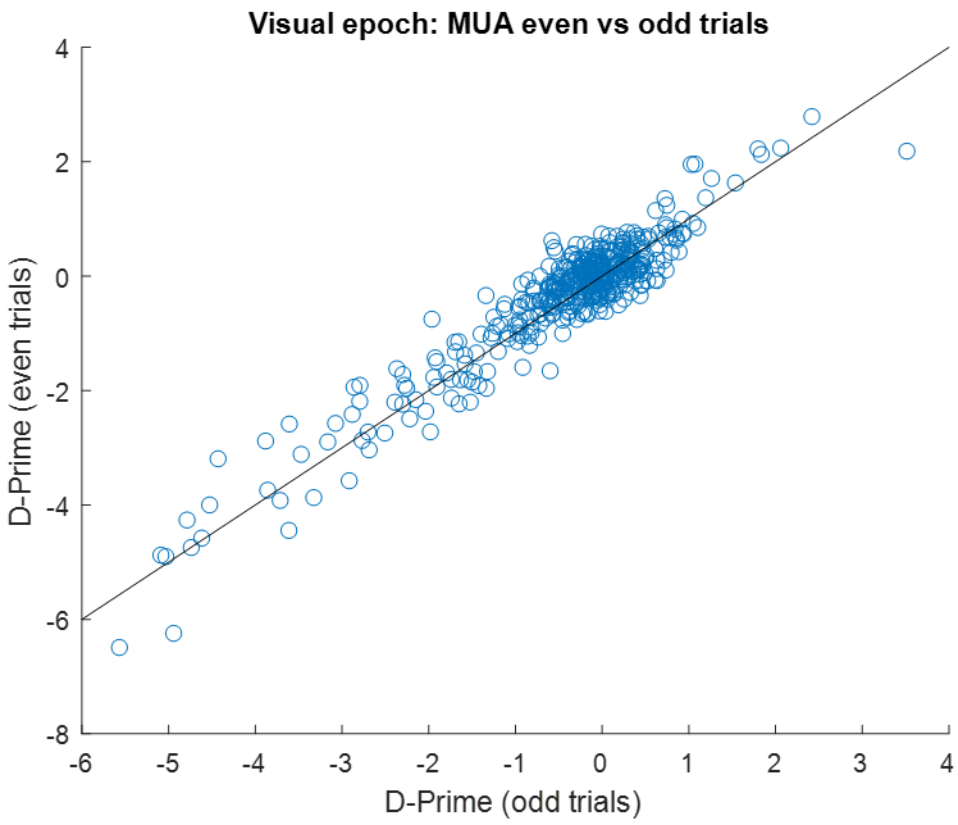

Figure 2-8. Visual epoch: MUA d-prime split-half reliability analysis.

Split-half reliability analysis: MUA d-prime for each site during the visual epoch; [50:200] ms following target onset. Trials to each target location were split into odd and even trials. The d-prime was calculated between target locations using only spike counts from either odd or even trials. Each point represents the comparison between the d-prime calculated for even trials vs the d-prime for odd trials. The correlation coefficient between the two d-prime calculations is 0.9397 ($p < 0.01$), indicating that the d-prime of the MUA during the visual epoch is a reliable metric. The black line is the unity line.

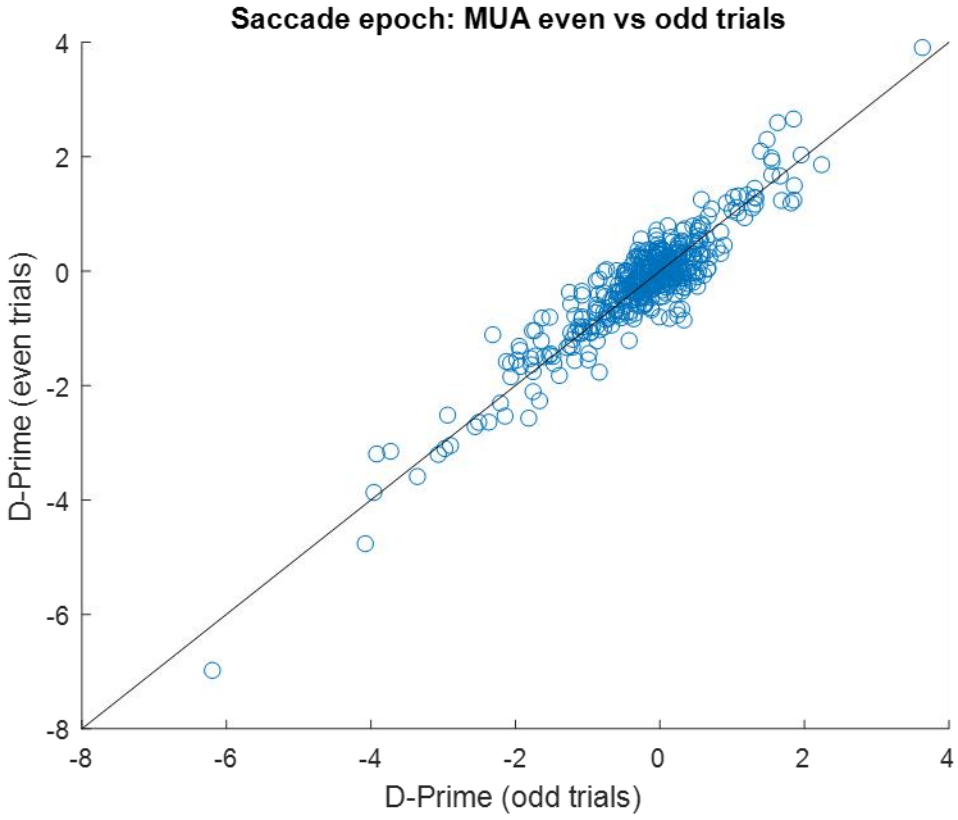

Figure 2-9. Saccade epoch: MUA d-prime split-half reliability analysis.

Split-half reliability analysis: MUA d-prime for each site during the saccade epoch; [-100:100] ms around saccade onset. Trials to each target location were split into odd and even trials. The d-prime was calculated between target locations using only odd or even trials. Each point represents the comparison between the d-prime calculated for even trials vs the d-prime for odd trials. The correlation coefficient between the two d-prime calculations is 0.9293 ($p < 0.01$), indicating that the d-prime of the MUA during the saccade epoch is a reliable metric. The black line is the unity line.

To account for noise that may be present in the LFP signals we paired the split-half reliability analysis of the LFP power with bootstrapping analysis (1000 iterations). For the visual and saccadic activity, we again calculated the d-prime values for odd and even trials with the LFP power at each frequency. For this analysis we combined the frontal and parietal sites. The blue line in Figure 2-10 shows the mean correlation coefficient between the odd and even d-prime values that resulted from the bootstrapping analysis at each frequency along with the 95% confidence bounds indicated by the shaded area. The orange line represents the mean correlation coefficient between the MUA d-prime and the LFP power d-prime that resulted from the bootstrapping analysis and its 95% confidence bounds. The correlation coefficients between the MUA and LFP power that resulted from the split-half reliability analysis appears qualitatively similar to the comparison of the full data set.

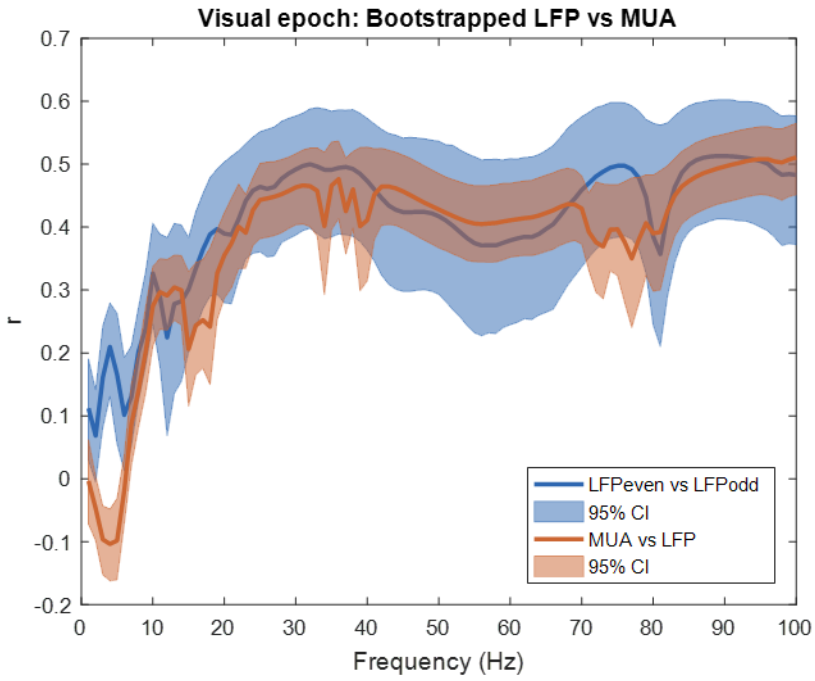

Figure 2-10. Visual epoch: Bootstrapped LFP power split-half reliability analysis.

Pearson's correlation coefficient vs frequency for the split-half reliability analysis of the LFP power d-prime for each site during the visual epoch; [50:200] ms following target onset. Trials to each target location were split into odd and even trials. The d-prime was calculated between target locations using only power from either odd or even trials. We used bootstrapping analysis to calculate the mean correlation coefficient between odd and even trials of the LFP power d-prime (blue line) and the mean correlation coefficient between the MUA d-prime and the LFP power d-prime (orange line). Shading indicates 95% confidence bounds. The correlation coefficient between the MUA and LFP falls within or slightly below the 95% confidence bounds of the LFPeven to LFPodd comparison.

As in Figure 2-5, we compared the selectivity metrics for parietal and frontal sites at 22, 36, 45, and 53 Hz following the onset of the visual stimulus. Figure 2-11A-D shows the comparison between the d-prime of the MUA and the d-prime of the LFP power for both odd and even trials, with odd trials being indicated by the open circles and even trials being indicated by the open triangles. As in the analysis of the full data set, we see a positive correlation at each of the example frequencies with the parietal sites having a stronger correlation than the frontal sites.

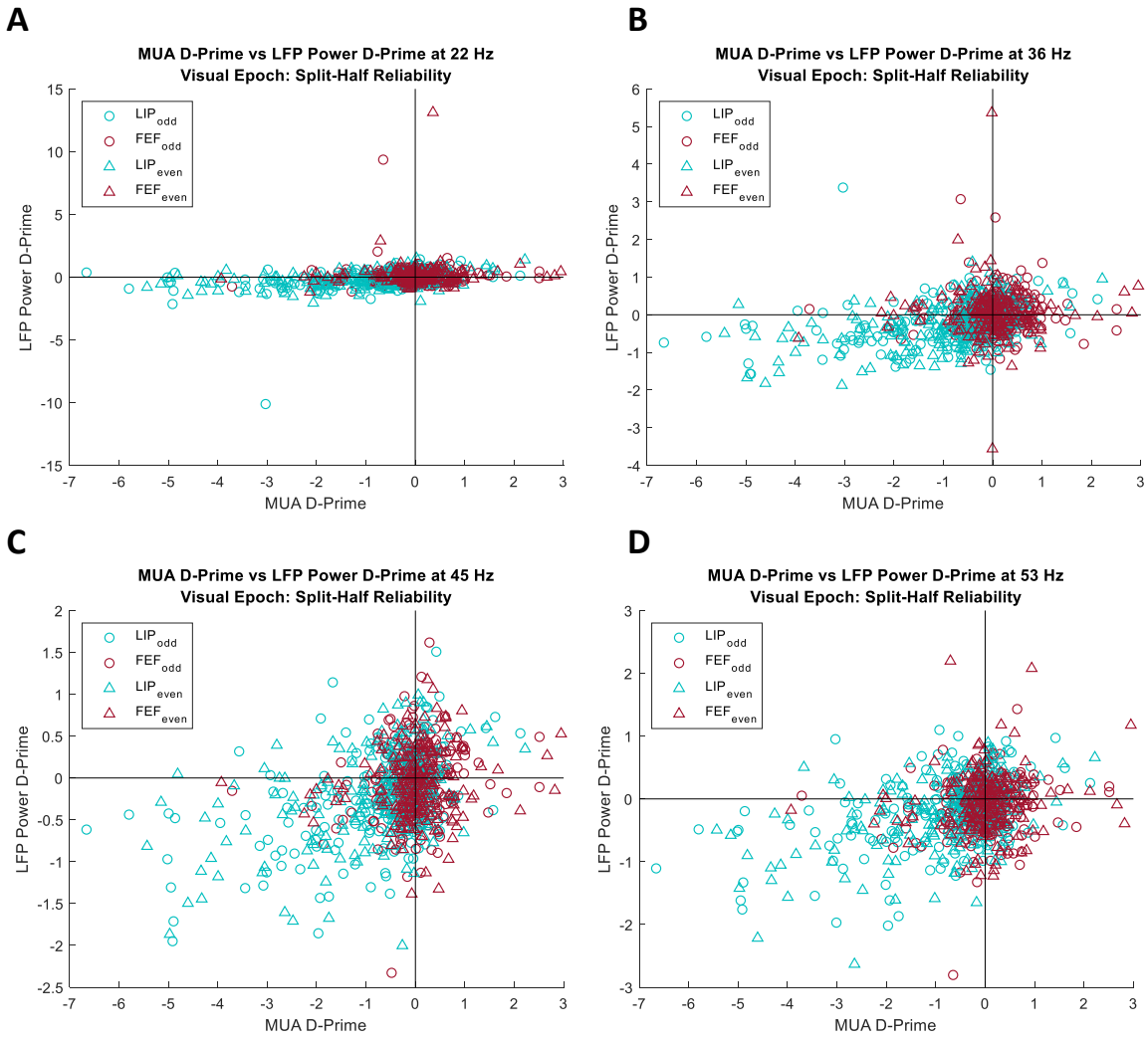

Figure 2-11. Visual epoch: Example frequencies of LFP power split-half reliability analysis.

Relationship between the d-prime of the MUA stimulus response and the LFP power stimulus response for odd and even trials at 22 Hz (A), 36 Hz (B), 45 Hz (C), and 53 Hz (D). Each point corresponds to a recording site (n=431; 215 parietal & 216 frontal). Color conventions are the same as in Fig 6. Open circles indicate odd trials while open triangles indicate even trials.

In contrast, we found that the relationship between the MUA d-prime and the LFP power d-prime had a much weaker relationship around the onset of the saccade. Following the same conventions as Figure 2-10, Figure 2-12 shows the correlation coefficients at each frequency between the odd and even LFP power d-primes (blue line and shading) as well as for the MUA d-prime and the LFP power d-prime that resulted from the bootstrapping analysis (orange line and shading). This indicates a weak relationship between the selectivity of a site as determined by the MUA and the selectivity determined by the LFP induced power when looking at the activity around the saccade. It also lends additional support to the hypothesis that there is more than just spatial preference information being carried in the LFP around the saccade.

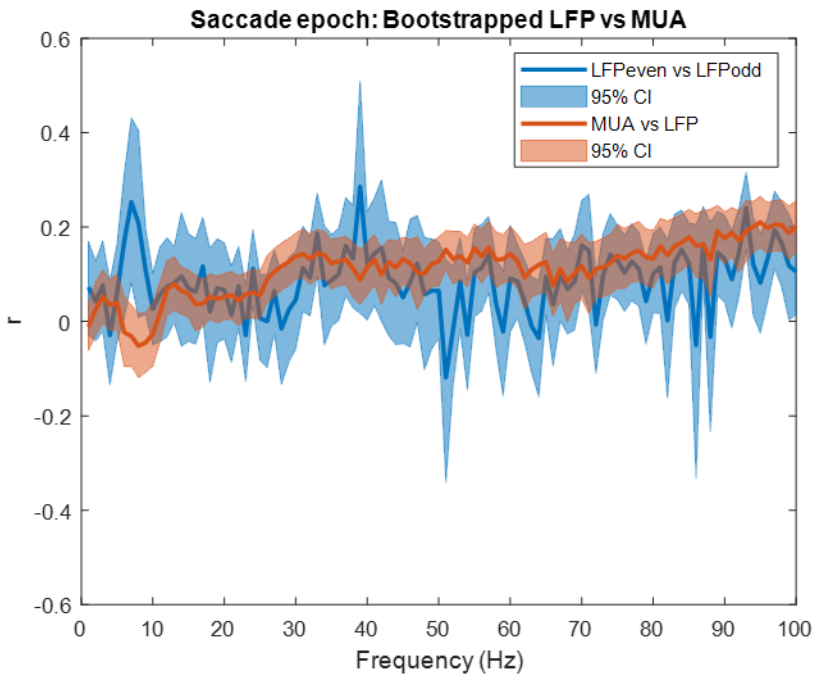

Figure 2-12. Saccade epoch: Bootstrapped LFP power split-half reliability analysis.

Pearson's correlation coefficient vs frequency for the split-half reliability analysis of the LFP power d-prime for each site during the saccade epoch; [-100:100] ms following saccade onset. Trials to each target location were split into odd and even trials. The d-prime was calculated between target locations using only power from either odd or even trials. We used bootstrapping analysis to calculate the mean correlation coefficient between odd and even trials of the LFP power d-prime (blue line) and the mean correlation coefficient between the MUA d-prime and the LFP power d-prime (orange line). Shading indicates 95% confidence bounds. The 95% confidence bounds of the MUA and LFP overlap with the 95% confidence bounds of the LFP_{even} to LFP_{odd} comparison.

As in Figure 2-7, we compared the selectivity metrics for parietal and frontal sites at 22, 36, 45, and 53 Hz around the onset of the saccade. Figure 2-13A-D shows the comparison between the d-prime of the MUA and the d-prime of the LFP power for both odd and even trials. Similar to the full data set, we see a very weak correlation at each of the example frequencies for both frontal and parietal sites.

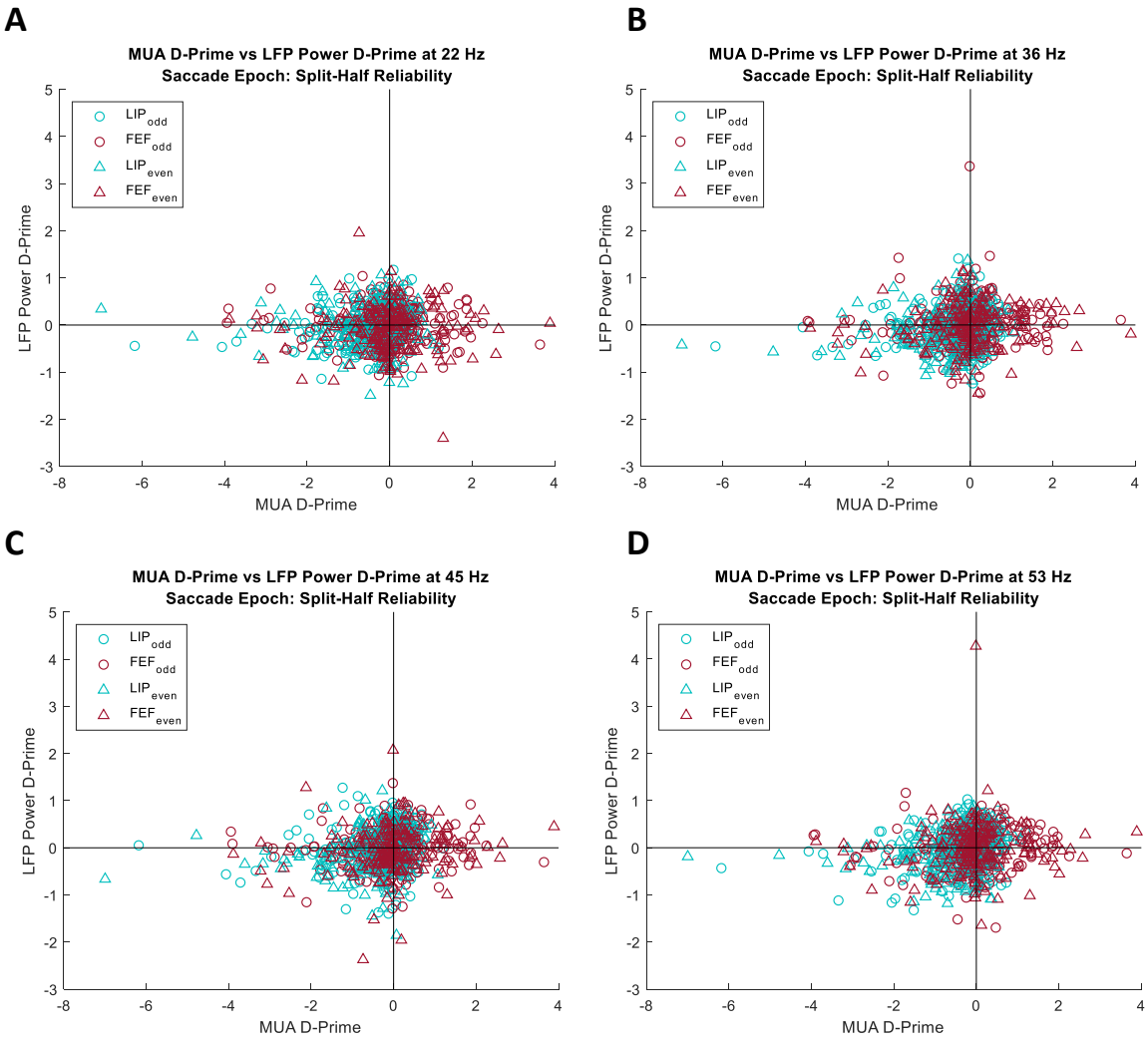

Figure 2-13. Saccade epoch: Example frequencies of LFP power split-half reliability analysis.

Relationship between the d-prime of the MUA peri-saccadic response and the LFP power stimulus response for even and odd trials at 22 Hz (A), 36 Hz (B), 45 Hz (C), and 53 Hz (D). Each circle corresponds to a recording site (n=431; 215 parietal & 216 frontal). Color conventions are the same as Fig 6. Open circles represent odd trials and open triangles represent even trials.

2.3.2 Field-Field Coherence

With the d-prime of the MUA being a robust means of measuring spatial selectivity of an LFP recording site following stimulus onset, we wanted to further explore the relationship between the LFPs recorded in FEF and those in LIP. We were particularly interested in the activity around the saccade for two reasons. First, in the above analyses we see what appears to be activity in the LFP power that is related to the spatial location of the saccade target, but is not correlated to the MUA. Second, in our lab's previous spike-count correlation analysis, which investigates interactions between the two areas, we found an unexpected decrease in correlation around the onset of the saccade when the target was at the preferred location (Hall et al, in review). Our overall goal was to determine whether this decorrelation was also present in other neural activity recorded across FEF and LIP. For an analogous correlation analysis in the frequency domain, we used the magnitude-squared coherence (MSC). We compared the MSC between trials when the saccade was made to the preferred target and trials when the saccade was made to the non-preferred target. The target preference of all recording sites was defined by the d-prime of the MUA. As in the previous spike-count correlation analysis, we limited our analyses to pairs of sites that shared a preferred target. We determined this using the product of the d-prime for each site. A matching preference resulted in a positive d-prime product and a non-matching preference resulted in a negative d-prime product. We further limited the pairs analyzed to those with a d-prime product of at least 0.4, as was done in Hall et al. This resulted in 109 pairs of LFP sites for analysis (14.29% of total pairs).

We calculated the MSC between each of the pairs and found that there was task related activity associated with both the onset of the visual stimulus and the onset of the saccade. The task related activity was also dependent on the spatial location of the target. Figure 2-14 shows an

example pair and the task related MSC for both the preferred and non-preferred target locations aligned to the onset of the stimulus. Fig 2-14A shows the average difference between the MSC during trials to the shared preferred target location and the non-preferred target location. At frequencies between ~ 20-50 Hz, we see higher coherence approximately 50 ms following stimulus onset when the stimulus is in the preferred location compared to the non-preferred location. We also see lower coherence 100-150 ms following stimulus onset. This is further illustrated in Figure 2-14B-C, which show the average MSC for trials to the preferred and non-preferred target locations. When looking at the LFP induced power for the frontal and parietal sites in the pair (Figure 2-15), we find increases in power that tend to correspond to increases in the MSC. In both frontal and parietal sites, we see an increase in power approximately 70 ms after the onset of the stimulus during trials in the preferred location. We also see an increase in power, though to a lesser degree, approximately 100 ms after the onset of the stimulus during trials in the non-preferred location. Interestingly, the magnitude of the increase in coherence does not correspond to the magnitude of the increase in corresponding power. We see a larger increase in coherence during trials to the non-preferred location compared to the preferred location, despite the corresponding power increase being smaller.

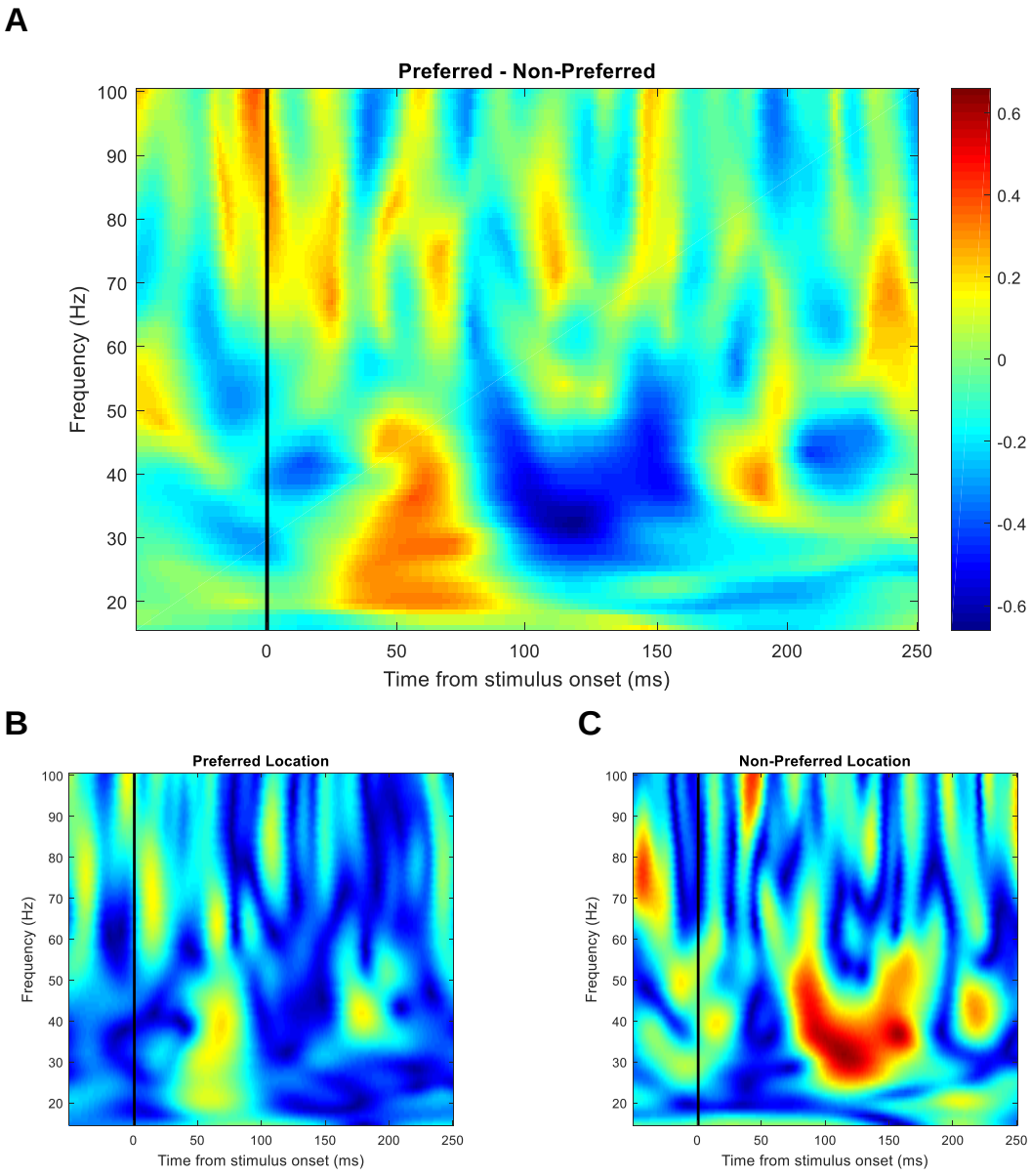

Figure 2-14. Visual epoch: Average MSC for example site pair.

Time-frequency plot of the magnitude-squared coherence when the stimulus appears at the preferred target location **(A)** and when the stimulus appears at the non-preferred target location **(B)** for an example pair of recording sites. **C)** Shows the difference between the MSC during trials at the preferred location and trials at the non-preferred location. Around 50 ms after the onset of the target, the coherence is slightly greater between ~20-45 Hz when the stimulus is at the preferred target location. This is immediately followed by ~50 ms of decreased coherence compared to the non-preferred target location. Coherence between the sites was averaged across trials. The selectivity product of this pair of sites is -4.5. Data is aligned to the onset of the visual stimulus.

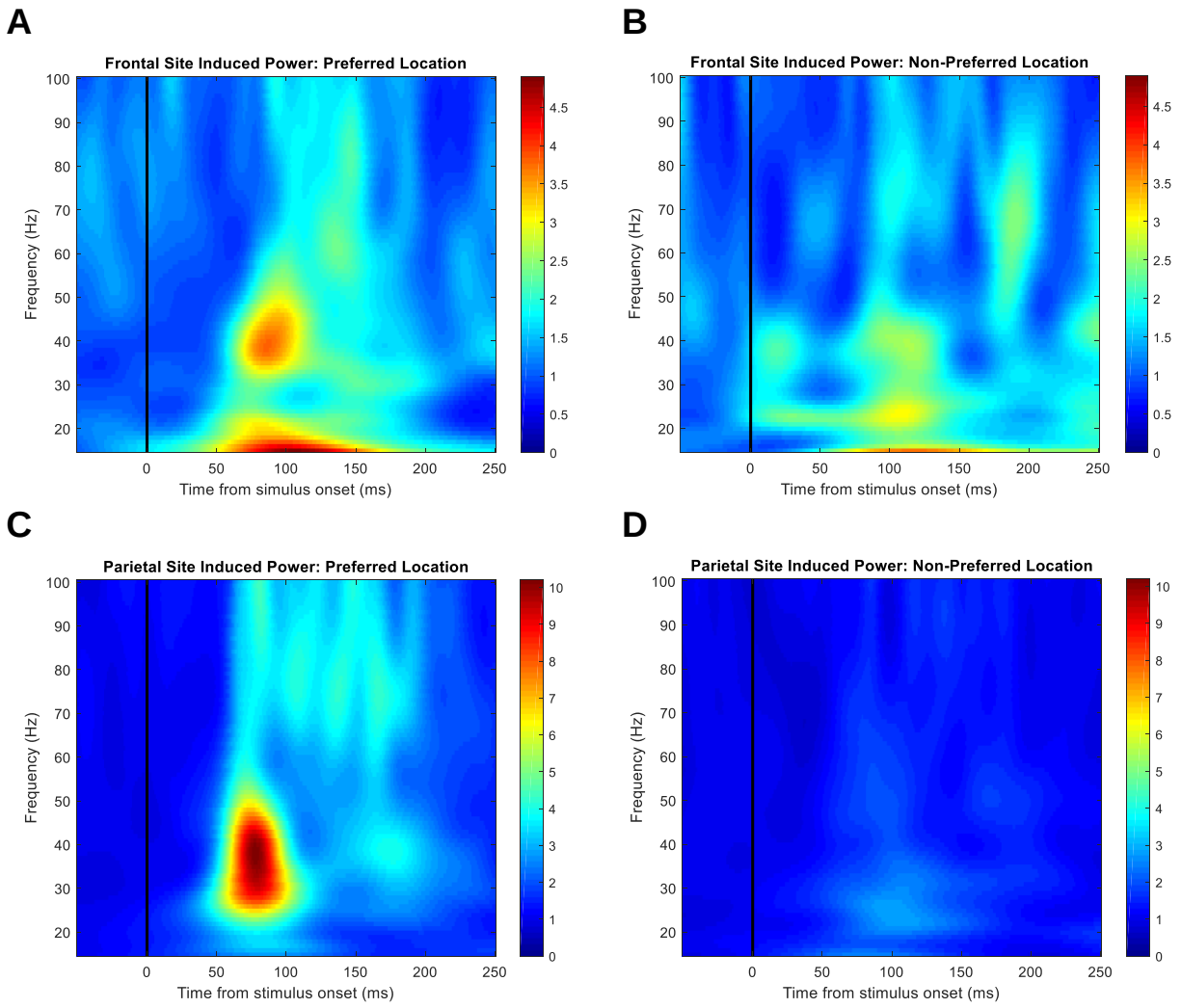

Figure 2-15. Visual epoch: Average LFP power for frontal and parietal example sites.

A) Average induced power over all trials to the preferred location for the frontal recording site. **B)** Average induced power over all trials to the non-preferred location for the frontal recording site. **C)** Average induced power over all trials to the preferred location for the parietal recording site. **D)** Average induced power over all trials to the non-preferred location for the parietal recording site. Approximately 70 ms following the onset of the visual stimulus, there is an increase in power during trials to the preferred target location. During trials to the non-preferred target location, we see a smaller increase in power that occurs approximately 100 ms following the onset of the visual stimulus. These increases in power correspond to increases in MSC, resulting in increased coherence immediately followed by decreased coherence from ~30-60 Hz when comparing the preferred target location to the non-preferred target location. Coherence between the sites was averaged across trials. Data is aligned to the onset of the saccade.

Figure 2-16 shows the same pair aligned to the onset of the saccade. In Figure 2-16A, which shows the average difference between trials to the preferred and non-preferred target locations, we see less coherence 50-100 ms following the onset of the saccade between 20-50 Hz when the target is in the preferred location compared to the non-preferred location. Additionally, there is lower coherence immediately preceding the onset of the saccade at higher frequencies (>75 Hz). Interestingly, when looking at the induced power for both the frontal and parietal recording sites of this example pair (Figure 2-17), we noticed that the average power was higher following saccades made to the non-preferred target. This appears to be a change in spatial preference between the visual and saccade epochs based on the LFP power. Based on the MUA, however, the target location preference is consistent throughout the trial, though stronger following the onset of the visual stimulus. This observation supports the hypothesis that the LFP around the onset of the saccade contains more information than just spatial selectivity.

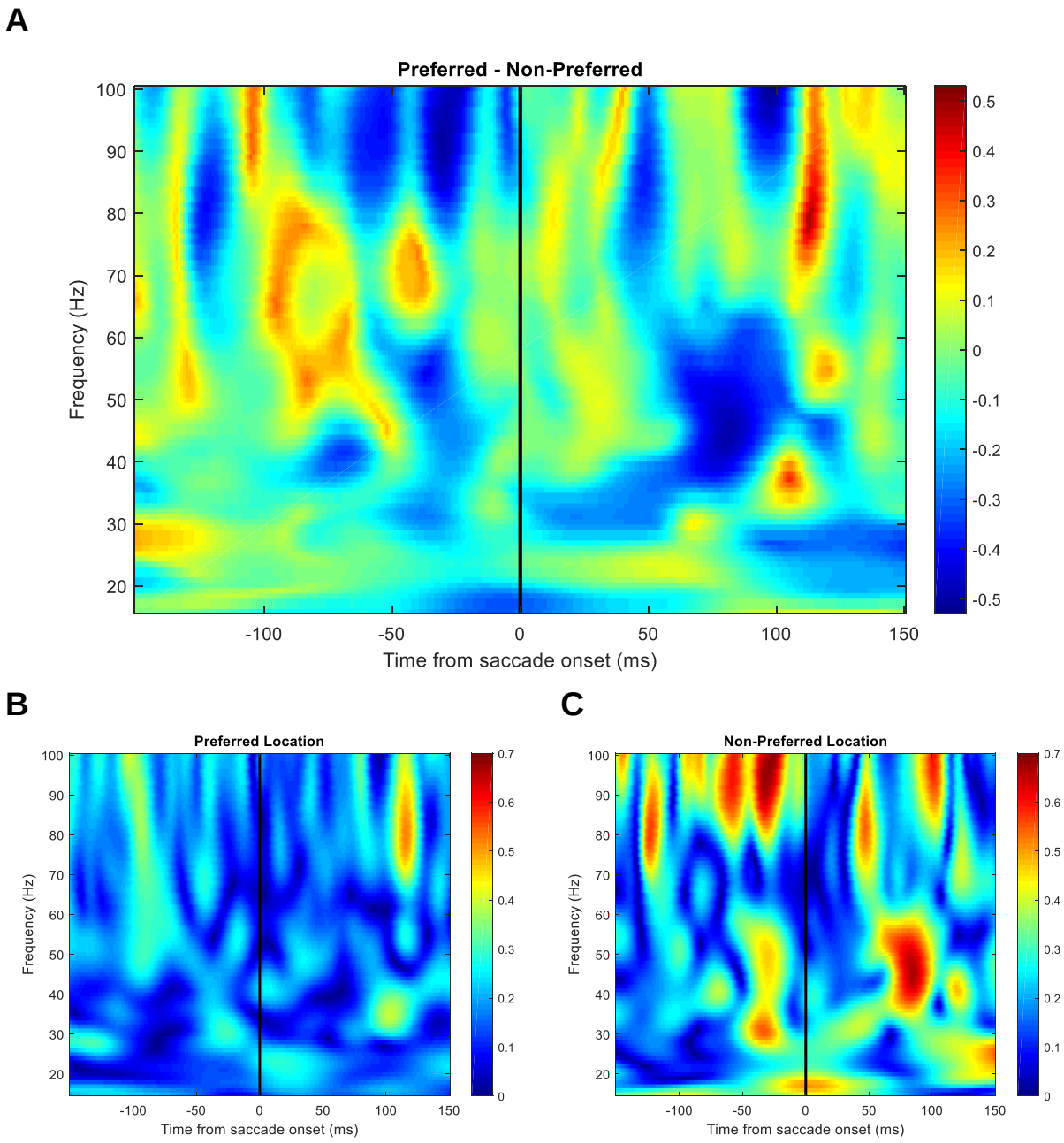

Figure 2-16. Saccade epoch: Average MSC for example site pair.

Time-frequency plot of the magnitude-squared coherence for the same example pair as in Fig 15. **A)** The average difference in MSC between trials when the saccade is directed to the preferred target location and when the saccade is directed to the non-preferred target location. **B)** Average MSC over all trials to the preferred target location. **C)** Average MSC over all trials to the non-preferred target location.

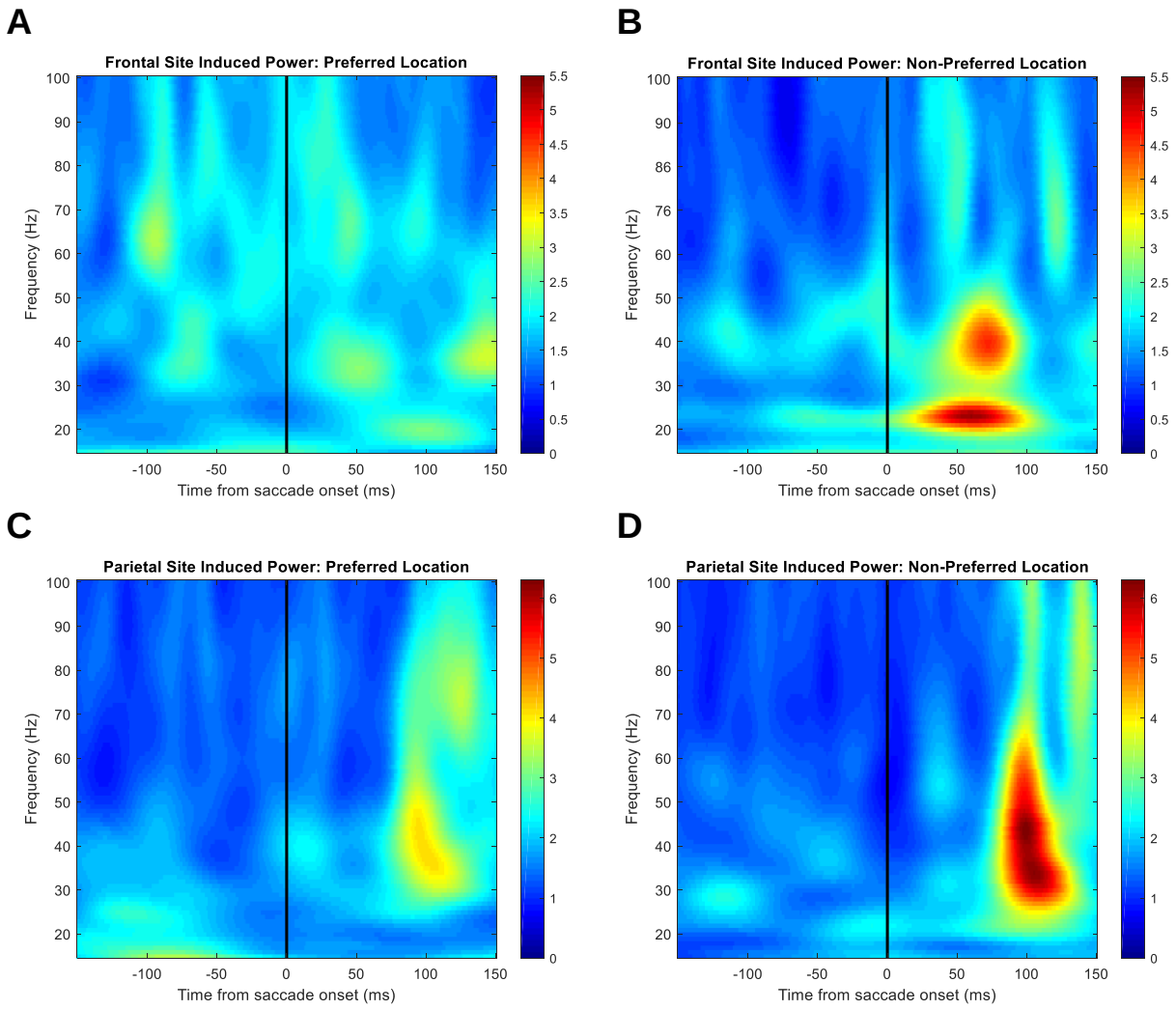

Figure 2-17. Saccade epoch: Average LFP power for frontal and parietal example sites.

A) Average induced power over all trials to the preferred location for the frontal recording site. **B)** Average induced power over all trials to the non-preferred location for the frontal recording site. **C)** Average induced power over all trials to the preferred location for the parietal recording site. **D)** Average induced power over all trials to the non-preferred location for the parietal recording site. Both before and after the onset of the saccade, the coherence is decreased between ~30-60 Hz when the saccade is towards the preferred target location compared to the non-preferred target location. At the same frequencies, the induced power on both the frontal and parietal recording sites is increased during trials to the non-preferred target location. Coherence between the sites was averaged across trials. Data is aligned to the onset of the saccade.

We wanted to determine whether the differences in task related activity due to target location were significant over the population of site pairs. As in Hall et al., we limited our analysis to pairs with a d-prime product of at least 0.4. To test for significance, we used a cluster-based permutation test (see Methods) that identified significant clusters of time-frequency points. This method addresses the issue of multiple comparisons and takes into account that the activity should be similar at adjacent frequencies and time points. We found that the decreased coherence associated with both the onset of the stimulus and the onset of the saccade were significant ($p < 0.01$). Figure 2-18 shows the difference between the MCS towards the preferred location and the non-preferred location when activity is aligned to the onset of the stimulus. As in Figure 2-14, from ~ 20-50 Hz there is increased coherence ~ 50 ms and decreased coherence 100-150 ms following the onset of the stimulus. As indicated by the full saturation, only the decrease in coherence 100-150 ms after the stimulus onset is significant.

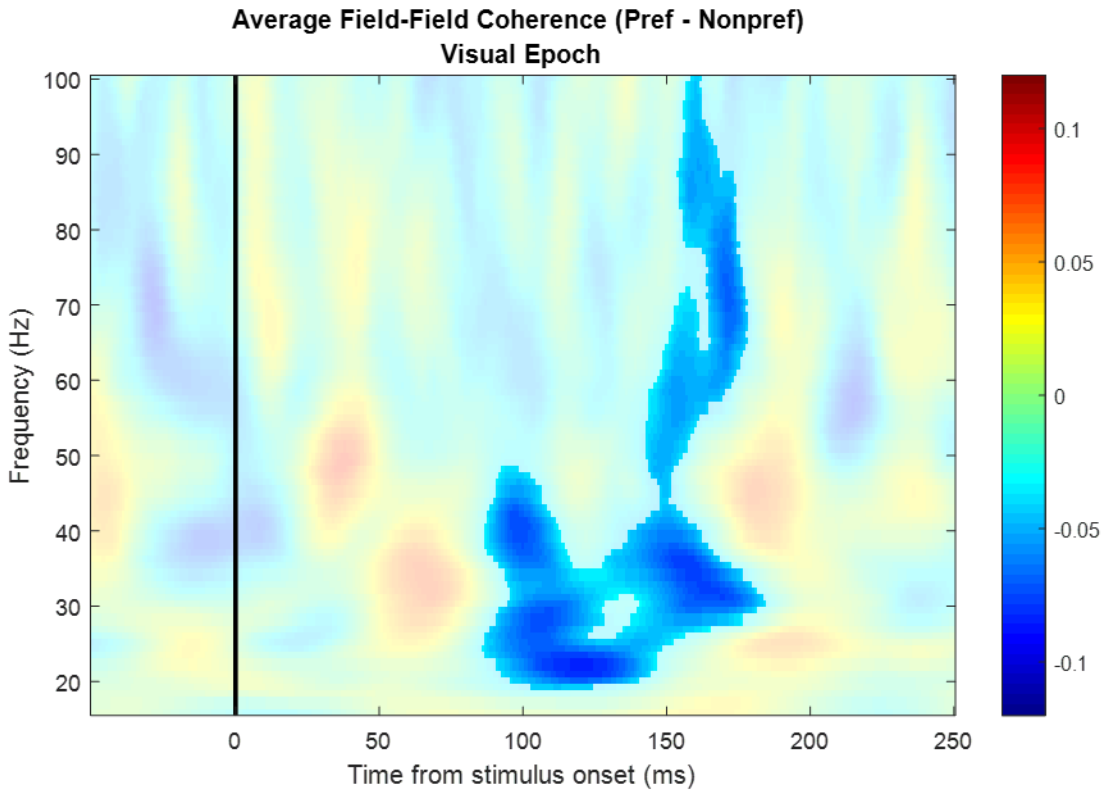

Figure 2-18. Visual epoch: Average difference in MSC (Pref. location – Nonpref. Location).

Population time-frequency plot of the difference between the magnitude-squared coherence when the stimulus appears at the preferred location and when the stimulus appears at the non-preferred location. Aligned to the onset of the stimulus. Full saturation indicates the cluster of time-frequency points is significant ($p < 0.01$).

At the population level, the significantly decreased coherence when the stimulus is at the preferred location also extends to higher frequencies (up to 100 Hz) at 150 ms following stimulus onset. When looking at the population response aligned to the onset of the saccade, we also see significantly less MSC when the target is in the shared preferred location. Figure 2-19 shows the average difference in MSC between the preferred location and the non-preferred location. Aligned to the saccade, there are three distinct time-frequency clusters with significantly lower MSC when the saccade is directed to the preferred target location. One occurs at low frequencies (< 25 Hz) and is centered approximately 25 ms before the onset of the saccade. The second occurs at higher frequencies (> 60 Hz) and is centered on saccade onset. The final significant time-frequency cluster occurs over a mid-frequency range (20 – 70 Hz) and is centered approximately 75 ms after the onset of the saccade.

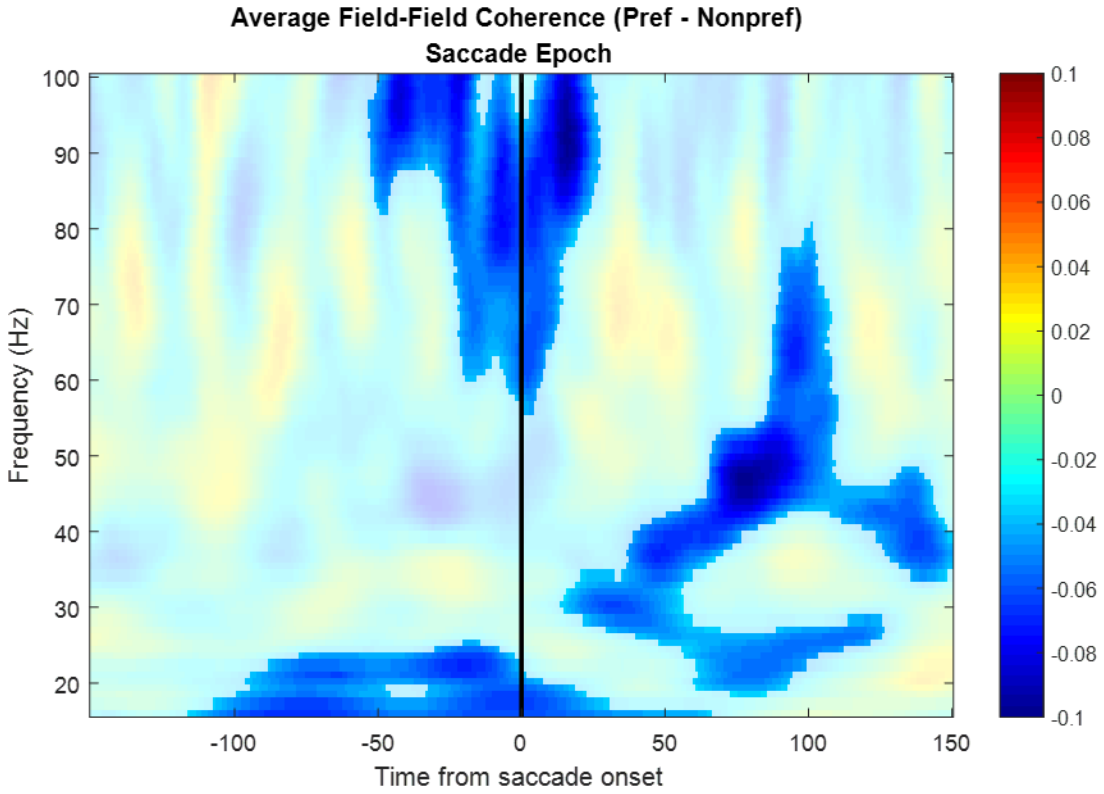

Figure 2-19. Saccade epoch: Average difference in MSC (Pref. location – Nonpref. location).

Population time-frequency plot of the difference between the magnitude-squared coherence when saccade is directed to the preferred location and when the saccade is to the non-preferred location. Aligned to the onset of the saccade. Full saturation indicates the cluster of time-frequency points is significant ($p < 0.01$).

These coherence findings provide interesting insight into the LFP power over the duration of the task. During the visual epoch of trials to the preferred target location, we see higher (but non-significant) coherence during the stimulus response and significantly lower coherence immediately afterwards. This suggests that after the stimulus response, the shared power across sites tends to be higher during trials to the non-preferred target location than during trials to the preferred target location. Similarly, for the saccade epoch, the lower coherence around the saccade during trials to the preferred location indicates that the LFP power is higher during trials to the non-preferred target location. One interpretation of this observation is a decoupling of neural activity between the frontal and parietal sites with shared spatial selectivity.

We next raised the question of whether this phenomenon of lower MSC in trials at the preferred location was dependent on the strength of the selectivity of the site pairs. To address this question, we looked at the average difference in MSC between the preferred and non-preferred location over site pairs with a d-prime product ranging from 0.1 – 4.0 in increments of 0.1. To better visualize a potential relationship between the average difference in MSC (ΔMSC), pair selectivity, and frequency we took the average of the ΔMSC over the epochs of interest. Figure 2-20A shows the ΔMSC over the visual epoch (50-250 ms after stimulus onset) as a function of frequency. The selectivity (as defined by the d-prime product) is indicated by the color of the line. The ΔMSC tends to be negative at lower selectivity and as selectivity increases so does ΔMSC until a d-prime product of ~1.5. Above a selectivity threshold of 1.5, the ΔMSC then starts to decrease and remains steady after a threshold of 2.5. Figure 2-20B better illustrates this by showing ΔMSC as a function of selectivity threshold for 25, 40, 50, and 70 Hz. The lines for 25, 40, and 50 Hz are grouped together and are positive above a d-prime product of ~0.7. The line for 70 Hz, however, remains negative at all selectivity thresholds. During the visual epoch, the ΔMSC

associated with a selectivity threshold above ~1 tends to be positive below 60 Hz, indicating a higher MSC when the stimulus is at the preferred location, but negative above 60 Hz (Figure 2-20A). Though these findings are averaged across the visual epoch, they suggest that the lower MSC for trials at the preferred location during the visual epoch depends on the selectivity threshold. One explanation for this is that the induced power, and therefore the MSC, primarily carries information about the site selectivity. As we showed earlier, the power during the visual epoch is highly correlated with the d-prime of the MUA, which is a function of the spike count. The correlations and the power response to the stimulus onset are typically high between 25 – 55 Hz (Figure 2-14 & 2-15). Higher power typically results in a higher coherence, which we see for trials at the preferred location compared to the non-preferred location for frequencies below 60 Hz. In sum, these results suggest that increased MUA to the preferred location is driving a higher induced power response between approximately 25 – 55 Hz, which in turn is causing the higher MSC seen at frequencies below 60 Hz for more selective site pairs.

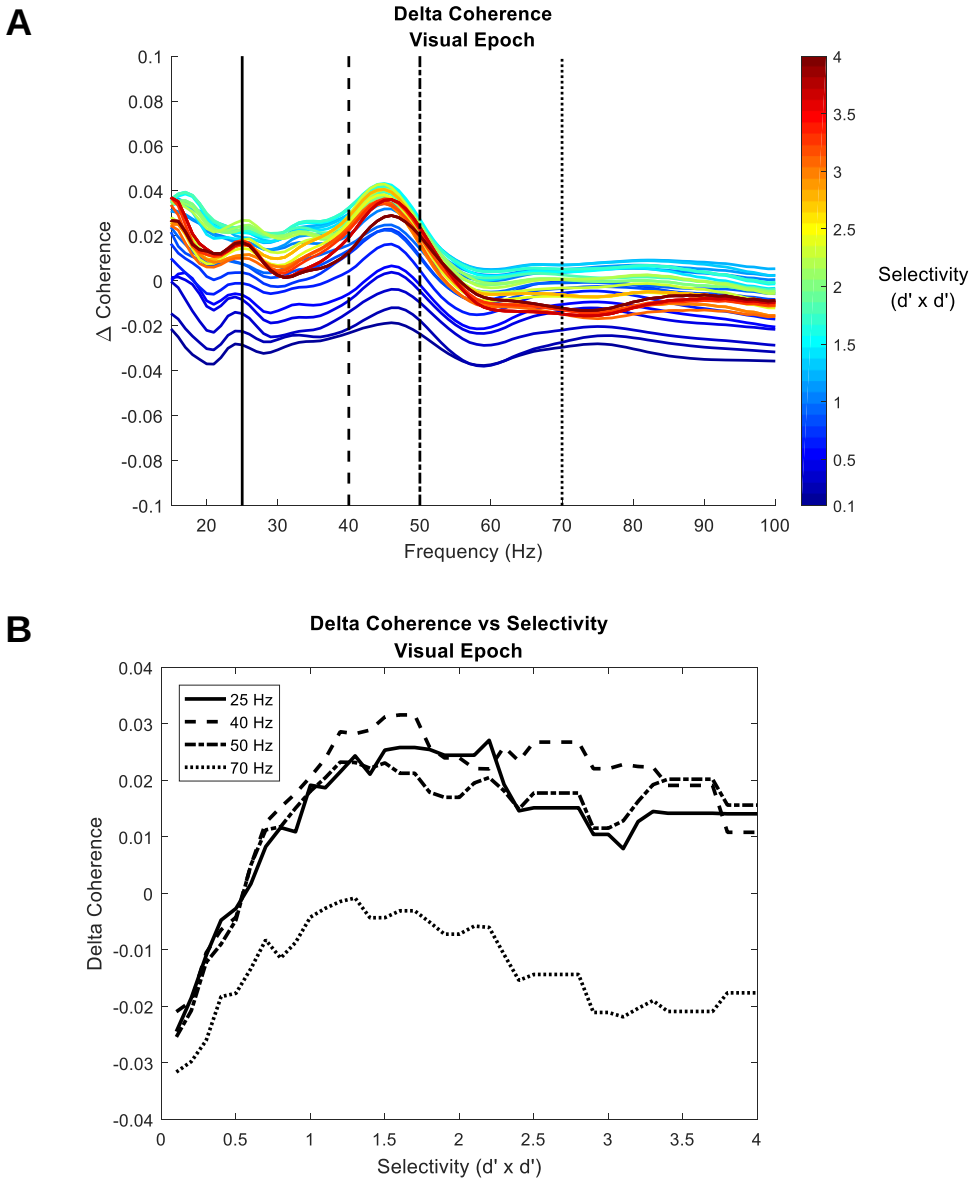

Figure 2-20. Visual epoch: Difference in MSC as a function of frequency.

A) Shows the difference in magnitude-squared coherence (ΔMSC) averaged over the visual epoch ([50:250] ms after stimulus onset) as a function of frequency for different selectivity thresholds. The selectivity threshold was determined using the product of the d-prime of the sites in a given pair. The range of the selectivity threshold is 0.1 – 4.0 and is indicated by the color of the line. Panel **(B)** further illustrates this relationship by showing ΔMSC as a function of selectivity for 25, 40, 50, and 70 Hz. At 25, 40, and 50 Hz the relationship is very similar and the ΔMSC is positive above a d-prime product of ~0.7. At 70 Hz, however, the ΔMSC remains negative at all selectivity thresholds.

Looking at the relationship between the ΔMSC and selectivity threshold during the saccade epoch (-150:150 ms around saccade onset), we again see evidence that the LFP power represents more than just the MUA. In Figure 2-21A we see that the ΔMSC follows a similar trend as in the visual epoch when the selectivity threshold increases. For low selectivity thresholds the ΔMSC starts low then increases until a d-prime product of ~1, where ΔMSC begins to decrease again. This trend is better illustrated in Figure 2-21B for 25, 40, 50, and 70 Hz. During the saccade epoch the lines representing 25, 50, and 70 Hz are grouped together and tend to hover around a ΔMSC of 0 above selectivity thresholds of ~1. At 40 Hz, however, the ΔMSC is markedly negative at each selectivity threshold, particularly at higher thresholds (> DPP = 2). This supports our earlier conclusions that the LFP signal around the onset of the saccade carries more information than just spatial selectivity. These findings also suggest that the decorrelation around the saccade we have seen in our previous spike-count correlation findings is also present in the LFP activity. A decorrelation of activity could suggest that around the onset of the saccade, frontal and parietal cortex are working independently of each other.

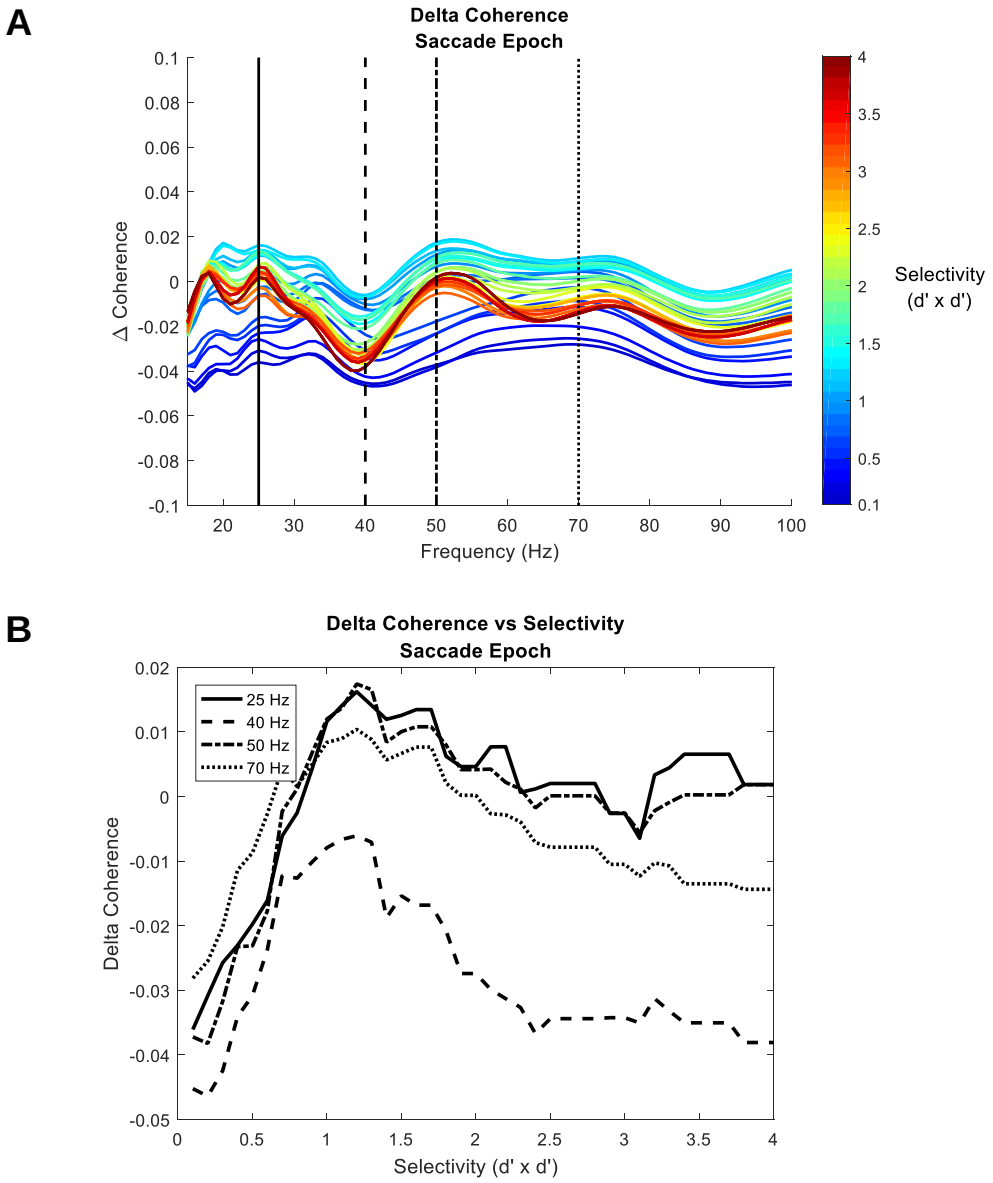

Figure 2-21. Sacce epoch: Difference in MSC as a function of frequency.

A) Shows the difference in magnitude-squared coherence (ΔMSC) averaged over the saccade epoch ([-150:150] ms after stimulus onset) as a function of frequency for different selectivity thresholds. Conventions are the same as in Fig 16. As in the visual epoch, the ΔMSC appears to depend on both frequency and selectivity. Panel **(B)** further illustrates this relationship by showing ΔMSC as a function of selectivity for 25, 40, 50, and 70 Hz. At 25, 50, and 70 Hz the relationship is very similar and the ΔMSC hovers around 0 above a d-prime product of ~0.7. At 40 Hz, however, the ΔMSC is negative at all selectivity thresholds, particularly for thresholds > 2.

2.4 Discussion

The aims of this study were two-fold: to determine whether the spatial selectivity of the MUA is also present in the LFP power and to better understand the relationship between LFP activity across frontal and parietal cortex. We addressed the first aim by determining the spatial preference between the two target locations using the magnitude of the LFP induced power and then asking whether it was congruent with the spatial preference as determined by the MUA. We found that following the onset of the visual stimulus the spatial preference of the LFP power was well correlated with the spatial preference of the MUA, particularly at parietal recording sites. During the saccadic response, however, the spatial preference of the LFP power was poorly correlated with the spatial preference of the MUA at both frontal and parietal recording sites. To address the second aim, we calculated the magnitude-squared coherence between pairs of recording sites that met the following criteria: pairs were comprised of one frontal site and one parietal site, the spatial preferences of the sites (as determined by the MUA during the visual epoch) were congruent, and the selectivity index was greater than or equal to 0.4. Under these conditions, we found that the spatial location of the stimulus/target had a significant effect on the MSC. More specifically, during trials to the preferred location the MSC was significantly lower following the stimulus response and around the onset of the saccade when compared to trials to the non-preferred location.

2.4.1 LFP Power Carries Spatial Preference of The Visual Stimulus in LIP

We found that the induced power of the LFP appeared to encode the spatial selectivity of the visual response. This is evidenced by the spatial preference as determined by the LFP power

being generally congruent with the spatial selectivity as determined by the MUA during the stimulus response. The correlations between the d-prime vales were especially prominent at parietal recording sites for all frequencies above 9 Hz. At frontal recording sites, significant correlation was only present at certain frequencies: 9-11 Hz, 13-20 Hz, 42-73 Hz, and 77 Hz and above. We were not surprised to see a strong correlation between the MUA and the LFP recorded at LIP sites following the visual stimulus. Activity in area LIP typically thought of as more of a sensory area than FEF is. Also, area LIP has anatomical inputs from many extrastriate visual areas (Blatt et al, 1990). In the standard view of visual processing, information about a visual stimulus is sent from these extrastriate areas to LIP. Our findings of a robust visual response in the LFP power is in line with the theory that LFPs are the summed synaptic input to an area. The high correlations between the MUA and LFP power also provide insight into the cortical processing of the spatial location of the visual stimulus in LIP. With the spiking activity thought of as the output of an area, the similar responses of the MUA and the LFP power, as indicated by the high correlations, suggest that there is little cortical processing with respect to the spatial location of the visual stimulus being computed locally in LIP.

We were surprised to find that the LFP power recorded at FEF sites did not robustly encode spatial selectivity. We found that the spatial preference as determined by the LFP power was not well correlated with the MUA selectivity to the visual stimulus in FEF. We expected to see a similar effect to that in LIP, where the selectivity of the LFP power was significantly correlated to the selectivity of the MUA above very low frequencies. Instead we see a multimodal response (red trace Figure 2-4), where only certain frequency bands are significantly correlated to the MUA selectivity. In previous studies that compared the spatial selectivity of the LFP evoked response to the spatial selectivity of the spiking in FEF, they found that during the MGS the spatial tuning of

the spiking and the evoked response were well aligned (Monosov et al., 2008). Additionally, there are previous studies in other cortical areas where the LFP stimulus selectivity is congruent with the stimulus selectivity of the MUA (Berens et al., 2008; Brosch et al., 2002; Jia et al., 2011; Kreiman et al., 2006; Liu & Newsome, 2006; Perel at al., 2015). One explanation of our findings is that the spatial selectivity is being computed locally at the FEF recording sites. This interpretation assumes that if the activity of the LFP activity is not reflected in the activity of the MUA, there is information processing occurring within that area. This is consistent with the view that LFP is the summed input to an area while the MUA is the summed output of that area. As in any system, non-matching input and output implies a transformation of the input data. This explanation could be further investigated by calculating the spike-field coherence. Another explanation is that the relationship between the LFP activity and the MUA is flexible. Previous studies in V1 have shown that how well the spatial tuning of the MUA matched the spatial tuning of the LFP power at gamma frequencies was dependent on the size and noisiness of the stimulus (Jia et al 2011). This explanation would suggest that for the task used in our study, the LFP power was representative of information other than the spatial location of the visual stimulus. In addition, the parameters of the task, particularly the target locations, may have contributed to the weak correlations between the LFP power selectivity and the MUA selectivity at certain frequencies. Because we used linear microelectrode arrays in both areas for this study, we attempted to place the targets such that one was in the population receptive field of the majority of the recorded neurons and the other was outside it. We require that one target was always in the upper contralateral quadrant and the other was always in the lower contralateral quadrant, with a separation of at least 90° relative to fixation. This resulted in a site's preferred target not necessarily falling at the center of that site's receptive field. One way to determine whether this is a valid

explanation, would be to repeat the task and place the targets at the center of the sites' receptive fields. As this is a daunting task with acute linear microelectrodes that could result in low number of trials for each condition, we think that any future approach would benefit from the use of a chronic array. The chronic array would provide the benefit of largely stable receptive field locations across recording sessions and high data yield.

2.4.2 LFP Induced Power Poorly Encodes the Spatial Selectivity of The Motor Response

The spatial tuning of the motor response is not well represented in the LFP power of either LIP or FEF. This is evidenced by the poor correlations of the spatial preference metric of the LFP power and the spatial preference metric of the MUA around the onset of the saccade. Despite the overall findings of poor encoding of the spatial preference, there were some instances where the two metrics of spatial selectivity were significantly, though weakly, correlated. In LIP, frequencies above 20 Hz exhibited a significant correlation but with a maximum correlation coefficient of $r = 0.37$ occurring at 99 Hz. As higher frequencies may be subject to contamination from spiking activity (Waldert et al., 2013), we also noted local maxima in the gamma and beta frequency bands. Though both significant, the maximum correlation coefficients within these frequency bands were smaller still ($r = 0.27$ at 31 Hz and $r = 0.26$ at 52 Hz). We found a significant correlation between MUA d-prime values and LFP power d-prime values at frequencies 33-57 Hz in FEF. As in LIP, the correlation coefficients, while significant, were small. The maximum correlation coefficient in FEF was $r = 0.15$ and occurred at 52 Hz. The low but significant correlations generate some interesting questions.

The first question being does the LFP power carry information about the spatial location of the upcoming saccade? One theory, mentioned above, posits that a decorrelation of the MUA and LFP activity indicates cortical processing. Following this, the weak correlations we have found suggest that around the onset of the saccade both LIP and FEF are carrying out some degree of processing related to the spatial location of the saccade target. One interpretation could be that the LFP coming into both FEF and LIP contains some information about the spatial location of the saccade target, but that it needs further refining and that this refining is carried out separately in both FEF and LIP. Support for the theory of independent computation in FEF and LIP comes from studies of attentional priority in both areas (Sapountzis et al., 2018). In a free-viewing visual search task, they found that both FEF and LIP exhibited neuronal responses to features of the target (either color or shape). Comparing the latencies of when the feature attention effects emerged, they found that, overall, FEF exhibited a shorter latency. However, when examining individual units there was a substantial portion of the LIP units that had latencies in line with those of FEF units. From this they conclude that LIP has a heterogenous neuronal population and that a subpopulation of LIP neurons compute feature attention independently of FEF influence. This could also be the case for the computation of an upcoming saccade in the MGS task.

What remains unclear is whether the magnitude of the correlation between the LFP and MUA could be indicative of the "amount" of cortical processing being carried out in a given area. One concern regarding answering this question is that LFP recordings are vulnerable to noise, which could degrade the magnitude of the correlations regardless of the degree of cortical processing being conducted in a given area.

2.4.3 MUA Is More Selective Than LFP Power for Both Visual and Saccade Responses

We also observed that the strength of the selectivity measurements, the magnitude of the d-prime values, were generally much higher in the MUA than in the LFP power. This is clearly illustrated in the scatter plots in Figures 2-5 and 2-7. The MUA d-prime values fall within the range of -7 to 3, while the LFP power d-prime do not exceed a range of -2.5 to 2 at the frequencies of interest. This observation could be explained in several ways. One explanation falls in line with the view of LFP as the synaptic input to an area. It is well established that the synaptic input to an area is comprised of spiking from many neurons in different areas. These neurons have different sized receptive fields and may also have different spatial preferences, if they exhibit spatial preferences at all. It reasonably follows that the input resulting from combining the outputs of these neurons, the LFP, would have a diminished spatial preference signal.

Another explanation is due to the parameters around the calculation of the LFP spatial selectivity. For the purposes of this investigation, we wanted to determine how well the LFP power reflected the MUA recorded at the same site. To do so, we kept the time windows used to compute the d-prime the same for both the MUA and the LFP power. The findings of Monosov et al. (2007) showed that in response to the stimulus onset of the MGS the spatial selectivity of the LFP evoked potential preceded that of the spiking recorded at the same site by an average of 9.9 ms in FEF. However, their results show the earliest displays of spatial selectivity occurring 48 ms following the onset of the visual stimulus. The time window we use to calculate the d-prime for both the LFP power and the MUA (50 to 200 ms following the stimulus onset) should encompass all but the very beginning of the earliest responses. Therefore, we do not believe that our calculation time window of choice would lead to lower magnitude d-prime values for the LFP power compared to the MUA. Another parameter that may affect the LFP power d-prime is the frequency used in the

calculation. In our analyses, we calculated a d-prime for each frequency 1 to 100 Hz in 1 Hz steps. It is expected for LFP activity at adjacent frequencies to be similar. This is one reason behind investigating LFP activity in frequency bands, rather than at particular frequencies. We opted against using frequency bands in our analyses for several reasons. One reason was to avoid obscuring interesting findings due to averaging over frequency ranges and to keep our view of the results as broad as possible. In Figure 2-4, where the correlation coefficient between the MUA d-prime and the LFP power d-prime is plotted as a function of frequency, you see that adjacent frequencies have similar correlation coefficients. This was expected and suggests that our approach of calculating d-prime in 1 Hz steps is not generating biologically irrelevant findings. It also revealed the drop in the correlation coefficient around 30 Hz in FEF, which could have been obscured if we had used typical frequency bands in our calculations. Another reason was to avoid circular results, which could arise by defining the frequency range of interest to only include frequencies where the LFP power is highest. While using 1 Hz steps in our analyses could have diminish the overall magnitude of the LFP power d-prime, we do not believe it altered the qualitative results of our analyses. Our approach also revealed interesting findings in the correlations in FEF while remaining non-circular.

2.4.4 FEF and LIP Function Independently Around Saccade Onset and at the Start of the Delay Period

In our analysis of the interaction between FEF and LIP, our findings suggest that these two areas function independently of one another during both the start of the delay period and around the onset of the saccade. The evidence for this claim comes from our magnitude-squared coherence analysis. In this analysis we found that there is significantly less coherence between the

frontoparietal site pairs during trials where the target was at the preferred location compared to trials when the target was at the nonpreferred location (Figures 2-18 & 2-19). As we increased the selectivity threshold for the pairs used in our analysis, we noticed that the effect lessened at first and then became prominent again at higher thresholds (DPP > 2). At the higher selectivity thresholds, the effect also appears to narrow in frequency and becomes concentrated within the gamma frequency range (Figure 2-21). One interpretation of these findings is that neurons in FEF and LIP are generally functioning at some baseline degree of coherence when they are not otherwise involved in cognitive processing. Then, when the neurons in these areas do become utilized for a cognitive function, they begin to operate independently, thus lowering the magnitude of the coherence between them.

This interpretation would also fit with previous findings from our laboratory, where we found negative noise coherence around the onset of the saccade between frontoparietal neuron pairs using the same inclusion criteria (Hall et al., in press). Within the larger body of literature there are both studies that support and contradict our findings. There are numerous publications that have found evidence to suggest that communication between distant brain areas is carried out using gamma frequency LFPs. Similarly, there are numerous studies that advocate for the beta band frequencies being the primary method of synchronization via LFPs.

In the camp of long-range synchronization at are studies involving saccade/reaching paradigms (Pesaran et al., 2008), covert visual attention (Gregoriou et al., 2009 & 2012), as well as the MGS (Gregoriou et al., 2012; Premereur et al., 2012). In these studies which measured the magnitude-squared coherence, their findings were that coherence was enhanced at gamma frequencies when the target/stimulus was in the neuron's RF (Fries 2005). This directly contradicts what we found, where there was less coherence at gamma frequencies during trials where the target

was in the preferred location. However, during the MGS only the LFP power was analyzed by Gregoriou et al. (2012), who found a decrease in the FEF beta band power (15-25 Hz) during trials where the saccade was directed to the RF compared to trials directed outside the RF. We see a similar phenomenon in the beta frequencies of our results. In Figure 2-17A-B, we show the average induced power of the LFP sites used in the coherence calculations. We see that the magnitude of the power spanning the high beta (as well as gamma) frequency ranges is higher for trials directed to the nonpreferred target compared to those directed to the preferred target. As mentioned previously, the magnitude of coherence is dependent on the magnitude of the power in the underlying signals. The findings of Gregoriou et al. (2012) would support our findings of decreased coherence during trials to the RF around the time of the saccade in the beta frequency range. It does not support our findings, however, of decreased power and coherence throughout the gamma frequency range. When looking at the power at gamma frequencies, they report higher power to trials to the RF compared to trials outside the RF. This would suggest higher gamma frequency coherence during trials to the RF and was found in both the covert attention task and the MGS task. It also aligns with their 2009 conclusions that gamma coherence is increased when covert attention is directed to the RF. Overall, these studies suggest that during cognitive processes gamma frequency coherence is enhanced when the target or stimulus is within the response field of the neurons.

In contrast to the findings of gamma frequency coherence enhancement during cognitive processes, Buschman and Miller (2007) report coherence enhancement during a cognitive task at 22 to 34 Hz, what is typically defined as the beta frequencies. The beta frequency enhancement was observed during a visual search task, while gamma frequency (35 to 55 Hz) enhancement was observed during a visual pop-out task. One would expect that higher cognitive load would be

required to successfully complete the visual search task compared to the visual pop-out task. Similarly, Salazar et al. (2012) found that content-specific increases of the magnitude-squared coherence between PFC and PPC during a working memory task was typically in the 12 to 22 Hz range. These studies support the theory that synchronization between distant brain areas during higher-order cognitive processing occurs at beta frequencies, rather than gamma frequencies.

The findings in our study tend to support elements of both schools of thought – that distant communication operating through gamma frequencies or beta frequencies – while adding a new insight. In our comparison of the MSC around the onset of the saccade between trials to the preferred location and trials to the nonpreferred location, we see that the differences are time and frequency dependent (Figure 2-19). Centered around the onset of the saccade we see that the coherence is significantly decreased in both the beta (< 25 Hz) and high frequency (> 60 Hz) ranges. Whereas, centered approximately 75 ms after the onset of the saccade we see a significant difference between the two conditions in the gamma range. Most of the previous analyses collapse their coherence measurements over an epoch rather than taking a time-varying measurement. This could be one reason behind the variety of conclusions in previous publications. Additionally, we find that in contrast to the previous studies, the MSC is significantly lower during trials to the preferred target location compared to trials to the nonpreferred target location. This has not been shown before that we know of, but is supported by the findings of decreased power in FEF during the MGS task when the saccade is made into the RF (Gregoriou et al 2012). This finding is also in line with the previous spike-count correlation studies from our laboratory (Hall et al., in review). Together with those findings, this suggests that during the planning and execution of a saccade FEF and LIP operate in a competitive relationship.

2.4.5 FEF and LIP Interact to Maintain Visual Stability During Saccades to the Nonpreferred Target Location

Another interpretation of our findings could be the following: during trials where the saccade is made to the nonpreferred target location, FEF and LIP interact to maintain spatial information about visual stimuli. This interpretation comes largely from Lawrence et al. (2005), in which they found movement cells in FEF that exhibited increased postsaccadic firing after saccades made opposite of the preferred direction. In our magnitude-squared coherence analysis around the onset of the saccade (Figure 2-19) we see that the coherence is lower for trials to the preferred target location compared to the nonpreferred target location and that this difference is significant largely during the postsaccadic epoch. The increased activity during saccades to the nonpreferred target could be specifically sent to LIP, rather than other downstream targets of FEF that would elicit a saccade. This feedback activity to LIP could then contribute to priority/salience mapping within LIP. This interpretation could fit into the previously presented interpretation as a theory of how FEF and LIP are interacting during trials when the target is not in the preferred location. The next step in exploring the possibility of this interpretation would be to analyze information that is typically thought to represent communication between brain areas, spike-field coherence. Finding increased coherence between FEF and LIP during saccades to the nonpreferred target compared with the preferred target, particularly within pairs where the FEF sites exhibited a purely movement response, would strengthen the validity of this interpretation.

3.0 Spike-Field Coherence

3.1 General Introduction

Spike-field coherence is a measure of shared power between a spiking time series and a local field potential time series. This measurement is a particularly useful analysis when examining interactions between brain areas. With the spiking thought of as the neural output of an area and the LFPs thought of as the summed synaptic input to an area, the spike-field coherence (SFC) can serve as means for measuring how much the output of one area influences the input to another area. How the SFC is calculated, however, is not standardized across studies in the literature. There are several methods for calculating SFC, with two prominent methods being based on multi-taper spectral analysis and spike-triggered average based analysis.

3.1.1 Multi-taper Spectral Analysis

Multi-taper spectral methods of calculating SFC have become a prominent method in the literature due to the promotion of the Chronux toolbox. Chronux is an open-source library of functions for use in MATLAB that was developed by Partha Mitra and Hemant Bokil (Mitra & Bokil, 2007). The multi-taper spectral methods that I used from this toolbox for calculating SFC are described in the following methods section. The tapers utilized by the Chronux toolbox are computed using discrete prolate spheroidal sequences, or Slepian sequences. This process derives from the problem of spectral concentration. This refers to finding a time sequence of a given length where the maximum spectral concentration is localized within the desired frequency interval. The

toolbox features a large number of customizable parameters, which can be a double-edged sword. On one hand, the user has the ability to focus on specific characteristics of his/her data. On the other hand, the wide array of customizable parameters leads to ambiguity when comparing results across studies – even those that use the same toolbox. As I will show in this chapter, small but significant findings can be gained or lost from adjusting the time-bandwidth product and the number of tapers used.

This is consistent with what you would expect from changing the number of tapers in the calculation. The motivation for using multiple tapers is to solve the issue of bias inherent in conventional Fourier analysis. In multi-taper methods, orthogonal tapers are generated to obtain multiple independent spectral estimations of the same sample. The addition of tapers smooths out the noise in the spectra, up to the "right" amount. When too many tapers are used there is an over-representation of the spectral concentration. This over-representation leads to features in the data being blurred together and spectral data that is prone to noisy fluctuations. Differences in recording equipment, electrode impedance, background noise, etc. can all have an effect on the signal to noise ratio (SNR) of data collected across laboratories and even across days within the same laboratory. These differences in the SNR can make finding the "right" number of tapers (the number that will smooth out the noise without blurring features) a process with little rigor.

Employing the use of multiple tapers, however, comes at the cost of temporal resolution. This can lead to the obfuscation of dynamic interactions between areas that occur over a short period of time. This is not a concern when the data epochs of interest are on the order of seconds. However, when using these methods to examine data epochs that are only a few hundred milliseconds in length, loss of temporal resolution can be an issue. Another issue that I will demonstrate is a transient, artifactual increases in coherence. This increase in coherence appears

to correlate to the length of the data segment used in the analysis. This may or may not be due to the nature of the multi-taper transformation, but it does highlight a previously unreported limitation with this method.

3.1.2 Spike-triggered Average Analysis

Another prominent method for calculating the SFC is based on the spike-triggered average (STA) of the LFP (Fries et al., 1997)(Fries, Roelfsema et al. 1997). The STA is the average voltage trace of the LFP centered on every instance of a spike. The intuition behind this method is that if the spikes from one area are influencing the LFP (either locally or at another area) then we might see consistent oscillations in the LFP around the onset of each spike. Calculating the STA is as simple as taking the voltage trace of the LFP, extracting a segment of some duration aligned to the onset of each spike, and taking the average of each of those segments. The calculation of the SFC is given as the power of the STA normalized by the average power of each individual LFP segment used to calculate the STA. The exact methods I used in the following analysis will be described below in Section 3.2.2.

As with the multi-taper spectral methods, there are several parameters that you could adjust when calculating the SFC using spike-triggered average methods. The first is the segment length of the LFP trace centered around each spike. A typical segment length is ±100 ms around the onset of the spike, but there is no consensus within the field. The second ambiguity with this method is how to calculate the power of both the STA and the individual LFP segments. There are a multitude of spectral transformations, including but not limited to multi-taper methods, Morlet wavelet, P-Welch, and other. Each method has its advantages and disadvantages and can be used to highlight

(or obscure) various features that might be present in the spectral data. Again, there are no standard parameters when using this method across the literature.

3.2 Methods

3.2.1 Multi-taper Spectral Methods

The first set of spike-field coherence analyses was conducted using the *coherencycpb.m* function from the Chronux toolbox. The following describes the particulars of those methods.

Data selection

The neuronal spiking and local field potential data were recorded and collected as described in Chapter 2. Data that were selected for spike-field coherence analysis was also subject to the same inclusion criteria that was utilized in the previously presented results.

Spike-field coherence with continuous LFP data and binned point-process spiking data

Once the relevant data for the epoch of interest was extracted and put into the proper form, it was input into the *coherencycypb.m* function of the Chronux toolbox. This function calculated the tapers using Slepian sequences. The number of tapers that are calculated are one of the input parameters. For this study we analyzed the results with 9 tapers and the accompanying time-bandwidth products of 5. After the tapers are calculated, the LFP data is multiplied by the tapers. The Fast Fourier Transform (built-in Matlab function) of this product is then taken and divided by the sampling frequency. This results in the spectrum, J_1, of the LFP data.

To find the spectra of the binned point-process data of the spike times, the spiking data is first multiplied by the tapers, as in the LFP analysis. The Fast Fourier Transform of this product is then taken, as above. To normalize this calculation, the mean spiking rate is found for each channel. The mean spike rate for each channel is then multiplied by the Fast Fourier Transform of the tapers. Then this product is used to normalize the spectrum, J_2, of the spiking data for each channel.

To find the SFC, the auto-spectra of the LFP, S_1, and the spiking, S_2, is calculated as shown in Eq 3-1. The cross-spectrum, S_{12}, is found in much of the same way, as shown in Eq 3-2. And finally, the SFC is calculated by normalizing the cross-spectrum by the square root of the product of the auto-spectra, as shown in Eq 3-3.

$$S_n = (J_n^* \times J_n) \quad \text{Eq. 3-1}$$

$$S_{nm} = (J_n^* \times J_m) \quad \text{Eq. 3-2}$$

$$SFC = \frac{S_{nm}}{\sqrt{S_n \times S_m}} \quad \text{Eq. 3-3}$$

The SFC was found for every pair of channels across areas. This resulted in 109 pairs with FEF spiking and LIP LFPs and 109 pairs with FEF LFP and LIP spiking. For simplicity, we refer to these descriptors of the SFC calculations as “directions”, following the presumption that spiking information is sent from one area to another.

3.2.2 Spike-triggered Average Methods

The general methods for the spike-triggered average based methods were briefly described in the introductory section. For this study, all of the analysis code for this method of calculating

the SFC was custom written in MATLAB. The specifications of this analysis are detailed below. We used the spike-triggered average methods to calculate the SFC for 109 pairs with FEF spiking and LIP LFP and 109 pairs with FEF LFP and LIP spiking.

Spike-Triggered Average

The spike-triggered average (STA) was found for each trial by first identifying the time at which each spike occurred within the epoch of interest. The epoch of interest we used was ±125 ms around the onset of the saccade. For each spike that occurred during the epoch, we extracted a segment of the LFP data. The extracted LFP segment was ±100 ms around the onset of the spike. The average of all LFP segments is the STA.

Spectral Transformation

The next component of this SFC calculation was to find the power of both the STA and the power of each of the LFP segments used to calculate the STA. We calculated the power using a Morlet wavelet transform, as described in Section 2.3.3. This resulted in separate time-varying power spectra for the STA and each of the LFP segments.

Spike-Field Coherence

Finally, the SFC was calculated by normalizing the power of the STA by the average power of the component LFP segments, as shown below in Eq 3-4.

$$SFC = \frac{S_{STA}}{\left(\frac{S_{LFP1}+\cdots S_{LFPn}}{n}\right)} \quad \text{Eq. 3-4}$$

3.2.3 Shuffle correction for inherent or evoked coherence

To correct for any inherent or evoked coherence that may appear in the raw SFC calculation, we used a shuffle correction. In the calculation of the SFC, spiking and LFP data are matched by trial. To correct for inherent coherence, we shuffled the trial order of only the LFP data. This resulted in pairs of spiking and LFP data that were not from the same trial. We then used this shuffled data to calculated the SFC. We repeated this process 1000 times to generate a pseudo-distribution of the inherent coherence. From this distribution, we could identify the 95% confidence bounds, which were then used to determine whether there was statistically significant coherence. This shuffle correction method was utilized for both Multi-Taper-based and STA-based methods of calculating SFC. Iterations of shuffled trials were within a pair of sites, within a target location, and within an analysis direction.

3.2.4 Cell Type Classification

The MUA recorded on each site was classified as either visual (V), visuomotor (VM), or motor (M). To determine the classification of a particular site we used a visuomotor index (VMI).

$$VMI = \frac{(FR_M - FR_{BM}) - (FR_V - FR_{BV})}{(FR_M - FR_{BM}) + (FR_V - FR_{BV})}$$ Eq. 3-5

Where FR_M is the firing rate during the motor epoch, -50 to 150 ms around saccade onset. FR_{BM} is the firing rate during the baseline period before the motor epoch, -450 to -350 ms before saccade onset. FR_V is the firing rate during the visual epoch, 50 to 250 ms after the target onset. And FR_{BV} is the firing rate during the baseline period preceding the visual epoch, -150 to 0 ms before target onset. Due to the convention of the index, sites were classified as visual if they had a VMI less than -0.6. Motor sites had a VMI greater than 0.6. And all remaining sites were classified as visuomotor. From the 109 pairs of sites included in the population analysis, 16 were VM-VM, 13 were M-M, 72 were VM-M. The 72 VM-M sites were composed of 64 sites with VM activity in FEF and M activity in LIP and 8 sites with M activity in FEF and VM activity in LIP.

3.3 Results

Our SFC analysis was largely incited by our findings described in Section 2.4.2 and in previous work completed in the lab (Hall et al., in review). Namely, that in both the field-field coherence and the spike-count correlation analyses between FEF and LIP we see a decrease in correlated activity around the onset of the saccade. With these two previous findings we anticipated seeing a similar decrease in SFC between the two areas. We calculated the SFC for each of the 109 pairs of sites across areas. Since MUA spiking and LFP were recorded on both sites in a pair, we have 109 pairs when analyzing either direction (FEF spiking and LIP field activity or LIP spiking and FEF field activity). We used two approaches to calculate the SFC. In the first approach,

we used multi-taper analysis (Chronux toolbox, Mitra & Bokil, 2007) to find the SFC around the onset of the saccade (± 150 ms). In the second approach, we used a spike-triggered average based method. To control for evoked activity in both approaches, we generated a pseudo-distribution of the SFC by shuffling trial pairings, as described above in Section 3.2.3.

3.3.1 Multi-taper Analysis SFC Results

To determine whether the SFC for either direction of analysis was significantly outside of the pseudo-distribution, we compared the "raw" SFC calculation with the 99% bounds of the shuffle-generated pseudo-distribution. For the population of all recorded site pairings, we only found one condition/analysis direction combination where the SFC was significantly different from the inherent or evoked coherence (as determined by the pseudo-distribution). For FEF spikes and LIP LFPs, the "raw" calculated SFC was lower than the 99% confidence bounds of the pseudo-distribution at 29-30 Hz and 71-77 Hz during trials to the nonpreferred target location. All other condition/analysis direction combinations of the SFC were within the 99% confidence bounds of the inherent or evoked coherence (Figure 3-1).

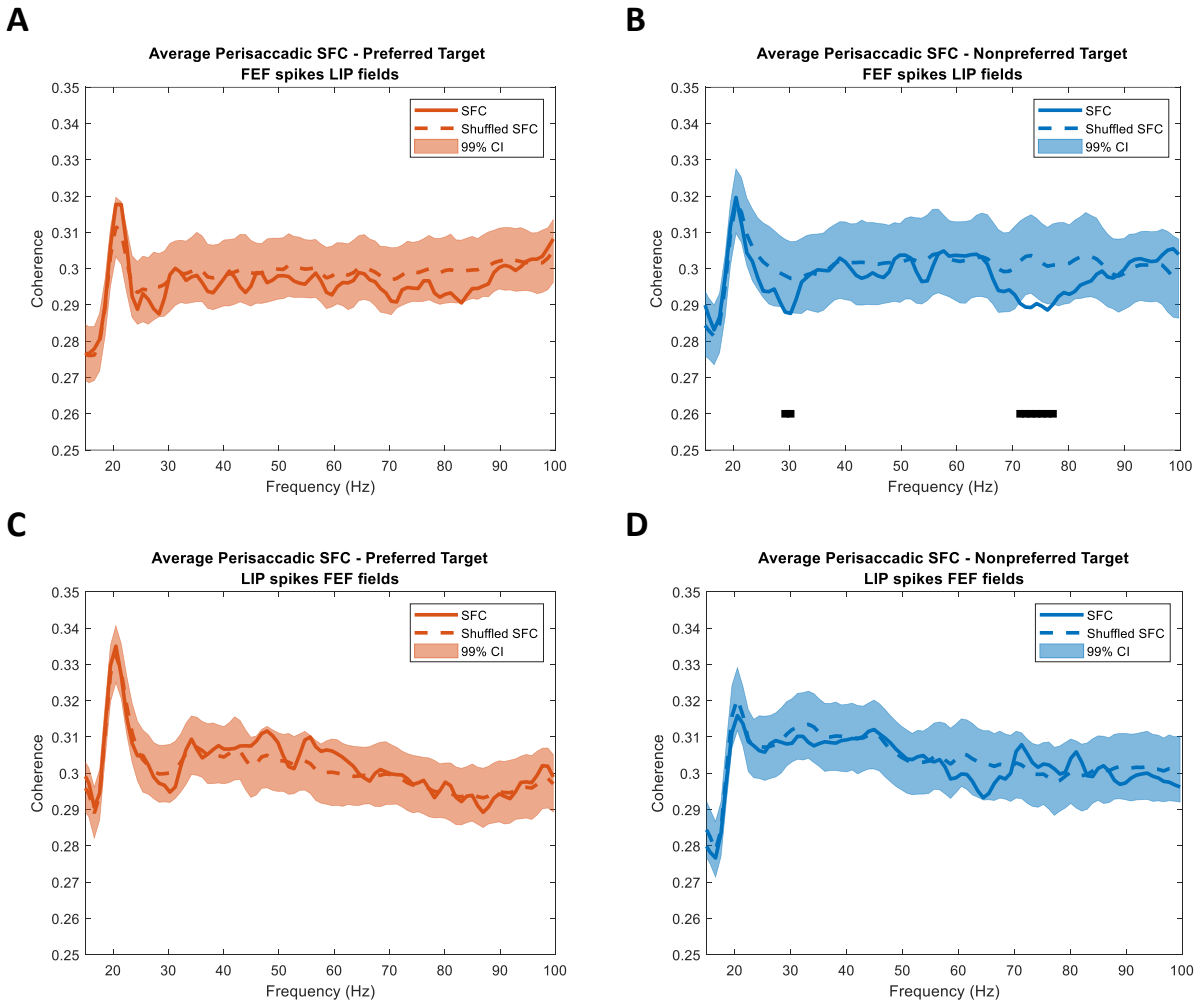

Figure 3-1. Population average perisaccadic SFC and shuffled pseudodistribution.

Average perisaccadic SFC for the population of recorded pairs. The solid lines indicate the "raw" SFC. The dashed lines indicate the average SFC of the shuffled pseudo-distributions. The shading indicates the 99th percentile bounds of the pseudo-distribution. (A) shows the SFC for trials directed to the preferred target for FEF spikes and LIP LFPs. (B) shows the trials to the nonpreferred target. We find that the "raw" SFC falls below the lower 99th percentile bounds of the pseudo-distribution at 29-30 Hz and 71-77 Hz. (C) and (D) show the corresponding results for LIP spikes and FEF LFPs.

Despite the lack of significant SFC to either target location, we wanted to investigate whether there was a difference in SFC between the two target locations. We subtracted the mean of the pseudo-distribution from the "raw" SFC calculation and then compared this shuffle-corrected SFC for saccades made to the preferred target to the shuffle-corrected SFC for saccades made to the nonpreferred target (Figure 3-2). We found that there was a significant difference between the preferred target and nonpreferred target locations between FEF spikes and LIP LFPs at 21-22 Hz and 72 Hz (Figure 3-2A; Wilcoxon rank-sum, $p < 0.05$). These results differed from our field-field magnitude-squared coherence results in two ways. The range of frequencies at which there was a significant difference in the population SFC was much more limited than in the population MSC. Also, at these frequencies the SFC was higher when the saccade was made to the preferred target. Given these differences and the relatively narrow range of frequencies where the difference was significant, we still questioned what these results meant.

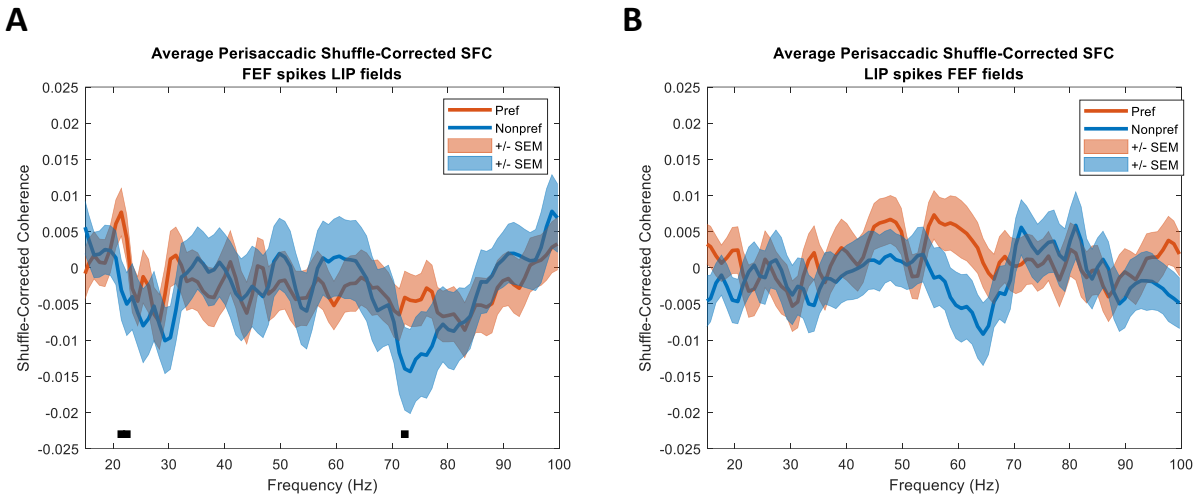

Figure 3-2. Population average SFC: Shuffle-Corrected.

Average spike-field coherence across areas around onset of the saccade (+/-150 ms). (A) SFC between FEF spikes and LIP LFPs was significantly higher during saccades towards the preferred target at 21-22Hz & 72Hz. (B) SFC between LIP spikes and FEF LFPs showed no difference across target locations. Orange trace represents trials when the target appeared at the preferred location. Blue trace represents trials when the target appeared at the non-preferred location. Shading indicates +/- SEM. Black lines indicate frequencies at which the coherence was significantly higher for the preferred target compared to the nonpreferred target (Wilcoxon rank sum test, $p < 0.05$).

We first wanted to see if the SFC within a target location and analysis direction was significant on its own. To do this we compared the calculation of SFC for each pair of recording sites to its respective shuffled distribution. Out of the 109 pairs analyzed, we found several instances where the "raw" SFC fell outside the 99th percentile bounds of that pair's individual pseudo-distribution. With the exception of one pair (pair 62), the deviations of the SFC outside of the 99th percentile bounds tended to be small. Across these individual pairs, the deviations outside the 99th percentile bounds did not occur at consistent frequencies for any combination of trial condition and analysis direction. Additionally, the range of continuous frequencies that fell outside the 99th percentile bounds was typically small, save for pair 62. These instances are summarized in Table 3.1.

Table 3-1. Multi-taper: Summary of individual pairs with significant SFC.

		FEF spikes LIP LFPs		**LIP spikes FEF LFPs**	
Target location		Pref.	Nonpref.	Pref.	Nonpref.
Number of pairs		32	26	41	31
Above upper bound:	Mean	0.0165 Omitting pair 62: 0.0081	0.0138	0.0124	0.0118
	Stdv.	0.0206 Omitting pair 62: 0.0062	0.0111	0.0099	0.0079
Below lower bound:	Mean	-0.0082	-0.0100	-0.0077	-0.0083
	Stdv.	0.0057	0.0083	0.0065	0.0084

As mentioned above, we did find one pair of recording sites (pair 62) with what appears to be a meaningful divergence outside of the 99th percentile bounds. Between FEF spikes and LIP LFPs, this pair shows an increase in SFC from 32-35, 38-47, 49-53, and 90 Hz during trials when the saccade is directed to the preferred target location. Particularly at 38-47 Hz we see a large deviation from the upper bounds of the shuffled pseudo-distribution. The shuffle-corrected SFC and corresponding bounds of the pseudo-distribution are illustrated below in Figure 3-3.

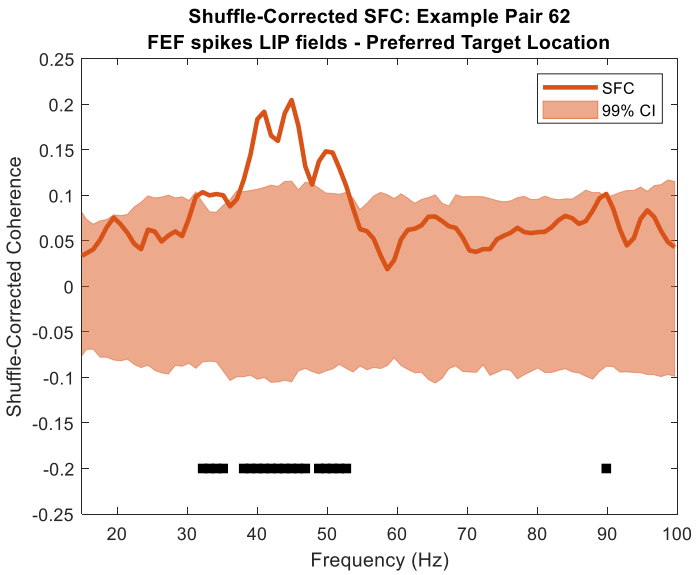

Figure 3-3. Multi-taper example pair with significant SFC.

Shuffle-corrected SFC (solid line) of pair 62 compared to the 99th percentile bounds of its pseudo-distribution (shading). At frequencies 32-35, 38-47, 49-53, and 90 Hz the SFC is above the upper bounds (black line) with an average deviation of 0.0394. SFC is between FEF spikes and LIP LFPs during trials to the preferred target location.

The frequency range that exhibits a large increase in SFC for pair 62 falls within the same range of frequencies where we see a significant decrease in coherence between target locations in the MSC analysis of the LFPs. Despite this one example, there are several factors that have led us

to believe that the SFC results, overall, are not biologically meaningful. First, the overall population of analyzed recording sites do not appear to exhibit any meaningful SFC outside of the pseudo-distribution for any combination of conditions of analysis directions. Another reason is that, even within the subpopulation of individual recording sites with significant SFC, we do not see a correlation between the frequencies at which the subpopulation's SFC and the population's SFC fall outside their respective shuffled distributions. Lastly, out of the subpopulation of individual pairs with significant SFC, only one pair exhibited a large deviation from its pseudo-distribution. The smaller deviations of the other pairs could very likely be explained by either chance, noisy signal, or both. Overall, we cannot make predictions as to the relevance of SFC at the level of the individual pairs of recording sites from this analysis.

3.3.2 Multi-taper Cell Type Specific SFC

Following the analysis on the full dataset, we asked whether there would be significant SFC between different combinations of cell types. In both FEF and LIP, previous studies have identified cells with different functional responses (Colby et al., 1996; Bruce & Goldberg, 1985). Though the activity responses are more likely to exist on a spectrum, the cell types are typically defined as visual (V), visuomotor (VM), and motor (M). We used these three cell types in our analysis, categorizing the MUA as described in Section 3.2.4. As mentioned above, we had a total of 109 site pairs, with 16 VM-VM pairs, 13 M-M pairs, and 72 VM-M pairs. To differentiate between VM-M pairs with VM activity in FEF (64 pairs) and those with VM activity in LIP (8 pairs), we will employ a naming convention that refers to the FEF cell type first. For example, a VM-M pair with VM activity in LIP and M activity in FEF will be furthermore referred to as a M-VM pair.

We repeated the analysis presented above for each of the four cell type pairings that were present in our data. As in the population analysis, we found few small deviations of the SFC outside of the 99th percentile bounds of the shuffled pseudo-distributions for the different cell types (Supplementary Figures 4-1 to 4-4). The one exception to this was for trials to the nonpreferred target between FEF spikes and LIP LFPs (Supplementary Figure 4-2). In this condition, the SFC fell considerably below the lower 99th percentile bound of the pseudo-distribution at 66-85 Hz. This will be detailed more in Section 3.4.2. However, we wanted to repeat the comparison between shuffle-corrected SFC for both target conditions within each cell type pairing. For the VM-VM pairs, we found that the SFC between FEF spikes and LIP LFPs was significantly higher during trials to the nonpreferred target at 80-83 & 85 Hz (Figure 3-4A, Wilcoxon rank-sum, $p < 0.05$). Between LIP spikes and FEF LFPs, we found that the SFC was significantly higher during trials to the preferred target. This difference occurred at 64-65 & 67-68 Hz (Figure 3-4B).

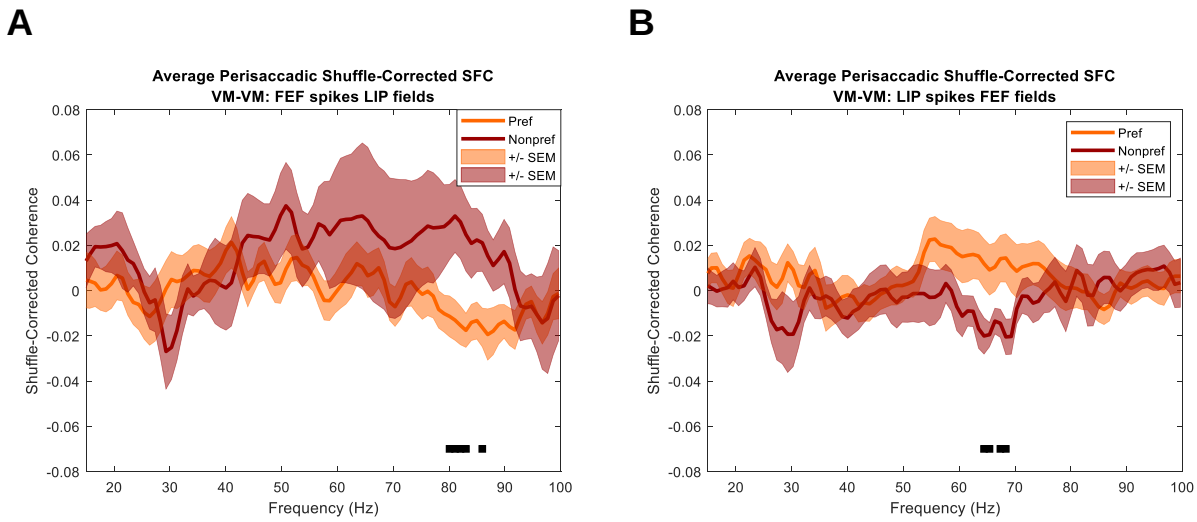

Figure 3-4. VM-VM Pairs: Average Shuffle-Corrected SFC

Shuffle-corrected SFC for all VM-VM pairs (n=16) for trials directed to the preferred target (orange) and trials directed to the nonpreferred target (red). (A) SFC between FEF spikes and LIP LFPs was significantly higher during saccades towards the nonpreferred target at 80-83Hz & 85Hz. (B) SFC between LIP spikes and FEF LFPs was significantly higher during saccades towards the preferred target at 64-65Hz & 67-68Hz. Shading indicates +/- SEM. Black lines indicate frequencies at which the coherence was significantly different between the preferred target and the nonpreferred target (Wilcoxon rank sum test, $p < 0.05$).

For the VM-M pairs, we found that the SFC between FEF spikes and LIP LFPs the trials to the preferred target location was significantly higher at 21-22 Hz and 72-77 Hz (Figure 3-5). Comparing the higher significant frequencies to those of the VM-VM pairs, we notice a difference in the range of significant frequencies as well as the trials that exhibit the higher SFC. For the SFC between LIP spikes and FEF LFPs in VM-M pairs, we only see a significant difference at 97 Hz, with the trials to the preferred target exhibiting higher SFC. Compared to the VM-VM pairs, the significant differences between the two conditions occur at different frequencies, but both show the SFC as higher for the preferred target location.

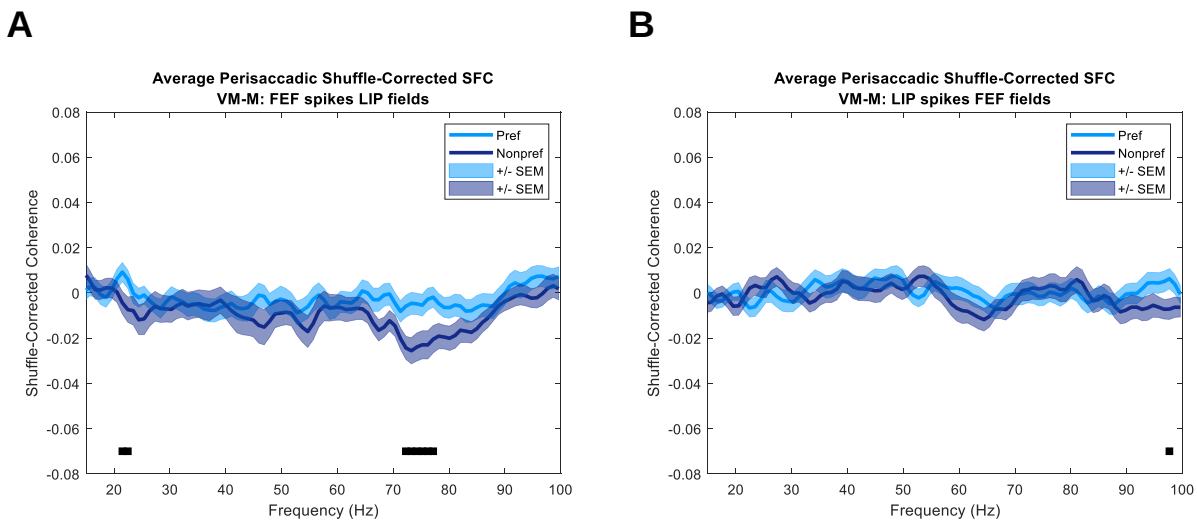

Figure 3-5. VM-M Pairs: Average Shuffle-Corrected SFC

Shuffle-corrected SFC for all VM-M pairs (n=64) for trials directed to the preferred target (light blue) and trials directed to the nonpreferred target (dark blue). (A) SFC between FEF spikes and LIP LFPs was significantly higher during saccades towards the preferred target at 21-22Hz & 72-77Hz. (B) SFC between LIP spikes and FEF LFPs was significantly higher for saccades towards the preferred target at 97Hz. Other conventions the same as Fig 3-4.

Looking at M-VM pairs, we again see little in common with either the VM-VM or VM-M pairs. Between the FEF spikes and LIP LFPs, we see that the SFC is significantly higher for trials to the preferred target at 21 Hz but significantly higher for the nonpreferred target from 59-60 Hz (Figure 3-6). And between the LIP spikes and FEF LFPs, the SFC is significantly higher for trials to the nonpreferred target at 59-60 & 71-74 Hz.

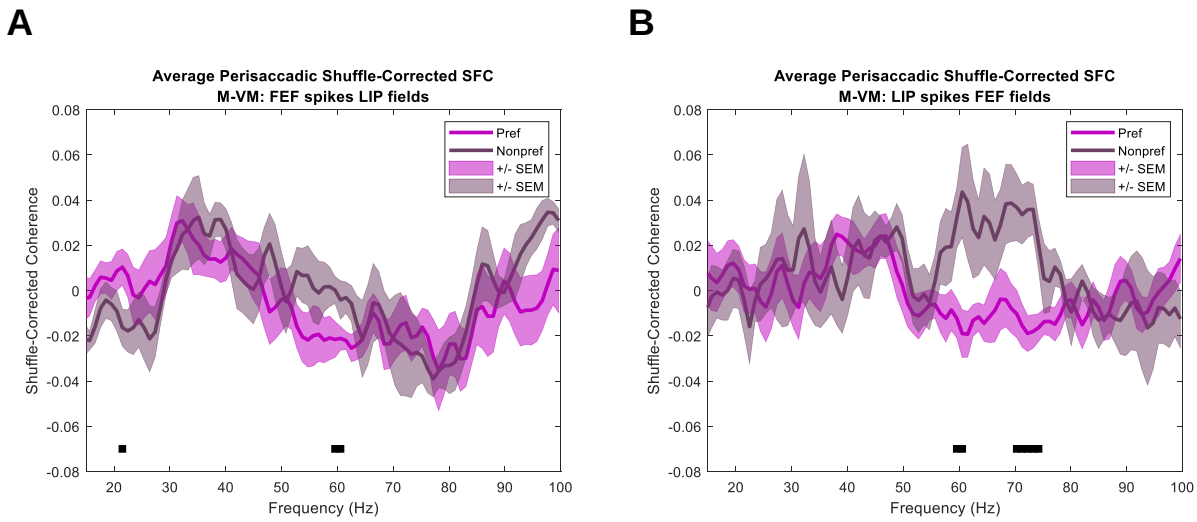

Figure 3-6. M-VM Pairs: Average Shuffle-Corrected SFC

Shuffle-corrected SFC for all M-VM pairs (n=8) for trials directed to the preferred target (light purple) and trials directed to the nonpreferred target (dark purple). (A) SFC between FEF spikes and LIP LFPs was significantly higher during saccades towards the preferred target at 21Hz and towards the nonpreferred target at 59-60Hz. (B) SFC between LIP spikes and FEF LFPs was significantly higher for the nonpreferred target at 59-60Hz & 71-74Hz. Other conventions the same as Fig 3-4.

Lastly, for the M-M pairs we found no significant differences in SFC between trials to the preferred target and trials to the nonpreferred target in either analysis direction. This is illustrated in Figure 3-7.

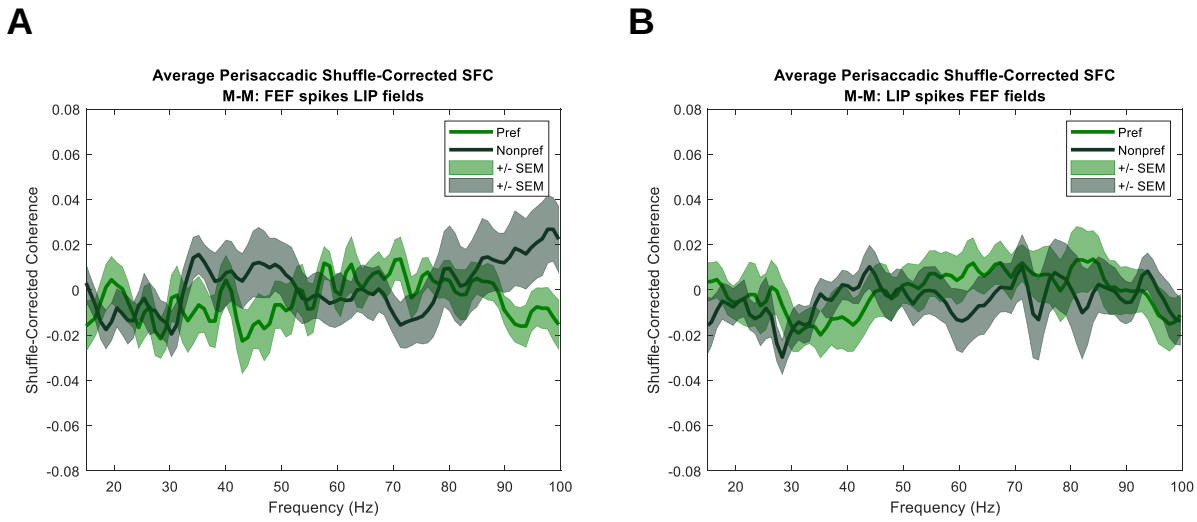

Figure 3-7. M-M Pairs: Average Shuffle-Corrected SFC

Shuffle-corrected SFC for all M-M pairs (n=13) for trials directed to the preferred target (light green) and trials directed to the nonpreferred target (dark green). We found that there were no significant differences between the SFC during the preferred and nonpreferred conditions between FEF spikes and LIP LFPs (A) or between LIP spikes and FEF LFPs (B). Other conventions the same as Fig 3-4.

Overall, the cell-type SFC analysis findings (summarized in Table 3-2) suggest that there could be a meaningful difference between trial conditions in the VM-M pairs, specifically between FEF spikes and LIP LFPs. The range of frequencies exhibiting significantly higher SFC during trials to the preferred target was relatively large (72 – 77 Hz) and continuous. When coupled with the comparison between the SFC and its pseudo-distributions, however, this finding is inconclusive. Though we see a significant difference in SFC between preferred and nonpreferred

target conditions during the memory-guided saccade, we do not see a significant deviation of the SFC from its shuffled pseudo-distribution. It remains unclear whether a significant difference between conditions could be biologically meaningful if there is not significantly difference from the coherence inherent to the system.

Table 3-2. Multi-taper: Summary of Cell-Type SFC Analysis

	FEF spikes LIP LFPs		**LIP spikes FEF LFPs**	
	Sig. Freqs (Hz)	**Higher Cond.**	**Sig. Freqs (Hz)**	**Higher Cond.**
VM-VM	80-83, 85	Nonpref	64-65, 67-68	Pref
VM-M	21-22, 72-77	Pref	97	Pref
M-VM	21, 59-60	Pref, Nonpref	59-60, 71-74	Nonpref
M-M	-	-	-	-

3.3.3 Spike-triggered Average SFC

We next turned to a method that was more suitable for analyzing small windows of interest, the SFC derived from the spike-triggered average. As described in Section 3.2, the spectral transformation used in this method was a Morlet Wavelet. This provided us with 1 ms temporal resolution, but did result in spectral smearing at low frequencies (< 15 Hz). Using this method, we repeated the analysis presented above in Sections 3.3.1 and 3.3.2. As in Section 3.3.1, we generated a pseudo-distribution of the inherent spike-field coherence for the population of site pairs for each trial condition and analysis direction. We compared the mean "raw" SFC to the mean SFC of each

shuffle iteration used to generate the pseudo-distribution as well as the distribution's 99th percentile bounds (Figure 3-8). We found that during trials to the preferred target location, the SFC between FEF spikes and LIP LFPs and the SFC between LIP spikes and FEF LFPs fell within their respective 99th percentile bounds for all analyzed frequencies (Figure 3-8 A, C). During trials to the nonpreferred target location, we found that the SFC between FEF spikes and LIP LFPs fell below the 99th percentile bounds of the distribution from 15-18 Hz (Figure 3-8B). Between LIP spikes and FEF LFPs the SFC fell below the 99th percentile bounds at 68-73 Hz during trials to the nonpreferred target location (Figure 3-8D).

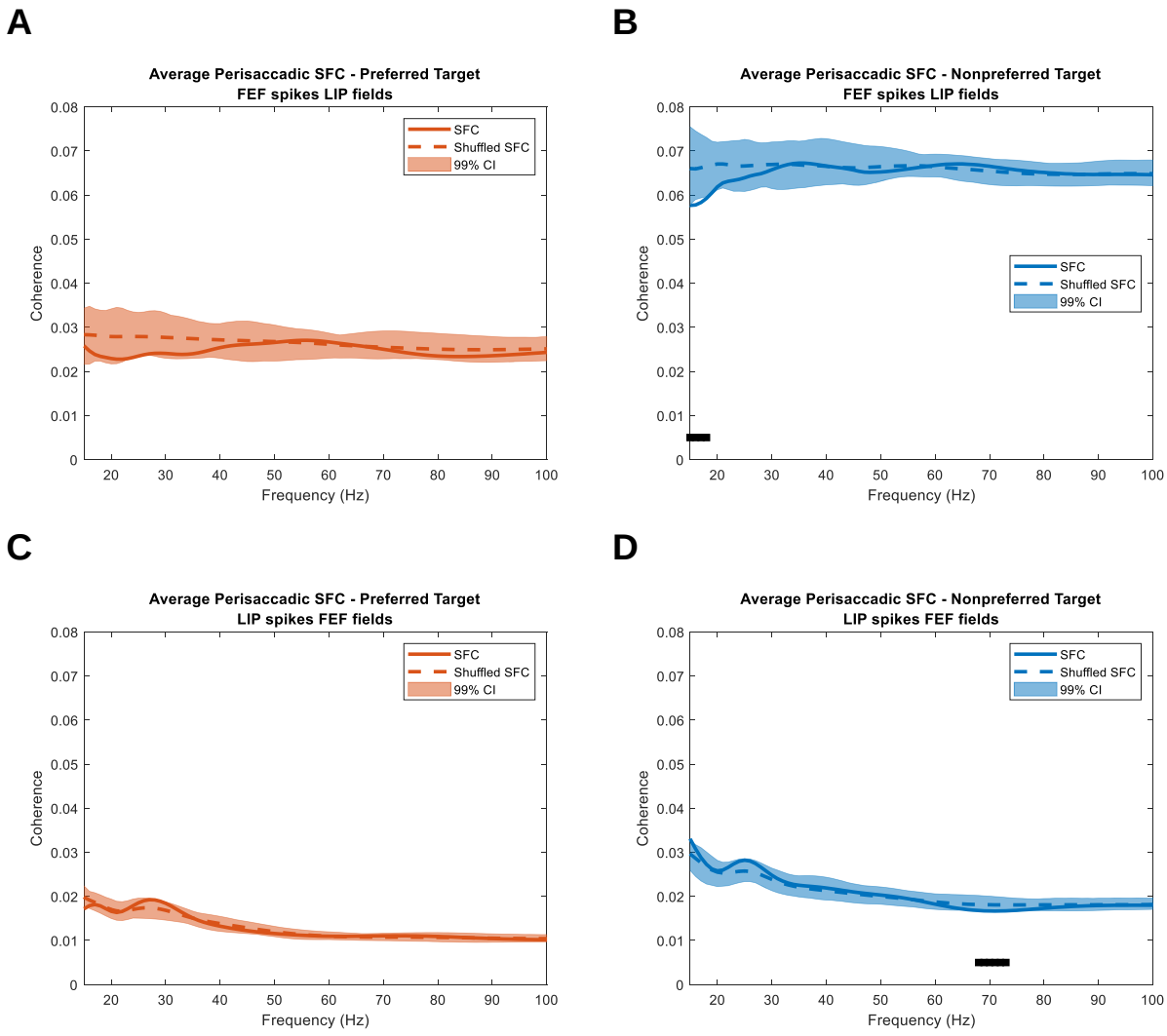

Figure 3-8. Population average perisaccadic SFC and shuffled pseudodistribution.

Average perisaccadic SFC for the population of recorded pairs calculated using the spike-triggered average methods. (A) shows the SFC for trials directed to the preferred target for FEF spikes and LIP LFPs. (B) shows the trials to the nonpreferred target. We find that the "raw" SFC falls below the lower 99th percentile bounds of the pseudo-distribution at 15-18Hz (C) and (D) show the corresponding results for LIP spikes and FEF LFPs with the "raw" SFC falling below the 99th percentile bounds of the shuffled pseudo-distribution during trials to the nonpreferred target at 68-73Hz. Conventions as in Fig 3-1.

Again, we next looked to see if there was a difference in the SFC for the different trial conditions. As in the previous analysis, we compared the SFC following a correction using the mean of the shuffled pseudo-distribution. Looking at the SFC between FEF spikes and LIP LFPs, we found that the SFC was higher during trials to the nonpreferred target at 79-80 Hz (Fig 3-9A, Wilcoxon rank-sum, $p < 0.05$). Between LIP spikes and FEF LFPs, we found that the SFC was higher during trials to the preferred target from 61-78 Hz (Fig 3-9B, Wilcoxon rank-sum, $p < 0.05$).

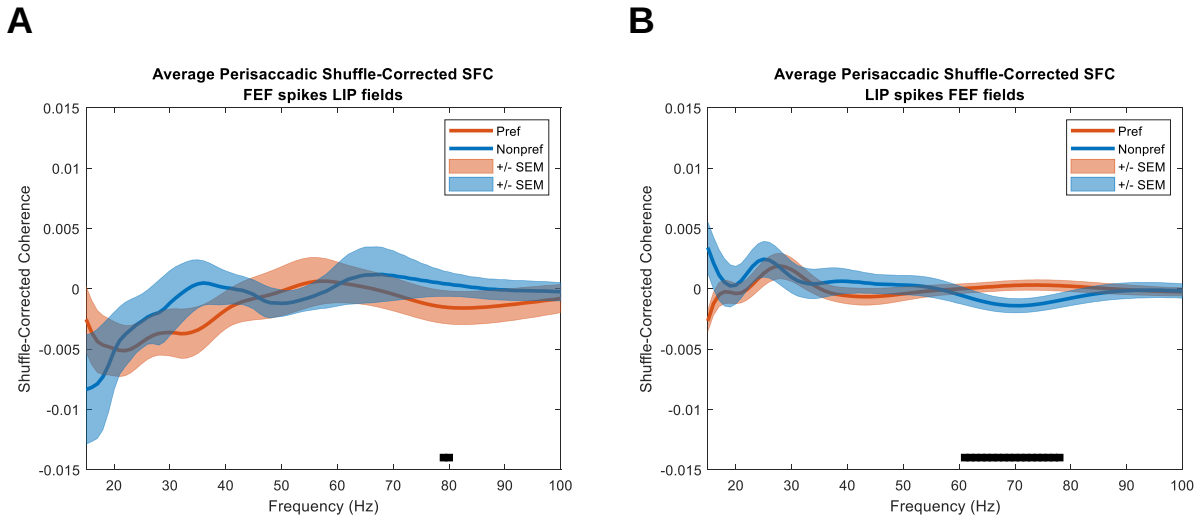

Figure 3-9. Population average SFC: Shuffle-Corrected.

Average spike-field coherence across areas around onset of the saccade (+/-100 ms) calculated using the spike-triggered average methods. (A) SFC between FEF spikes and LIP LFPs was significantly higher during saccades towards the nonpreferred target at 79-80Hz. (B) SFC between LIP spikes and FEF LFPs was significantly higher during trials to the preferred location from 61-78HZ (Wilcoxon rank sum test, $p < 0.05$). Conventions as in Fig 3-2.

We next wanted to examine whether any individual recording sites exhibited significant SFC relative to their own shuffled pseudo-distribution. As in the multi-taper analysis we found several pairs of recording sites where the "raw" SFC fell outside the 99th percentile bounds of that

pair's individual pseudo-distribution. Again, the deviations outside of the bounds tended to be very small and are summarized below in Table 3-3. Contrary to the last analysis there were a handful of pairs, rather than just one, that had relatively large deviation. These larger deviations usually indicated a greater "raw" SFC. Also, the range of continuous frequencies that fell outside the 99th percentile bounds tended to be larger than in the multi-taper methods. This is likely due to the STA-based methods using a Morlet Wavelet transform, which has less optimal spectral resolution than the multi-taper spectral transform.

Table 3-3. STA-Based: Summary of individual pairs with significant SFC.

		FEF spikes LIP LFPs		**LIP spikes FEF LFPs**	
Target location		Pref.	Nonpref.	Pref.	Nonpref.
Number of pairs		43	33	31	41
Above upper bound:	Mean	0.0097	0.0130	0.0059	0.0058
	Stdv.	0.0178	0.0187	0.0093	0.0106
Below lower bound:	Mean	-0.0018	-0.0012	-0.0009	-0.00098
	Stdv.	0.0027	0.0008	0.0009	0.0011

Interestingly, the pair that showed a significant deviation outside of its 99th percentile bound in the previous analysis methods, pair 62, also showed a significant deviation with these methods. Fig 3-10 shows the average SFC across trials with the shuffled pseudo-distribution of that pair. We found that the SFC is greater than the 99th percentile bounds of the pseudo-distribution from 24-42 Hz. While these are not exactly the same significant frequencies from the multi-taper methods (32-35, 38-47, & 49-53 Hz), the two frequency ranges do overlap quite a bit.

The finding of significant SFC for this pair using both analysis methods lends support to the idea that, at the very least, there are some sites within LIP and FEF that might utilize SFC as a means of communication during the planning/execution of a saccade.

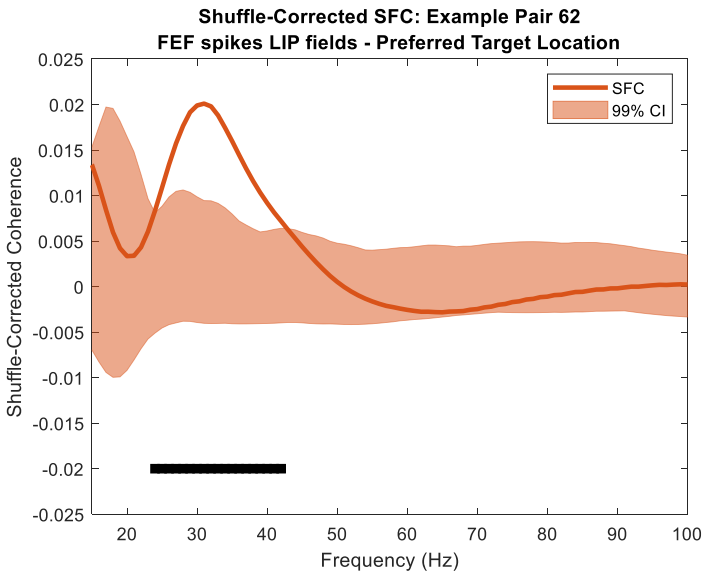

Figure 3-10. STA-based example pair with significant SFC.

SFC of pair 62 compared to the 99th percentile bounds of its pseudo-distribution, calculated using the STA-based methods. The SFC is greater than the distribution at 24-42 Hz, with an average deviation of 0.0060. SFC is between FEF spikes and LIP LFPs during trials to the preferred target location. Conventions as in Fig. 3-3.

3.3.4 STA-based Cell Type Specific SFC

Using the STA-based methods, we repeated our cell type specific SFC analysis. As in Section 3.3.2, we classified the activity at each recording site using a visuomotor index (VMI). Because the VMI is calculated using the firing rate, the VMI for each recording site was the same

as in the previous analysis. Therefore, we had the same pairs in each of the four categories: VM-VM pairs (n=16), VM-M pairs (n=64), M-VM pairs (n=8), and M-M pairs (n=13).

We first analyzed whether there was significant SFC for each of the pair types. We did this by comparing the average SFC across all pairs within a type to the 99th percentile bounds of its respective shuffled pseudo-distribution. These comparisons were made for each trial condition and analysis direction (Supplementary Figures 4-5 to 4-8). Overall, we found that there was little deviation of the mean SFC outside of the 99th percentile bounds and that those deviations were small. The one exception to this finding was for VM-VM pairs during trials to the nonpreferred target location between FEF spikes and LIP LFPs (Supplementary Figure 4-5B). Under these conditions, we found that the SFC was significantly higher than the 99th percentile bounds at 59-73 Hz. This finding suggests that if meaningful information is being carried in the SFC under these conditions that it would occur within these frequencies.

Continuing with the VM-VM pairs, we compared the shuffle-corrected SFC for trials where the target was at the preferred location to trials where the target was at the nonpreferred location. Between FEF spikes and LIP LFPs, we see that the SFC is significantly higher during trials to the nonpreferred target location at 40-47 & 49-54 Hz (Figure 3-11A, Wilcoxon rank-sum, $p < 0.05$). We notice that these is no overlap between these frequencies and those at which the average SFC for VM-VM pair to the nonpreferred target are significant. Between LIP spikes and FEF LFPs, however, we found no difference between the two target locations (Figure 3-11B). Comparing this analysis to the results of the multi-taper analysis, we find that for FEF spikes and LIP LFPs, both analyses showed that the SFC was higher during trials to the nonpreferred target, albeit at different frequency ranges.

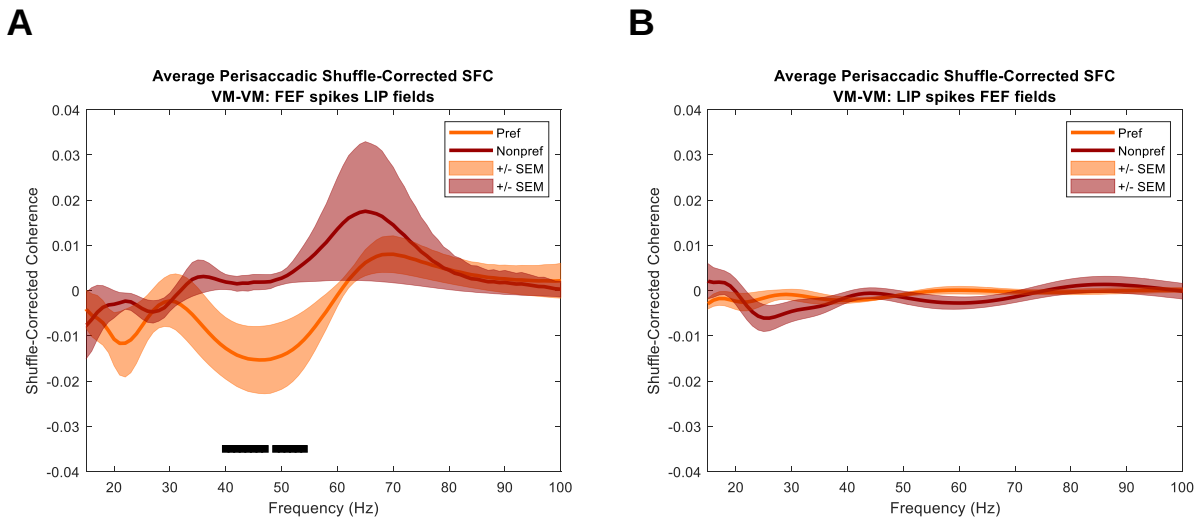

Figure 3-11. STA-Based VM-VM Pairs: Average Shuffle-Corrected SFC

Spike-triggered average methods: Shuffle-corrected SFC for all VM-VM pairs (n=16) for trials directed to the preferred target (orange) and trials directed to the nonpreferred target (red). (A) SFC between FEF spikes and LIP LFPs was significantly higher during saccades towards the nonpreferred target at 40-47Hz & 49-54Hz. (B) SFC between LIP spikes and FEF LFPs showed no significant difference across target locations (Wilcoxon rank sum test, $p < 0.05$). Conventions as in Fig 3-4.

Looking next at the VM-M pairs, the majority of pairs that we analyzed, we find that between FEF spikes and LIP LFPs the SFC is, again, significantly higher during trials to the nonpreferred target location, but at a frequency range of 73-89 Hz (Fig 3-12A). Between LIP spikes and FEF LFPs, we see a significant difference between the two conditions for this cell type pairing. From 65-72 Hz the SFC is significantly higher during trials to the preferred target location compared to trials to the nonpreferred target location (Fig 3-12B). Neither of these frequency ranges overlap with the ranges of significant frequencies for VM-VM pairs. Comparing these findings to those of the multi-taper analysis, we again see few similarities between the results. Though there is some overlap between the significant frequencies between FEF spikes and LIP LFPs, in this analysis the SFC during trials to the nonpreferred target is higher while in the multi-taper analysis the SFC during trials to the preferred target is higher. Between LIP spikes and FEF LFPs, though both analyses show the trials to the preferred target as having higher SFC, the frequencies at which this occurs do not overlap.

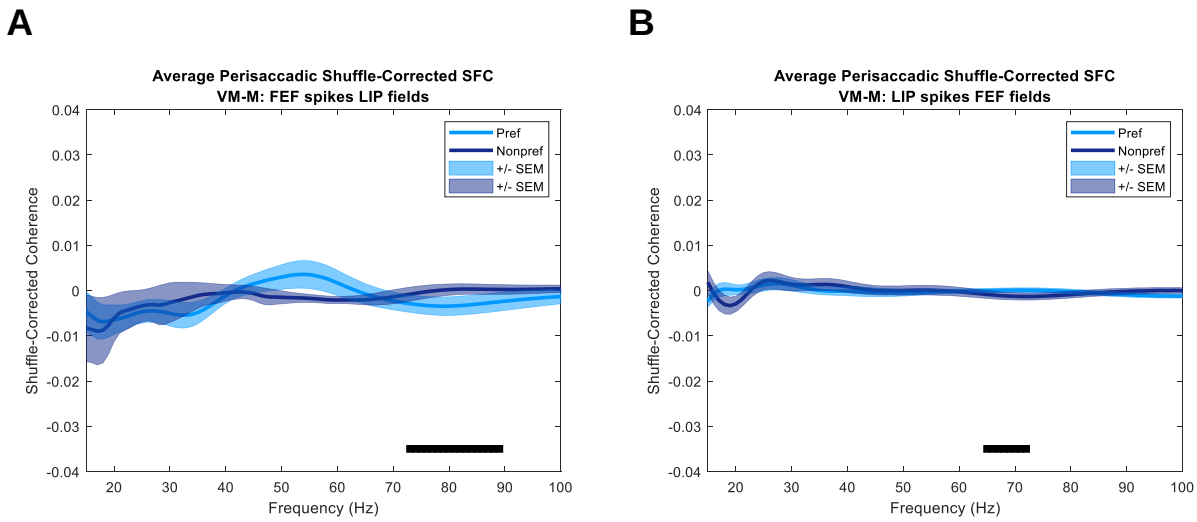

Figure 3-12. STA-Based VM-M Pairs: Average Shuffle-Corrected SFC

Spike-triggered average methods: Shuffle-corrected SFC for all VM-M pairs (n=64) for trials directed to the preferred target (light blue) and trials directed to the nonpreferred target (dark blue). (A) SFC between FEF spikes and LIP LFPs was significantly higher during saccades towards the nonpreferred target at 73-89Hz. (B) SFC between LIP spikes and FEF LFPs was significantly higher for saccades towards the preferred target at 65-72Hz (Wilcoxon rank-sum, $p < 0.05$). Other conventions the same as Fig 3-4.

We next analyzed the M-VM pairs. Between FEF spikes and LIP LFPs we found that the SFC is significantly higher during trials to the preferred target location at a frequency range of 17-23 Hz (Fig 3-13A). Between LIP spikes and FEF LFPs, we see that the significant difference between conditions falls on a much narrower range. From 22-25 Hz the SFC is significantly higher during trials to the nonpreferred target location (Fig 3-13B). Again, we see no overlap in the ranges of significant frequencies between this cell type pairing and VM-VM or VM-M pairs. As in the previous two cell type pairings, the comparison to the multi-taper analysis yields very little in common. Neither analysis direction has any common frequencies at which the SFC is different between target locations. The only similarities between the two sets of results is that between FEF spikes and LIP LFPs the low frequency results show the SFC for the preferred target location as being significantly higher and that between LIP spikes and FEF LFPs both analyses show the nonpreferred target location as having higher SFC.

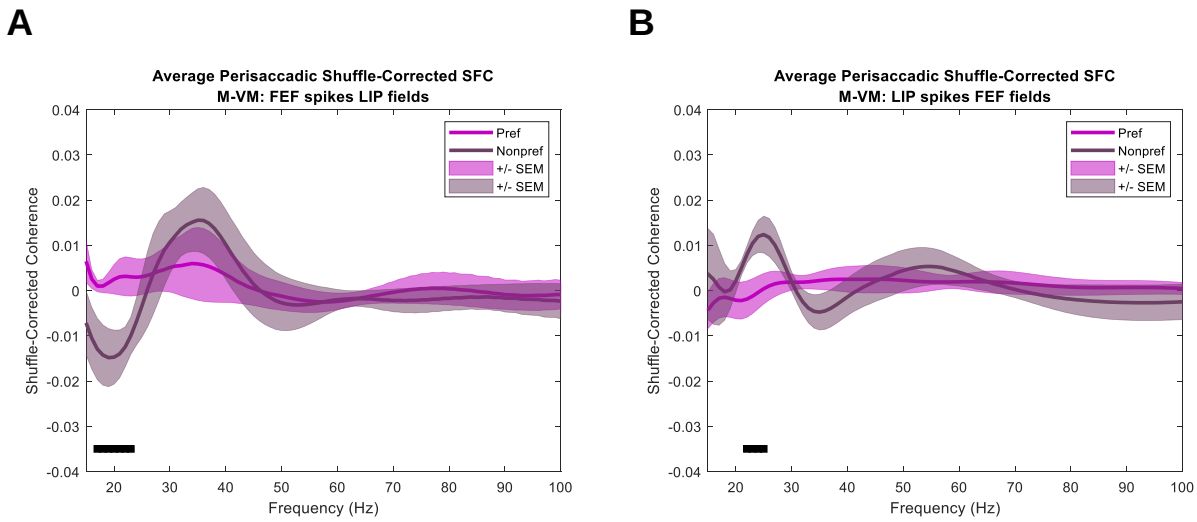

Figure 3-13. STA-Based M-VM Pairs: Average Shuffle-Corrected SFC

Spike-triggered average methods: Shuffle-corrected SFC for all M-VM pairs (n=8) for trials directed to the preferred target (light purple) and trials directed to the nonpreferred target (dark purple). (A) SFC between FEF spikes and LIP LFPs was significantly higher during saccades towards the preferred target at 17-23Hz. (B) SFC between LIP spikes and FEF LFPs was significantly higher for the nonpreferred target at 22-25Hz (Wilcoxon rank-sum, $p < 0.05$). Other conventions the same as Fig 3-4.

Lastly, we concluded our STA-based analyses by looking at the M-M pairs. Using the multi-taper methods, we found no difference between the trial conditions for either analysis direction. However, for the STA-based methods we did have some frequencies where the difference was significant for both analysis directions. Between FEF spikes and LIP LFPs, we found that the SFC was significantly higher during trials to the preferred target location at 15, 40-41 Hz; a relatively small range compared to other analyses using the STA-based methods (Fig 3-14A). Between LIP spikes and FEF LFPs we also found that the SFC was significantly greater during trials to the preferred target locations, but at 77-100 Hz (Fig 3-14B). As noted in the methods, our analysis only included frequencies up to 100 Hz, so it is possible that this continuous range of frequencies with a significant difference between conditions extends beyond what we analyzed.

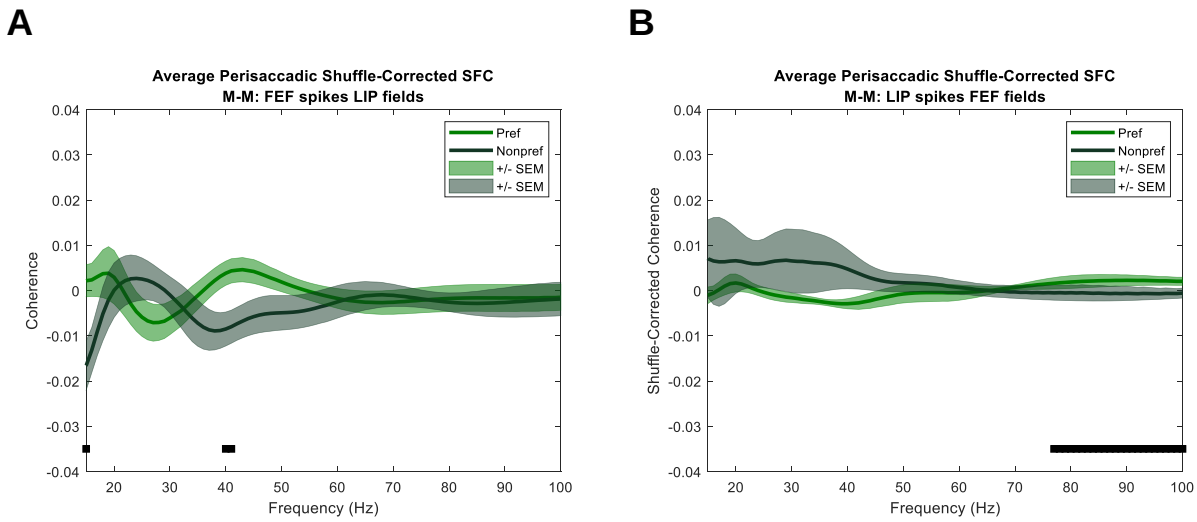

Figure 3-14. STA-Based M-M Pairs: Average Shuffle-Corrected SFC

Spike-triggered average methods: Shuffle-corrected SFC for all M-M pairs (n=13) for trials directed to the preferred target (light green) and trials directed to the nonpreferred target (dark green). (A) We found that the SFC was significantly higher during trials to the preferred target location at 15Hz & 40-41Hz between FEF spikes and LIP LFPs. (B) The SFC during trials to the preferred target was also significantly higher between LIP spikes and FEF LFPs from 77-100Hz (Wilcoxon rank-sum, $p < 0.05$). Other conventions the same as Fig 3-4.

For the STA-based SFC, the cell-type analysis findings (summarized below in Table 3-4) on their own suggest that the differences between conditions for the VM-VM, VM-M, and M-M pairings could be meaningful. However, as in the multi-taper methods cell-type analysis, just looking at the differences between trial conditions is not the whole story. When comparing the SFC to the shuffled pseudo-distributions we again see that there is little deviation outside of the 99th percentile bounds. And where we do see deviations of a larger magnitude (VM-VM pairs between FEF spikes and LIP LFPs to the nonpreferred target location), the frequencies at which there is a deviation from the pseudo-distribution are not the same frequencies where there is a difference between trial conditions. Though the SFC findings using the STA-based methods are a little more compelling than the multi-taper method findings, they still are largely inconclusive.

Table 3-4. STA-Based: Summary of Cell-Type SFC Analysis

	FEF spikes LIP LFPs		**LIP spikes FEF LFPs**	
	Sig. Freqs (Hz)	**Higher Cond.**	**Sig. Freqs (Hz)**	**Higher Cond.**
VM-VM	40-47, 49-54	Nonpref	-	-
VM-M	73-89	Nonpref	65-72	Pref
M-VM	17-23	Pref	22-25	Nonpref
M-M	15, 40-41	Pref	77-100	Pref

3.4 Discussion

The aim of this study was to study communication between FEF and LIP during a memory-guided saccade. This set of analyses centered on measuring the spike-field coherence (SFC) between the areas, which is thought to be a method of assessing direct communication. The previous section detailed the results of the SFC analysis around the onset of the saccade for both the population of recorded pairs and cell-type specific pairings. This section will present the overall conclusion from the SFC analysis and its context within the larger body of literature. In addition, we will outline some methodological concerns and considerations.

3.4.1 Communication Between FEF and LIP Is Not Widespread During a Memory-Guided Saccade.

Across both methods of analysis, the overwhelming conclusion is that there is little evidence to support widespread interaction between FEF and LIP during the planning/execution of a memory-guided saccade. This conclusion is supported by our comparison of the population average SFC and the respective shuffled pseudo-distribution (Figures 3-1 & 3-8). In both the multi-taper methods and the spike-triggered average methods we found that there was little deviation of the mean SFC outside of the 99^{th} percentile bounds of the pseudo-distribution. The deviations that we did see were typically very small in magnitude and/or did not span a wide range of frequencies. This suggests that the deviations outside of the pseudo-distribution are likely due to chance during the shuffling process and do not represent a biologically meaningful finding.

The absence of widespread interaction between FEF and LIP during the MGS is further supported by the SFC analysis we conducted on each individual pair of recording sites. As

previously detailed, we generated a shuffled pseudo-distribution using trials from each individual pair. When we compared the average SFC for each site pair to its pseudo-distribution we found several instances of the average SFC deviating outside of the 99th percentile bounds. As in the population analysis, these deviations were small in magnitude and persisted over a short frequency range. Again, indicating that these deviations were likely due to chance. There was one pair, however, that stood out across both analysis methods and exhibited significant SFC (Figs 3-3, 3-10). Though we found largely significant SFC in only 1 of 109 pairs, the pair's significant SFC across both analysis methods and the magnitude of the deviation outside of the pseudo-distribution suggests that the pair's SFC is meaningful. The presence of this individual pair does suggest that there is some degree of communication between FEF and LIP during the planning/execution of a memory-guided saccade. The communication could be limited to specific microcircuits between the two areas.

Our analysis of the cell-type specific pairing provides mixed support for our overall conclusion. With the STA-based methods we found that the SFC was significantly greater than the 99th percentile bounds at 59-73 Hz for the VM-VM pairs (Supplementary Figure 4-5B). This could indicate that the active circuits between FEF and LIP during the planning and execution of a memory-guided saccade are largely between visuomovement cells. However, this was not the case for the multi-taper methods, which found no instances of SFC being significantly greater than the pseudo-distribution for any cell type pairing or trial condition. When looking at the differences across target locations, the results become even more unclear. For both analysis methods we found significant differences between the target locations for each of the cell type pairings. However, there was little consensus in results across the analysis methods. In addition, the significant differences in the VM-VM pairs between FEF spikes and LIP LFPs did not occur at the same

frequencies at which the SFC was significantly greater than the bounds of the pseudo-distribution. As mentioned previously, one would expect that a signal conveying meaningful spatial information would occur where there is significant SFC. Consequently, though the cell-type specific SFC analysis provides some support for a limited network of communication between FEF and LIP, it does not offer evidence for a network based on specific cell types.

For the most part, our findings contradict the larger body of literature surrounding SFC studies across distant brain areas. Many of these studies have found that there is increased SFC across areas during trials with the preferred stimulus/movement (Salazar et al., 2012; Gregoriou et al., 2009 & 2012). One explanation for these results is that we corrected for inherent SFC in our analyses. Many of the previous studies mentioned do not appear to employ any methodology to correct for inherent SFC, which as this study and others (Snyder et al., 2018) have found is non-trivial. For example, if we were to compare the SFC across target locations between FEF spikes and LIP LFPs using the STA computational method without correcting for inherent SFC, we would see much higher SFC during trials to the nonpreferred target location than during trials to the preferred target location at all frequencies (Figs 3-8A&B). However, when the two SFC traces are shuffle-corrected we see that the SFC during trials to the nonpreferred target location is only significantly higher than the SFC during trials to the preferred target location at 79 & 80 Hz (Fig 3-9A). This is a considerable difference, making it evident that not accounting for the inherent SFC could have substantial effects on the conclusions of a study. Consequently, though our findings contradict much of the literature, the weight of these contradictions is questionable.

Another potential explanation for the contradictory findings is the widespread use of the Chronux toolbox for the SFC analysis in the previous studies. Over the course of our study, several concerns arose with the multi-taper methods employed by the Chronux toolbox. The two most

notable concerns we found both resulted in a transient, artifactual increase in coherence. The frequency at which this increase occurs appears to be associated with both the duration of the window of interest as well as the number of tapers used in analysis. The resultant effects are further detailed in Section 3.4.3.

3.4.2 Negative SFC?

Looking at the multi-taper methods, however, gives us a different result. Using that analysis method, we found no instances where the SFC was significantly greater than the 99th percentile bounds. Interestingly, we did find one instance where the average SFC was significantly lower than the 99th percentile bounds (Supplementary Figure 4-2B). This occurred between VM-M pairs when the saccade target was at the nonpreferred location.

This finding in and of itself raises some interesting questions. Coherence values, by definition, can only fall within the range of [0,1], thus it is impossible to have negative coherence. One assumption we've made in our analysis is that calculating the coherence of shuffled trial pairings is essentially the same as calculation the coherence between two unrelated signals, and thus should approximate noise. The expectation is that noise is incoherent. So, if noise should have a coherence value of 0, how can a measurement of SFC fall below that?

There are several explanations that we could envision. One explanation is that the seemingly negative SFC is due to noise in the recorded signals. Another explanation being that the divergence outside of the 99th percentile bounds was due to chance that is inherent to the shuffling process. And lastly, that we were wrong in our assumption that the signals recorded across different trials are unrelated. We have already provided evidence for inherent coherence between the two areas to be nontrivial. This could be indicative of a larger, global signal that is present between

FEF and LIP and exhibits a baseline level of coherence. One could imagine a scenario when coherence could fall below baseline, for example if the areas were operating independently or competitively.

3.4.3 Concerns with the Multi-taper Methods

Effect of additional tapers

As described previously, finding the optimum number of tapers to use in the multi-taper SFC analysis is typically done by trial and error. We conducted the analysis in Section 3.3.1 using four different numbers of tapers: 7, 9, 15, and 19. The results of the analysis with 9 tapers were reported in Section 3.3.1. In this section, we compare the population average SFC to the preferred and nonpreferred targets for each of the different number of tapers.

When using 7 tapers and an accompanying time-bandwidth product of 4, we found a significant difference between the SFC of FEF spikes and LIP LFPs during trials directed to the preferred target and trials directed to the preferred target at 18 Hz (Fig 3-15A; Wilcoxon rank sum, $p < 0.05$). For LIP spikes and FEF LFPs, we also found that there was a significant difference between the preferred and nonpreferred target locations at 52-53 and 94-100 Hz (Fig 3-15B; Wilcoxon rank sum, $p < 0.05$). For both analysis directions, the SFC during trials to the preferred target was higher than the SFC during trials to the nonpreferred target at all significant frequencies.

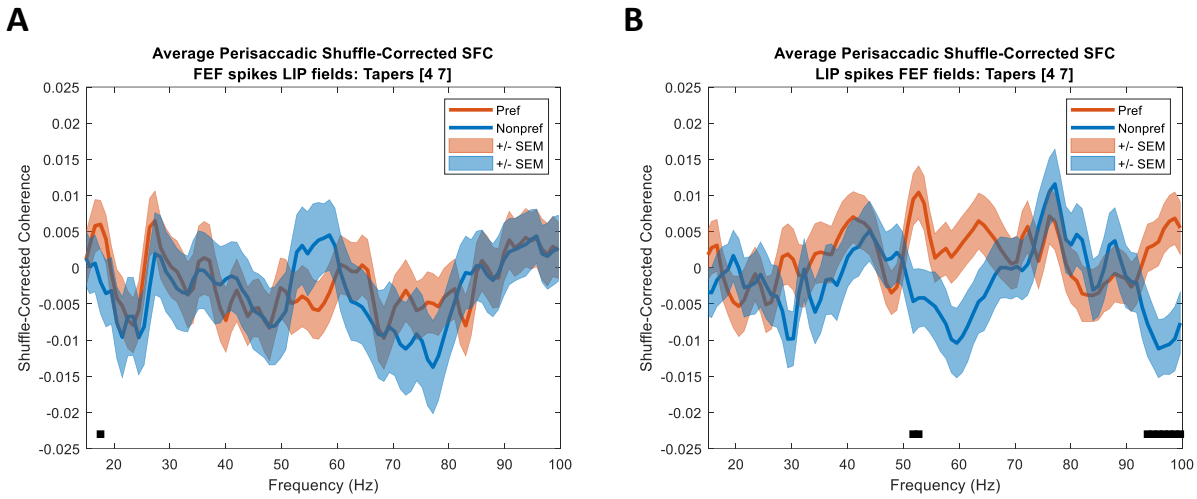

Figure 3-15. Population average perisaccadic SFC using 7 tapers.

Average spike-field coherence across areas around onset of the saccade (+/-150 ms) using 7 tapers and a time-bandwidth product of 4. (A) SFC between FEF spikes and LIP LFPs was significantly higher during saccades towards the preferred target at 18 Hz. (B) SFC between LIP spikes and FEF LFPs was significantly higher to the preferred target location at 52-53 Hz and 94-100 Hz. Conventions the same as Fig 3-2.

Our next highest number of tapers used in analysis was 9, with an accompanying time-bandwidth product of 5. These results were presented in their entirety Section 3.3.1. To restate the findings of the analogous analyses: between trials to the preferred and nonpreferred target location, we found that the SFC between FEF spikes and LIP LFPs was significantly higher during saccades towards the preferred target at 21-22Hz & 72Hz. The SFC between LIP spikes and FEF LFPs showed no difference across target locations.

We next used 15 tapers and an accompanying time-bandwidth product of 8. We found a significant difference between the SFC of FEF spikes and LIP LFPs during trials directed to the preferred target and trials directed to the preferred target. From 21-26 Hz the SFC is higher during trials directed to the nonpreferred target location (Fig 3-16A; Wilcoxon rank sum, $p < 0.05$). For

LIP spikes and FEF LFPs, we also found that there was a significant difference between the preferred and nonpreferred target locations. At 16 Hz and from 18-26 Hz we find that the SFC is greater during trials directed to the preferred target location (Fig 3-16B; Wilcoxon rank sum, $p < 0.05$).

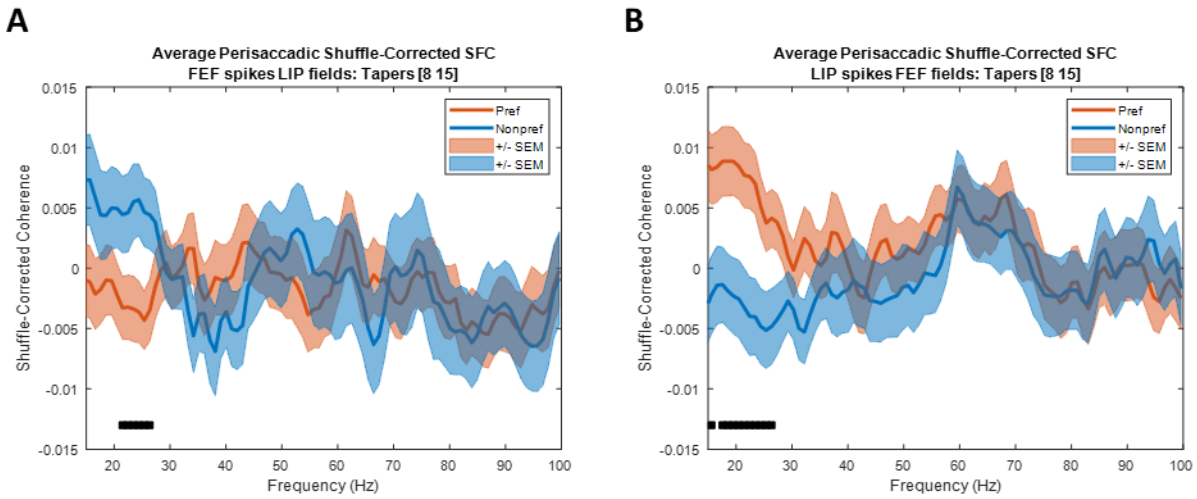

Figure 3-16. Population average perisaccadic SFC using 15 tapers.

Average spike-field coherence across areas around onset of the saccade (+/-150 ms) using 15 tapers and a time-bandwidth product of 9. (A) SFC between FEF spikes and LIP LFPs was significantly higher during saccades towards the nonpreferred target from 21-26 Hz. (B) SFC between LIP spikes and FEF LFPs was significantly higher to the preferred target location at 16 Hz and from 18-26 Hz. Conventions the same as Fig 3-2.

The greatest number of tapers we used in our analyses was 19 with an accompanying time-bandwidth product of 10. Similar to the analyses with 15 tapers, we found that the SFC was higher during trials to the nonpreferred target between the SFC of FEF spikes and LIP LFPs. The frequencies that exhibited the significant difference were 31-35 Hz (Fig 3-17A; Wilcoxon rank sum, $p < 0.05$). For LIP spikes and FEF LFPs, we also found that the SFC during trials to the

preferred target location was higher than the SFC during trials to the nonpreferred target location. This significant difference occurred at frequencies 15-23 Hz, 25-36 Hz, and 39-40 Hz (Fig 3-17B; Wilcoxon rank sum, $p < 0.05$).

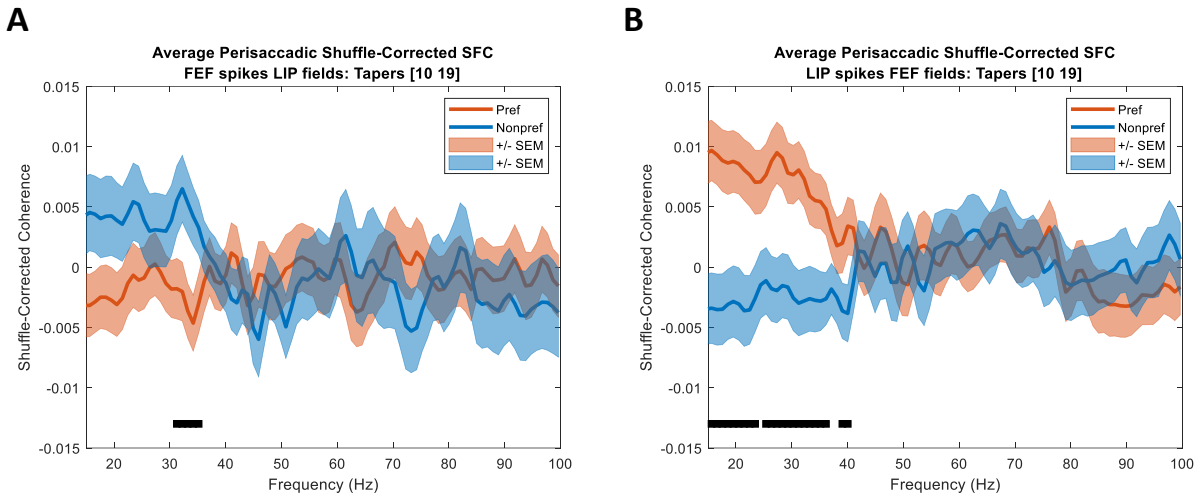

Figure 3-17. Population average perisaccadic SFC using 19 tapers.

Average spike-field coherence across areas around onset of the saccade (+/-150 ms) using 19 tapers and a time-bandwidth product of 10. (A) SFC between FEF spikes and LIP LFPs was significantly higher during saccades towards the nonpreferred target from 31-35 Hz. (B) SFC between LIP spikes and FEF LFPs was significantly higher to the preferred target location at 15-23 Hz, 25-36 Hz, and from 39-40 Hz. Conventions the same as Fig 3-2.

Overall, we find that changing the tapers affects the frequencies at which we see a significant difference between the preferred and nonpreferred target. Whatever the cause, this result is concerning, given that significant findings could be changed to fit a specific narrative by changing calculation parameters.

Artifactual coherence

Another oddity that became apparent when using the multi-taper methods to calculate SFC is an artifactual jump in coherence. The jump is seen in the non-shuffle-corrected population average SFC (Figure 3-1). We wanted to see under what parameters the artifact could be eliminated. The artifact also persisted despite changing the number of tapers used and changing the size of the analysis window. However, we noticed that changing either the number of tapers used or the size of the analysis window caused the artifact to appear at different frequencies. We used analysis windows of ±100, ±150, ± 225 ms around the onset of the saccade. 225 ms was the shortest amount of time between the saccade onset and the start of the inter-trial interval, making this the longest analysis window we could use without discarding trials on the basis of that criterion.

The previous section illustrated how changing the number of tapers can affect the findings of significant differences between trial conditions. That data presented in Figures 3-15 through 3-17 were shuffle corrected, so the artifact was effectively removed. Figure 3-18 shows the population average of the "raw" SFC along with the mean and the 99th percentile bounds of the shuffled pseudo-distribution for the four different tapers used in calculation. We only present the results for LIP spiking and FEF LFPs during trials to the preferred target location, as the artifact was most pronounced under this condition. However, the effect was seen at the same frequencies across all conditions. The full set of results for each condition can be found in Supplementary Figures 4-9 to 4-11.

We found that when we kept the duration of the time window of analysis consistent (± 150 ms around the onset of the saccade) but increased the number of tapers used in the analysis that the frequency at which the artifact appeared also increased. When 7 tapers were used the peak of

the artifact occurred at 16 Hz (Figure 3-18A). Using 9 tapers, the peak of the artifact occurred at 20 Hz (Figure 3-18B). With 15 tapers, the peak of the artifact occurred at 32 Hz (Figure 3-18C). And when using 19 tapers, the peak of the artifact occurred at 40 Hz (Figure 3-18D).

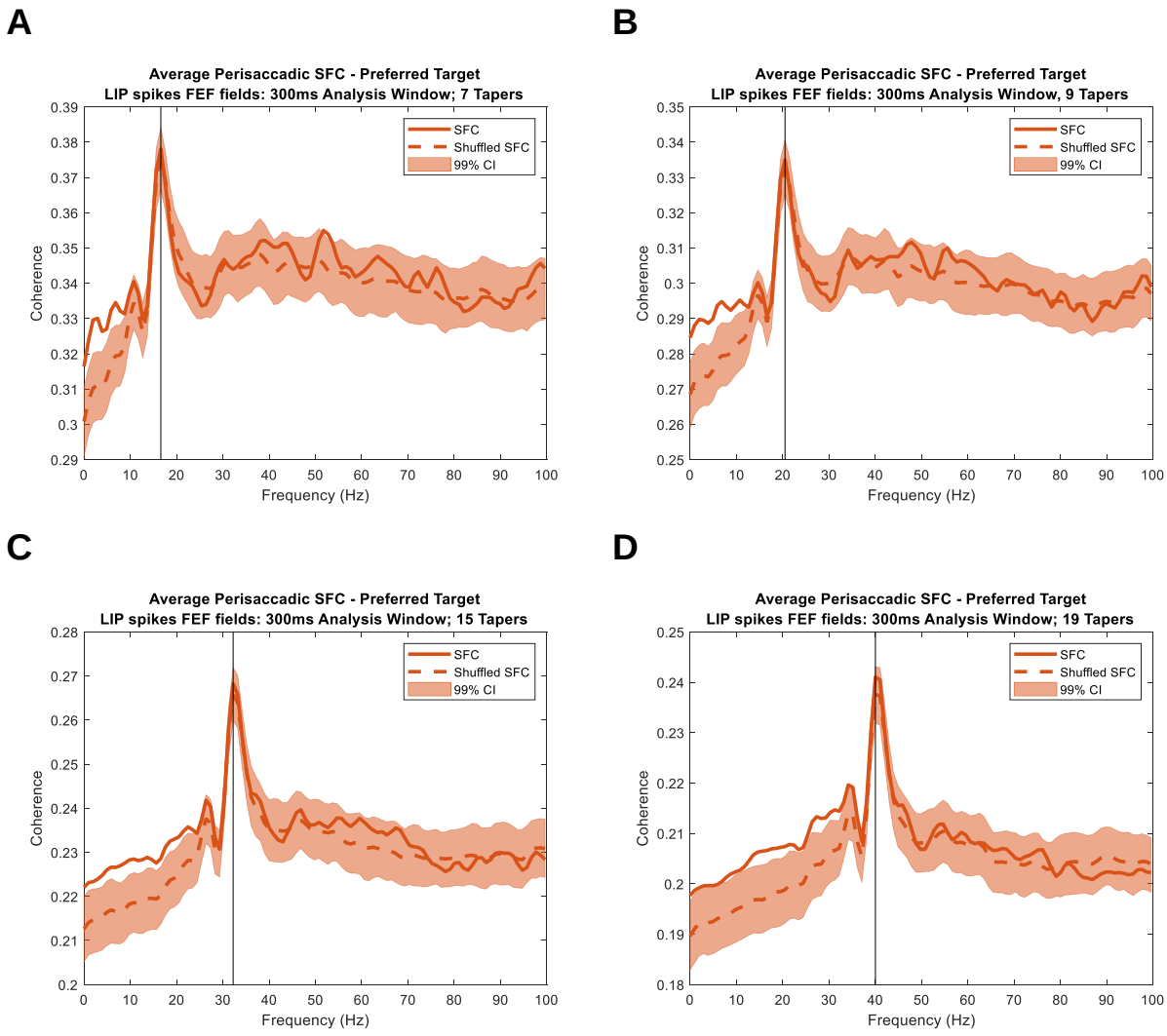

Figure 3-18. Effect of increasing tapers on frequency of artifact.

Artifact in raw SFC calculation using multi-taper methods increases in frequency as number of tapers are increased. (A) Shows the artifact occurring at 16 Hz when 7 tapers are used. (B) Shows the artifact occurring at 20 HZ when 9 tapers are used. (C) Shows the artifact at 32 Hz with 15 tapers. Lastly, (D) shows the artifact at 40 Hz with 19 tapers. All analyses used a time window of ± 150 ms around the saccade onset and show the results from the LIP spiking and FEF LFPs for the preferred target location. Conventions are the same as in Figure 3-2 with the black line indicating the frequency at which the peak of the artifact occurs.

When we held the number of tapers used consistent (with 9 tapers being used), we found that changing the size of the analysis window also changed the frequency at which the artifact occurred. Increasing the size of the analysis window appeared to correspond to a decrease in the frequency at which the artifact occurred. When using an analysis window of 200 ms (± 100 ms around saccade onset), the peak of the artifact occurred at 25 Hz (Fig 3-19A). As shown above in Figure 3-18B, an analysis window of 300 ms (± 150 ms around saccade onset) corresponded to an artifact with a peak at 20 Hz. Finally, an analysis window of 450 ms (± 225 ms around saccade onset) resulted in the peak of the artifact occurring at 12 Hz (Fig 3-19B).

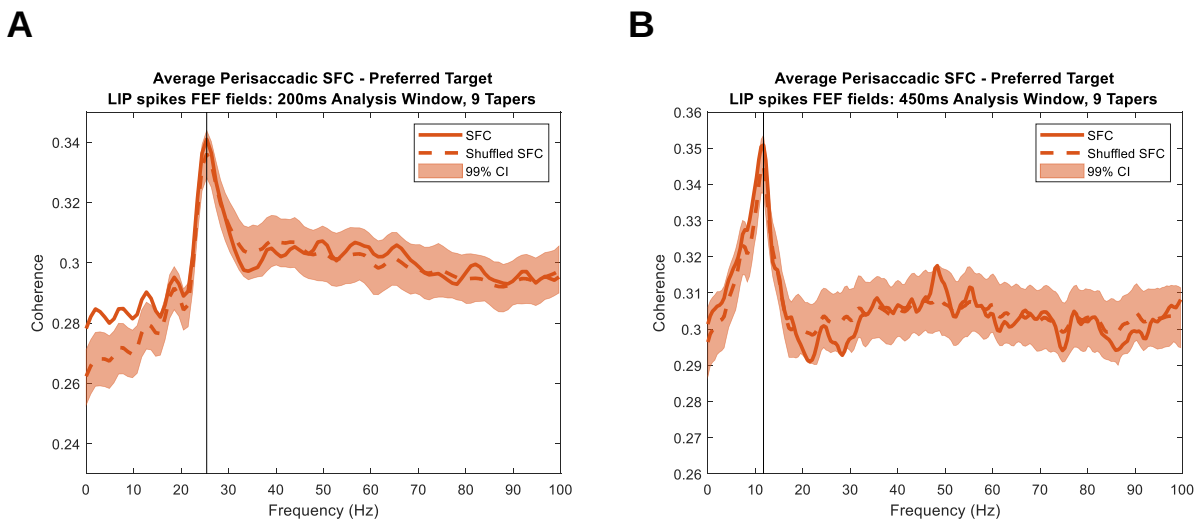

Figure 3-19. Effect of analysis window size on frequency of artifact.

Artifact in raw SFC calculation using multi-taper methods decreased in frequency as the size of the analysis window is increased. **(A)** Shows the artifact occurring at 25 Hz when a 200 ms window is used. **(B)** Shows the artifact occurring at 12 HZ when a 450 ms window is used. All analyses used 9 tapers and show the results from the LIP spiking and FEF LFPs for the preferred target location. Conventions are the same as in Fig 3-18.

Altogether, these results indicate that the artifact is in some way tied to both the number of tapers used and the length of the analysis window. We did not study this effect in enough depth to hypothesize as to the exact nature of the relationship, however there does appear to be a linear relationship based on the limited values we did test (Fig 3-20).

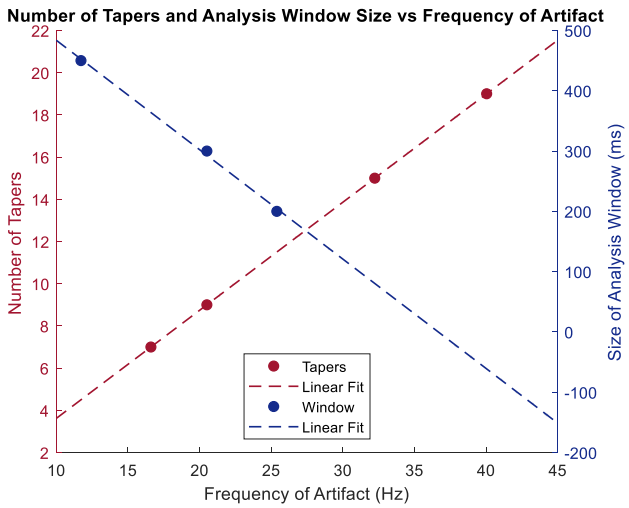

Figure 3-20. Summary of artifact findings.

The relationship between the frequency of the artifact and the number of tapers (left axis, red dots/line) as well as the size of the analysis window used (right axis, blue dots/line). There appears to be a direct relationship between increasing the number of tapers and the increase in the frequency of the artifact. While increasing the size of the analysis window appears to decrease the frequency at which the artifact occurs.

If the relationship between the analysis window and the artifact frequency holds true outside of this range, it could be possible to effectively remove the artifact with a large enough time window. The majority of studies that use the Chronux toolbox use large analysis windows, sometimes on the order of seconds. This could be the reason that this artifact has yet to be reported. It also suggests that this methodology for calculating SFC is not suitable for small time windows.

4.0 General Discussion

The overarching goal of this dissertation was to shed light on the content of information passed between distant brain areas. We specifically chose the frontal eye fields (FEF) and the lateral intraparietal area (LIP) as our areas of study for four main reasons: the dense reciprocal anatomical connections, similar functional responses, involvement in the generation/execution of saccades, and involvement in higher-order cognitive processes. Anatomical studies detail a complex, and sometimes sparse, network of connections between neurons in FEF and LIP. Previous studies that examine how FEF and LIP function, either independently or together, in the context of saccadic eye movements have reinforced that the activity within and across these areas is nuanced. Both areas have been shown to be necessary for normal execution of saccades (Dias & Segraves, 1999; Li et al., 1999). Evidence of a causal relationship between the spiking in FEF and the LFPs in LIP has been found during a visually-guided saccade, however not during a memory-guided saccade (Premereur et al., 2012). Spike-field coherence studies have also found that the interactions between FEF and LIP depend on the task. And yet a recent study suggests that in some contexts, FEF and LIP function independently but that this concurrent processing is limited to subsets of neurons (Sapountzis et al., 2018). Taken together, the current understanding of how FEF and LIP communicate information is limited to that communication being context dependent and occurring within complex networks of neurons.

In the second chapter of this dissertation, we started to address the overarching question by first examining whether spatial preference is encoded within the LFPs in both FEF and LIP. We found that the LFPs in both areas encoded the target location of the visual stimulus and that this effect was more prominent in LIP. This reinforces previous findings that LIP is the more sensory

area of the two. Another explanation for the difference in correlations between the spatial selectivity of the MUA and LFP in FEF and the spatial selectivity of the MUA and LFP in LIP could lie in the organization of the neurons within each area. Neurons in LIP tend to follow a topographical organization (Hamed et al., 2001), where the organization of neurons in FEF is less well defined. As we know, an LFP signal has a much larger cortical footprint than the activity of a single neuron. If the spatial tuning of neighboring MUA recording sites is very similar and one of those sites is well tuned with the local LFP, then it would follow that the neighboring MUA is also well tuned to its local LFP. This could result in a high correlation between the spatial selectivity of the MUA and the LFP across the population. In the case where there is a more heterogeneous population of spatial selectivity within the MUA, but the LFP still influences a relatively large cortical area, this could lead to poor correlations between the MUA and LFP selectivity on a given recording site.

Around the onset of the saccade we found that neither the LFPs of FEF nor of LIP encoded the target location. Interestingly, we found what appears to be a decrease in LFP power around the onset of the saccade when it is directed to the preferred target location. This is reminiscent of decreases in LFP power in primary motor cortex around the onset of movement (Donoghue et al., 1998). Donohue and colleagues (1998) found that LFP oscillations from 20-80 Hz increased in power during the time preceding an arm/finger movement but then ceased at the onset of the movement. The cessation in oscillations appeared to coincide with the onset of the MUA response to the reach. In this and other reaching studies with similar findings, the LFP oscillations have been interpreted as a global signal that may carry information on sensorimotor integration, movement planning, or coordination (Baker, 2007; Rubino et al., 2006). In our study, we also see weak LFP power during the saccadic eye movement. However, rather than seeing strong

oscillations leading up to the eye movement, we see strong oscillations following the offset of the saccade. These findings would not be consistent with LFP oscillations serving as a global movement planning signal, as we see them primarily after the movement has ended. However, as has been mentioned previously, the LFP signals could be used in the maintenance of a priority map. We also observe stronger LFP power when the saccade is made to the non-preferred target location than when it is made to the preferred target location. These findings might suggest that the updating of the priority map is carried out by neurons that are not involved in the planning/execution of an upcoming saccade. This theory would explain both the post-saccadic increase in LFP oscillations and the difference in power between preferred and non-preferred conditions.

As suggested by previous studies, the presence of spatial selectivity in the MUA but not in the LFPs could be indicative of cortical processing. The incongruence between the MUA selectivity and the LFP selectivity around the onset of the saccade suggests that there is cortical processing being carried out at that time. We further investigate this cortical processing around the saccade onset by calculating the magnitude-squared coherence across areas. Previous studies have found that coherence between FEF and LIP is enhanced under certain task conditions, such as during the presentation of a shared preferred stimulus (Salazar et al., 2012). We expected to find that coherence between FEF and LIP was enhanced around the onset of saccades to the shared preferred target, which could suggest that the cortical processing in FEF and LIP was coordinated. However, we found that the coherence between FEF and LIP actually decreased around the onset of a saccade to the shared preferred target. This finding implies that the relationship between FEF and LIP during the generation and execution of a saccade could be a competitive one when the saccade is in a preferred spatial location.

We dove deeper into the direct interactions between FEF and LIP during saccade generation and execution in the third chapter by calculating the spike-field coherence (SFC). SFC measures the shared power between spiking data and LFPs following the intuition that if a spike train is influencing the LFP, then the SFC will be high. When measuring the SFC between pairs of FEF and LIP recording sites we found that there was no significant SFC over the population of site pairs for any trial condition or analysis direction. Even when the population analysis was limited to combinations of particular cell types, we found no significant SFC. When looking at individual site pairs, we did find one pair that had significant SFC. Our finding of one pair with significant SFC supports the conclusion that the functional networks between FEF and LIP are complex and sparse. These findings, while contradicting much of the literature overall, are consistent with our MSC results. It supports the conclusion that FEF and LIP function independently or competitively during the generation and execution of a saccade.

This conclusion leads to the question of why FEF and LIP would be operating in a competitive role. One explanation could be that during the memory-guided saccade they function in competition for redundancy within the system. We see many instances of redundancy in the brain (for good reason). Support for this theory comes from lesion studies, where following lesions of either FEF or LIP memory-guided saccades are impaired. However, over time, the performance returns back to pre-lesion accuracy.

But why should these areas compete specifically during the memory-guided saccade? Microstimulation studies suggest that FEF and LIP are working together during a visually-guided saccade task, but not during a memory-guided saccade (Premereur et al., 2012). One reason could be that during the visually-guided saccade there is more reliance on sensory information and LIP is more of a sensory area than a motor area. Another could be tied to the invocation of working

memory. During the memory-guided saccade, working memory is employed to remember the location of the target in order to correctly saccade to it. This is not necessary in the visually-guided saccade. One way to test this theory would be to carry out these analyses during additional tasks, those that require working memory and those that do not.

One final speculation on why FEF and LIP would be functioning in a competitive relationship during the memory-guided saccade is that they are operating under push-pull dynamics. This could be conceived of as the combined output of both areas needing to reach a certain threshold in a downstream area. If activity in both areas is coordinated and firing intensely, this threshold may be reached too quickly. To prevent that, activity in either FEF or LIP might be reduced. This would result in a decorrelation of the activity across areas, which is what we see in both our previous spike-count correlation studies and in the findings presented in this dissertation.

Limitations for this study stem mainly from the experimental design. In our data collection, we recorded using an "economical" approach. That is, we positioned the target locations each day to elicit a response from as many recorded units as possible. This resulted in target locations that were within the response field of many units, but not necessarily at the center of the response field. This also could have resulted in units whose response field contained both of the target locations, which would be one explanation for why many units were either weakly or non-selective for spatial location of the targets. To map the response fields of each unit recorded on both linear arrays in order to more precisely place the targets, however, would have been a time-consuming task. This would have led to a reduced number of pairs with matching spatial preference. Additionally, more target locations would have resulted in less MGS trials being performed to any one target location during any one recording session. In order to generate a useful pseudo-distribution to correct for inherent coherence, the shuffling procedure we utilize requires, at a minimum, enough trials for

1000 unique trial combinations. With acute recording techniques, such as those used in the current experimental design, many trials suffer from movement artifact in the LFP data and thus need to be excluded from analysis. The reduction in trials to any given target location, which would result from including additional target locations, would have the most negative impact on the present study.

There are several things to consider for future studies that aim to address the question of deciphering the content of information that is passed between distant brain areas. The first would be to address the experimental design limitations detailed in the previous paragraph. One way to accomplish this would be to repeat the experiments using chronically implanted linear arrays instead of acutely implanted linear arrays. This would help reduce the movement artifacts that plague many trials. Also, the use of chronic arrays would, presumably, ensure that you are recording from the same recording sites for the duration of the study. This would allow for the collection of trials for each pair of sites across multiple recording days. Having a greatly increased number of trials for each site pair would allow for the incorporation of more target locations, particularly ones that are tailored to the RFs of the recoded neurons. A more precise measurement of RF overlap within a pair of recording sites could provide more robust population results of the communication of spatial preference across FEF and LIP. Additionally, being able to record from the same site pairs across sessions could offer an interesting insight into whether these networks between FEF and LIP change over time.

Secondly, future studies should also look at the coherence between recording sites across areas that do not share a target location preference. One explanation for the decreased coherence between sites with congruent spatial selectivity during saccades to the preferred target that we have previously mentioned is that there is a constant, baseline level of coherence between these sites

that is then disrupted around the saccade. Examining the coherence between sites with unmatched spatial selectivity could serve to further refine this theory. If the proposed baseline level of coherence is limited to sites with shared spatial selectivity, then you would expect little to no coherence between site pairs with differing spatial selectivity. However, if the coherence between FEF and LIP is global or unrelated to spatial selectivity the coherence between unmatched site pairs might be similar to the coherence between matched site pairs during saccades to the non-preferred target location. Results from analyzing these recording sites could provide valuable insight into the broader functional network between FEF and LIP.

Another consideration for future studies would be to incorporate differing levels of cognitive difficulty to the study. Several studies have found that the interactions between FEF and LIP differ across tasks that require different levels of cognitive difficulty. Some suggest that increased cognitive difficulty results in independent cortical processing within the two areas (Premereur et al., 2012). The tasks used in these studies, however, are often considerably different in ways other than just the cognitive difficulty. Therefore, it is difficult to conclude whether the differences in how FEF and LIP interact are due to cognitive load or the content of the task itself.

Additionally, future studies might want to reexamine the validity of current statistical testing methods performed in the time-frequency space. The study which we based our analysis methods on (Tallon-Baudry & Bertrand, 1999) developed the cluster-based permutation method to avoid the issue of multiple comparisons. The issue of multiple comparisons comes into play because the ultimate goal is to compare conditions, but in order to do so you must compare each time-frequency point that makes up a condition. Their multi-leveled statistical procedure alleviates that concern by ultimately comparing a “cluster statistic”, however, this method does not address the inherent indeterminacy between time and frequency. This indeterminacy essentially means that

it is possible to conclude that the conditions differ from each other (and if one condition has greater or lesser coherence) but that it is not possible to define where that difference occurs within time-frequency space. In the context of our findings, we would still be able to conclude that during a memory-guided saccade there is less coherence between recording sites when the target is in a shared, preferred location than there is when the target is in a shared, non-preferred location. However, we would not be able to confidently conclude that this difference occurs around the offset of the saccade in the gamma frequency range. Even taking this into consideration, our results imply that there is a decorrelation between FEF and LIP around the onset of a memory-guided saccade when the saccade is made to the preferred target location. However, the lack of specificity in time-frequency space muddies our conjectures of what this decorrelation could be achieving and the networks through which it may be operating. Future studies could limit their analyses to just comparing conditions in frequency (averaging over time) and/or in time (averaging over frequency/ies). This would avoid confounds between time and frequency, but would still suffer from a lack of specificity in time-frequency space. One option that could address this problem in future studies is to perform all three statistical analyses (over time, over frequency, and cluster-based) and use the results from each test to support or refute that of the cluster-based testing in time-frequency space.

Lastly, with the use of chronic linear arrays, future studies could examine the frontoparietal networks at the level of cortical layers. Due to their positioning along the banks of sulci, FEF and LIP are not ideal recording areas for laminar studies. As such, future studies could examine areas 46 and 7a, which are located on the cortical surface adjacent to FEF and LIP, respectively. Both of these areas also share many of the characteristics of FEF and LIP that drove us to target them for the research in this dissertation. By taking these three considerations into account, future

studies would be able to further connect the functional frontoparietal networks to the anatomical networks and further define the contextual bounds of spatial communication between frontal and parietal cortices.

Though taking into account all of the aforementioned considerations would result in more rigorous future studies, there remains a very fundamental question of whether coherence between LFPs should be studied. There are still many issues involved in the analysis of these signals that do not have a clear solution. One issue would be the susceptibility of LFPs to movement artifacts. This could be solved through the use of chronically implanted electrodes, but that inherently limits the number of different recording sites in your study. This also brings up the issue of extremely localized LFP signals. The spatial extent of a given LFP is unclear in many cortical areas. Therefore, using chronic implants could result in a study that compares what is functionally one LFP from frontal cortex and one LFP from parietal cortex. Another issue, which has been previously detailed, is that of using the proper statistical tests. The current approach does not address the indeterminacy between time and frequency. As a result, there is no way to observe any dynamic differences in LFP power or coherence over a time window. Since differences in power or coherence are often compared as the average frequency over a time window, this leaves findings susceptible to "p hacking" through the selection of the time window. Another step in the analysis of LFP power and coherence where "p hacking" could occur is during the selection of the spectral analysis methods. As detailed in previous sections and illustrated in the results of Chapter 3, different spectral methods can result in different statistically significant findings. Not only does the concern lie in the choice of spectral methods, but also in the choice of parameters within those methods. One solution would be for the field, as a whole, to adopt a standard way of analyzing these signals. However, this ignores that there are differences across each laboratory's recording

set up that make it necessary to use different signal processing parameters to account for things such as noise. Overall, these issues pose a serious threat to the rigor of studying LFP power and coherence. I believe that understanding these signals is essential to our understanding of how brain areas work together to generate a behavior. However, until common solutions arise for these issues and are adopted by the field as a whole, conclusions made about these signals should be looked at with very critical eyes.

Appendix A Supplementary Figures

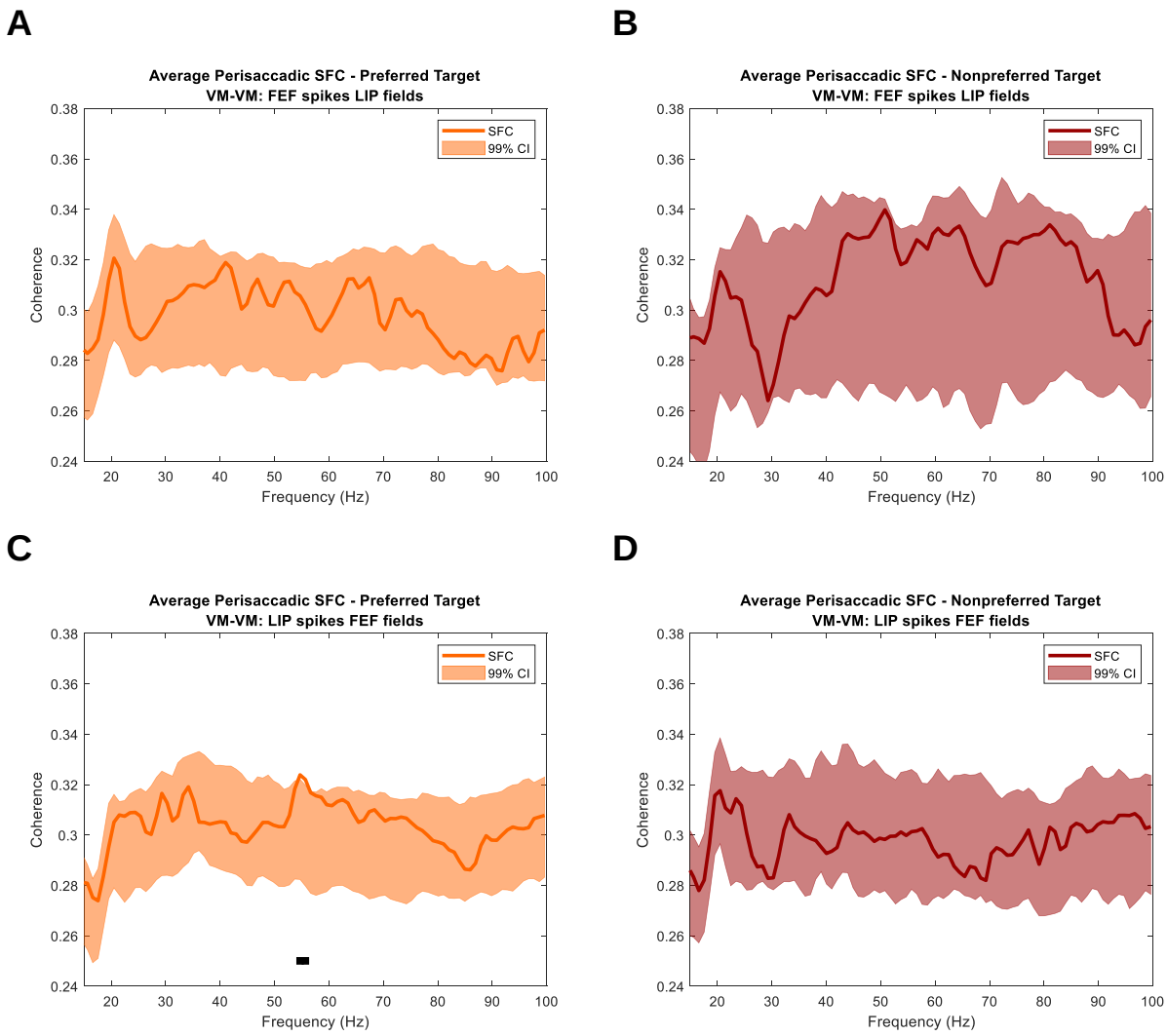

Figure 4-1. VM-VM Pairs: Average perisaccadic SFC and shuffled pseudodistribution.

Average perisaccadic SFC for the population of recorded VM-VM pairs (n=16). The solid lines indicate the "raw" SFC. The shading indicates the 99th percentile bounds of the pseudo-distribution. (A) shows the SFC for trials directed to the preferred target for FEF spikes and LIP LFPs. (B) shows the trials to the nonpreferred target. (C) shows the SFC for trials to the preferred target for LIP spikes and FEF LFPs. We find that the "raw" SFC exceeds the upper 99th percentile bounds of the pseudo-distribution at 55-56 Hz. (D) shows the trials to the nonpreferred target for LIP spikes and FEF LFPs.

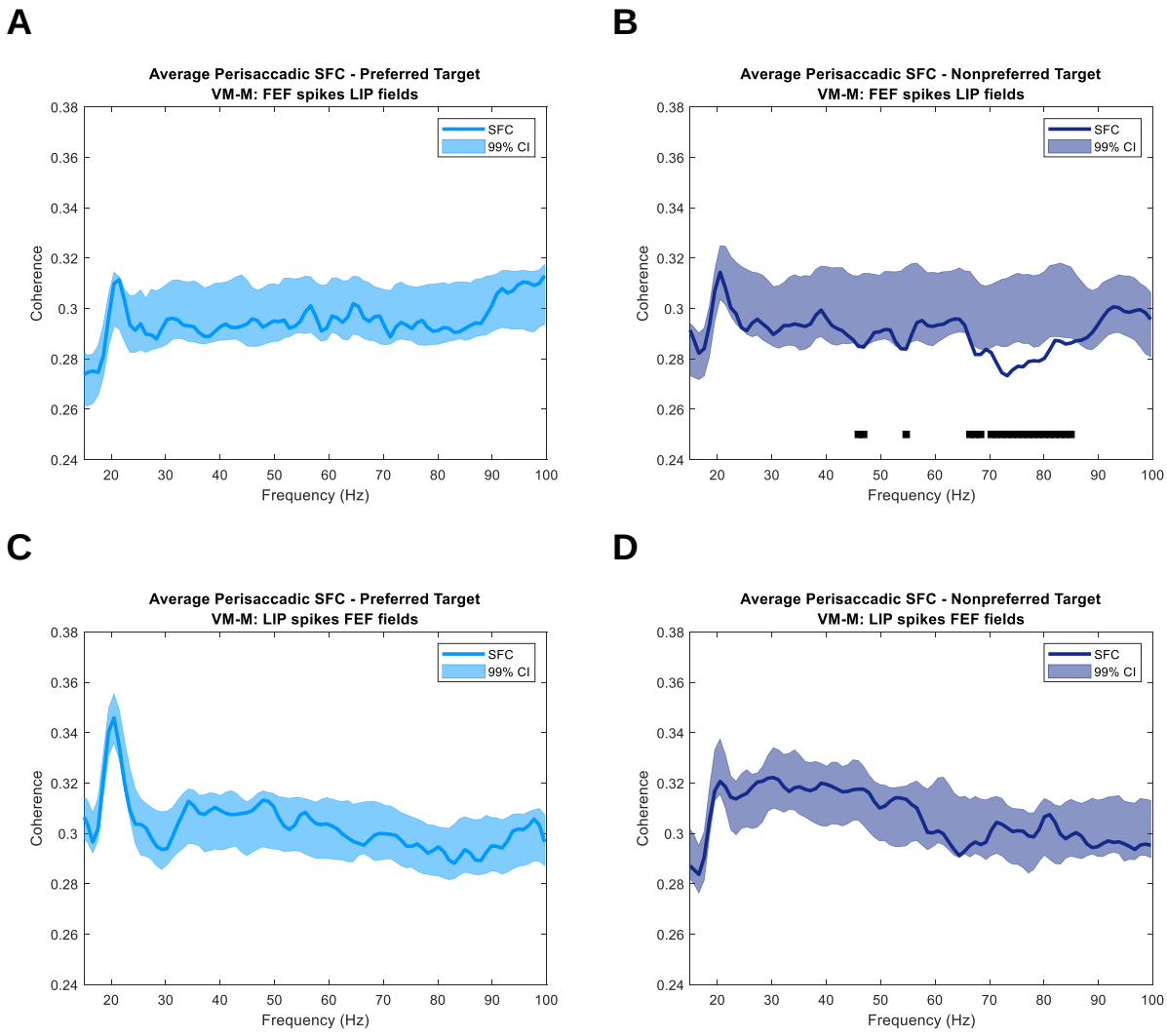

Figure 4-2. VM-M Pairs: Average perisaccadic SFC and shuffled pseudodistribution.

Average perisaccadic SFC for the population of recorded VM-M pairs (n=64). The solid lines indicate the "raw" SFC. The shading indicates the 99th percentile bounds of the pseudo-distribution. (A) shows the SFC for trials directed to the preferred target for FEF spikes and LIP LFPs. (B) shows the trials to the nonpreferred target. We find that the "raw" SFC falls below the lower 99th percentile bounds of the pseudo-distribution at 46-47 Hz, 55 Hz, and 66-85 Hz. (C) and (D) show the corresponding results for LIP spikes and FEF LFPs.

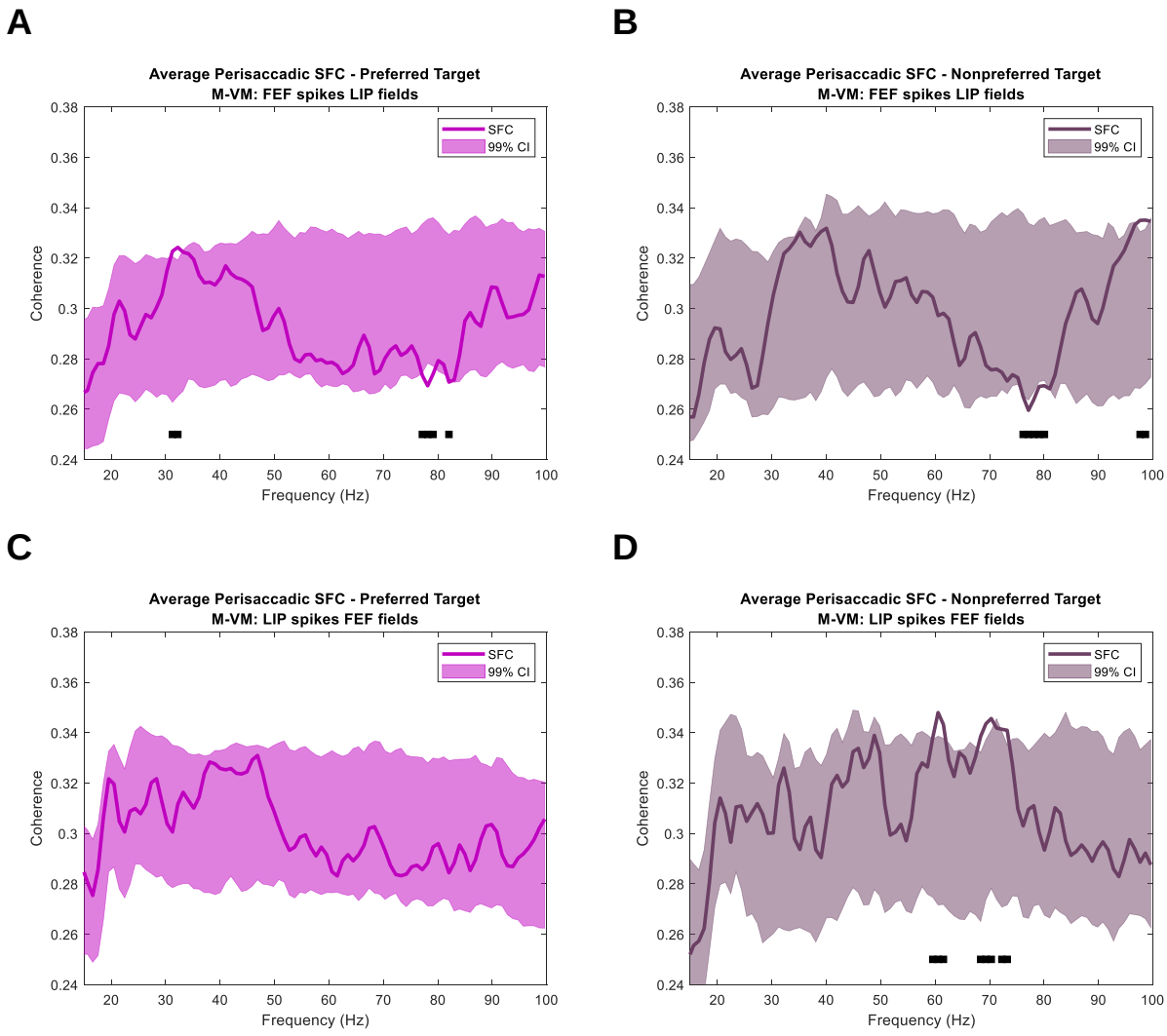

Figure 4-3. M-VM Pairs: Average perisaccadic SFC and shuffled pseudodistribution.

Average perisaccadic SFC for the population of recorded M-VM pairs (n=8). The solid lines indicate the "raw" SFC. The shading indicates the 99th percentile bounds of the pseudo-distribution. (A) shows the SFC for trials directed to the preferred target for FEF spikes and LIP LFPs. The "raw" SFC exceeds the upper 99th percentile bound at 31-32 Hz and falls below the lower bounds of the pseudo-distribution's 99th percentile at 77-79 & 82 Hz. (B) shows the trials to the nonpreferred target. The SFC exceeds the upper 99th percentile bound at 98-99 Hz and falls below the lower bounds of the pseudo-distribution's 99th percentile at 76-80 Hz. (C) shows the SFC for trials to the preferred target for LIP spikes and FEF LFPs. We find that the SFC exceeds the upper 99th percentile bounds of the pseudo-distribution at 59-61, 68-70, & 72-73 Hz. (D) shows the trials to the nonpreferred target for LIP spikes and FEF LFPs.

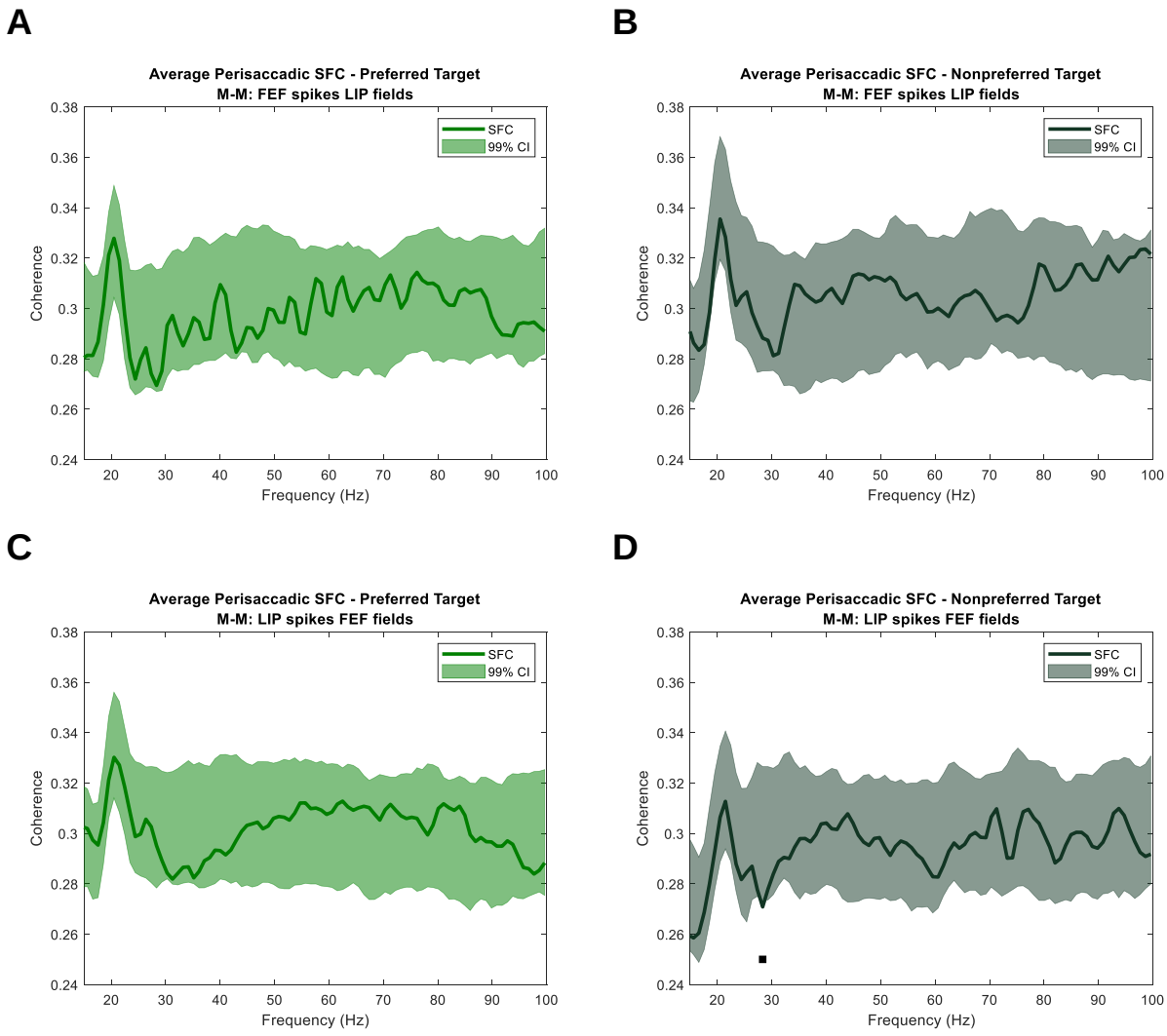

Figure 4-4. M-M Pairs: Average perisaccadic SFC and shuffled pseudodistribution.

Average perisaccadic SFC for the population of recorded M-M pairs (n=13). The solid lines indicate the "raw" SFC. The shading indicates the 99th percentile bounds of the pseudo-distribution. (A) shows the SFC for trials directed to the preferred target for FEF spikes and LIP LFPs. (B) shows the trials to the nonpreferred target. (C) shows the SFC for trials to the preferred target for LIP spikes and FEF LFPs. (D) shows the trials to the nonpreferred target for LIP spikes and FEF LFPs. In this condition we find that the SFC falls below the lower 99th percentile bounds of the pseudo-distribution at 28 Hz.

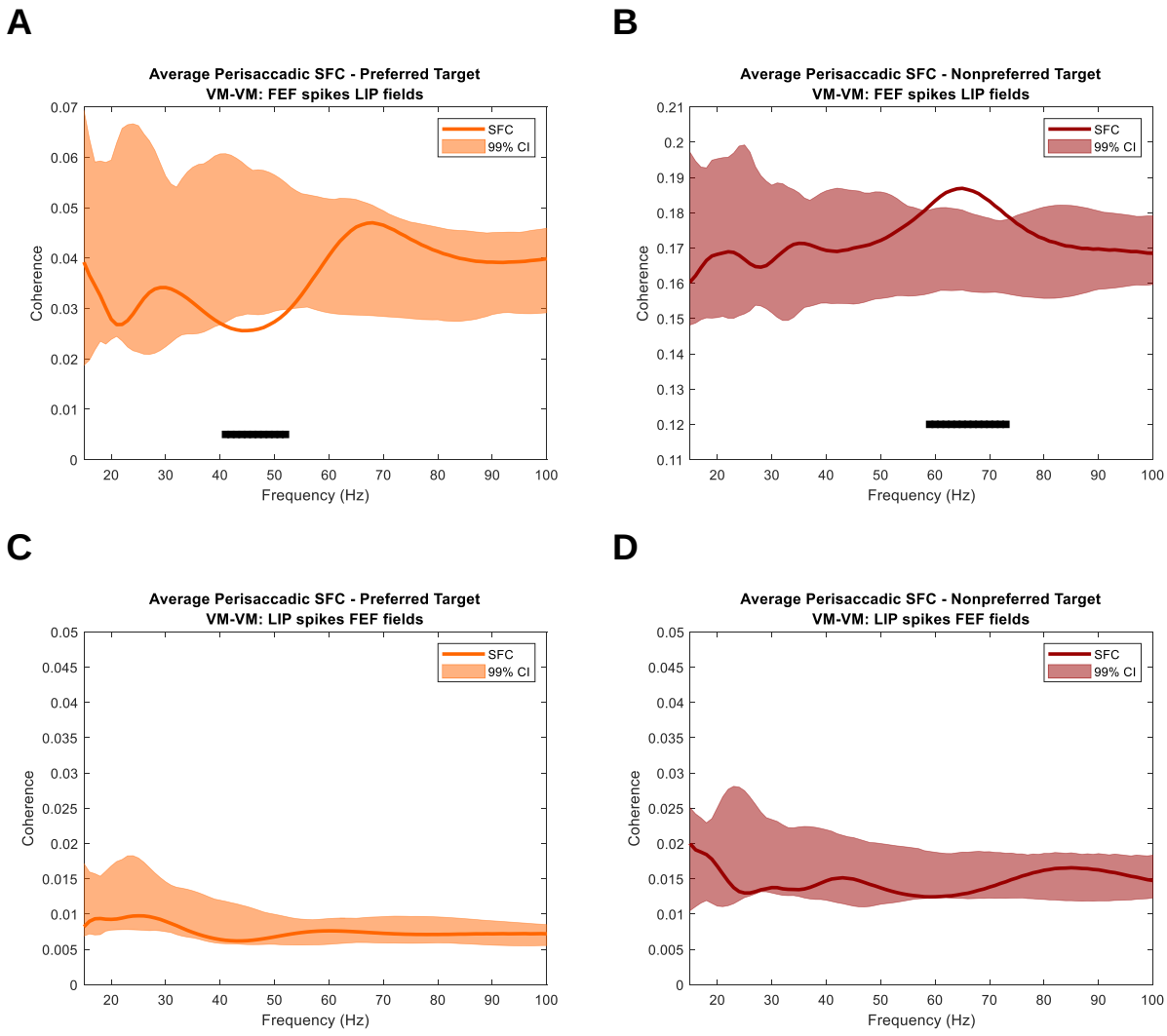

Figure 4-5. STA-Based VM-VM Pairs: Average perisaccadic SFC and shuffled pseudodistribution.

Average perisaccadic SFC for the population of recorded VM-VM pairs (n=16). (A) shows the SFC for trials directed to the preferred target for FEF spikes and LIP LFPs. Under this trial condition the SFC falls below the lower bound of the pseudo-distribution's 99th percentile at 41-52 Hz. (B) shows the trials to the nonpreferred target. Here the SFC exceeds the 99th percentile bounds at 59-73 Hz. (C) and (D) show the corresponding results for LIP spikes and FEF LFPs. Conventions as in Figure 4-1.

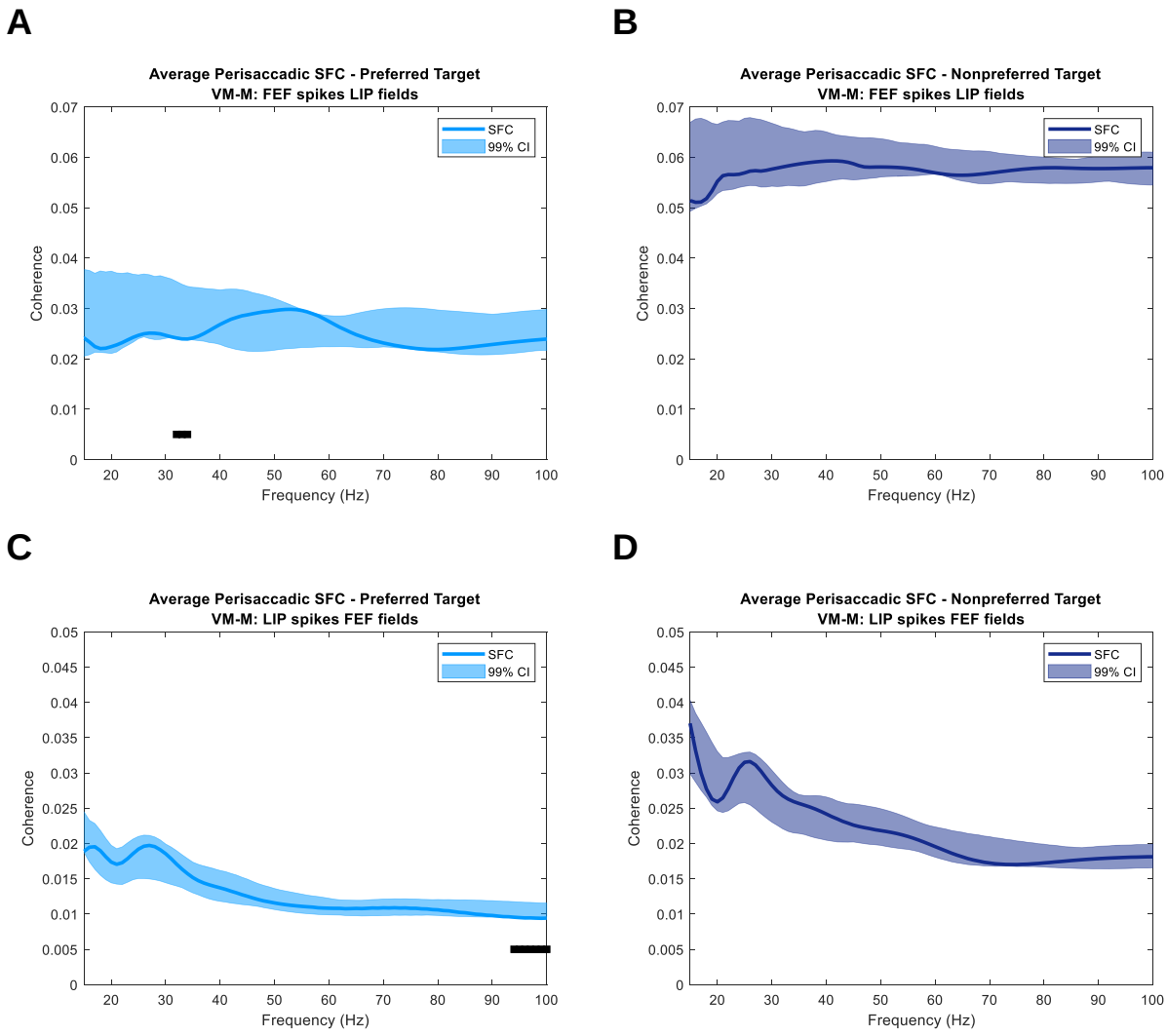

Figure 4-6. STA-Based VM-M Pairs: Average perisaccadic SFC and shuffled pseudodistribution.

Average perisaccadic SFC for the population of recorded VM-M pairs (n=64). (A) shows the SFC for trials directed to the preferred target for FEF spikes and LIP LFPs. The SFC falls below the 99th percentile bounds of the pseudo-distribution at 32-34 Hz. (B) shows the trials to the nonpreferred target. (C) shows the SFC for trials to the preferred target for LIP spikes and FEF LFPs. We find that the SFC falls below the lower 99th percentile bounds of the pseudo-distribution at 94-100 Hz. (D) shows the trials to the nonpreferred target for LIP spikes and FEF LFPs. Conventions as in Figure 4-2.

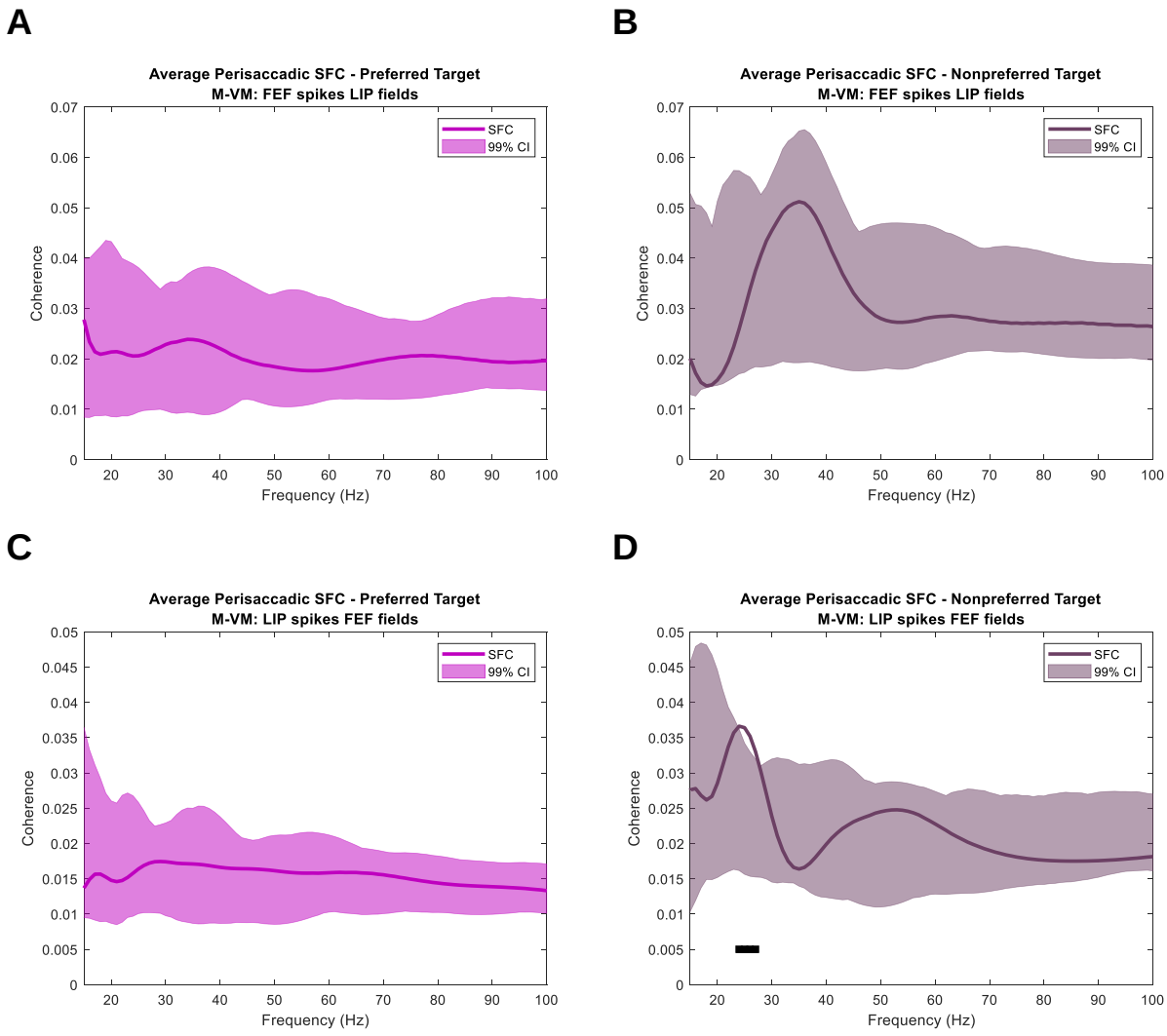

Figure 4-7. STA-Based M-VM Pairs: Average perisaccadic SFC and shuffled pseudodistribution.

Average perisaccadic SFC for the population of recorded VM-M pairs (n=8). (A) shows the SFC for trials directed to the preferred target for FEF spikes and LIP LFPs. (B) shows the trials to the nonpreferred target. (C) shows the SFC for trials to the preferred target for LIP spikes and FEF LFPs. (D) shows the trials to the nonpreferred target for LIP spikes and FEF LFPs. In this condition we find that the SFC exceeds the upper 99th percentile bounds of the pseudo-distribution at 24-27 Hz. Conventions as in Figure 4-3.

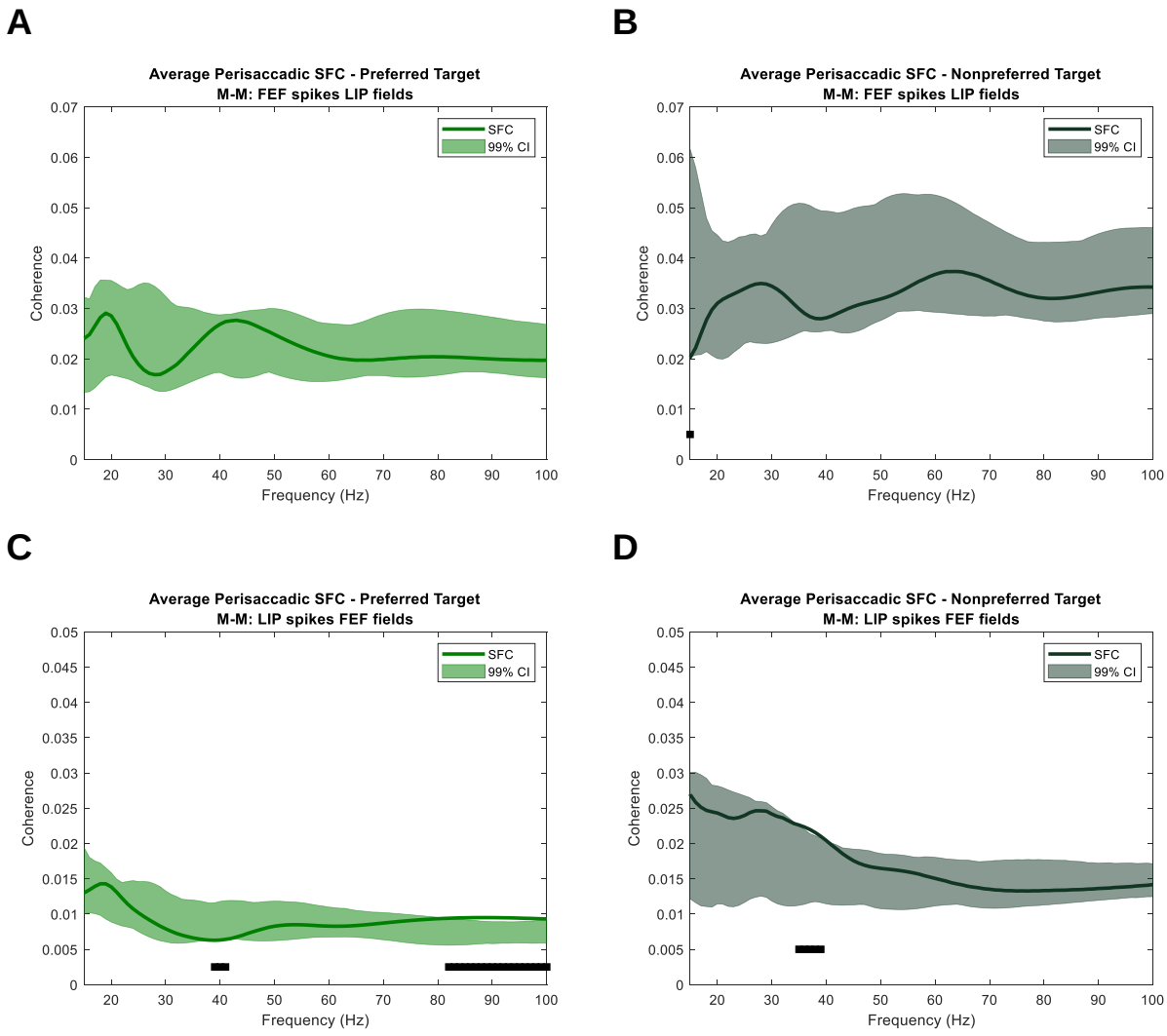

Figure 4-8. M-M Pairs: Average perisaccadic SFC and shuffled pseudodistribution.

Average perisaccadic SFC for the population of recorded M-M pairs (n=13). (A) shows the SFC for trials directed to the preferred target for FEF spikes and LIP LFPs. (B) shows the trials to the nonpreferred target. In this condition the SFC falls below the lower 99th percentile bounds at 15 Hz. (C) shows trials to the preferred target for LIP spikes and FEF LFPs. In this condition, the SFC falls below the 99th percentile bounds at 39-41 Hz and exceeds the bounds at 82-100 Hz. (D) shows the trials to the nonpreferred target for LIP spikes and FEF LFPs. Here we find that the SFC exceeds the 99th percentile bounds at 35-39 Hz. Conventions as in Figure 4-4.

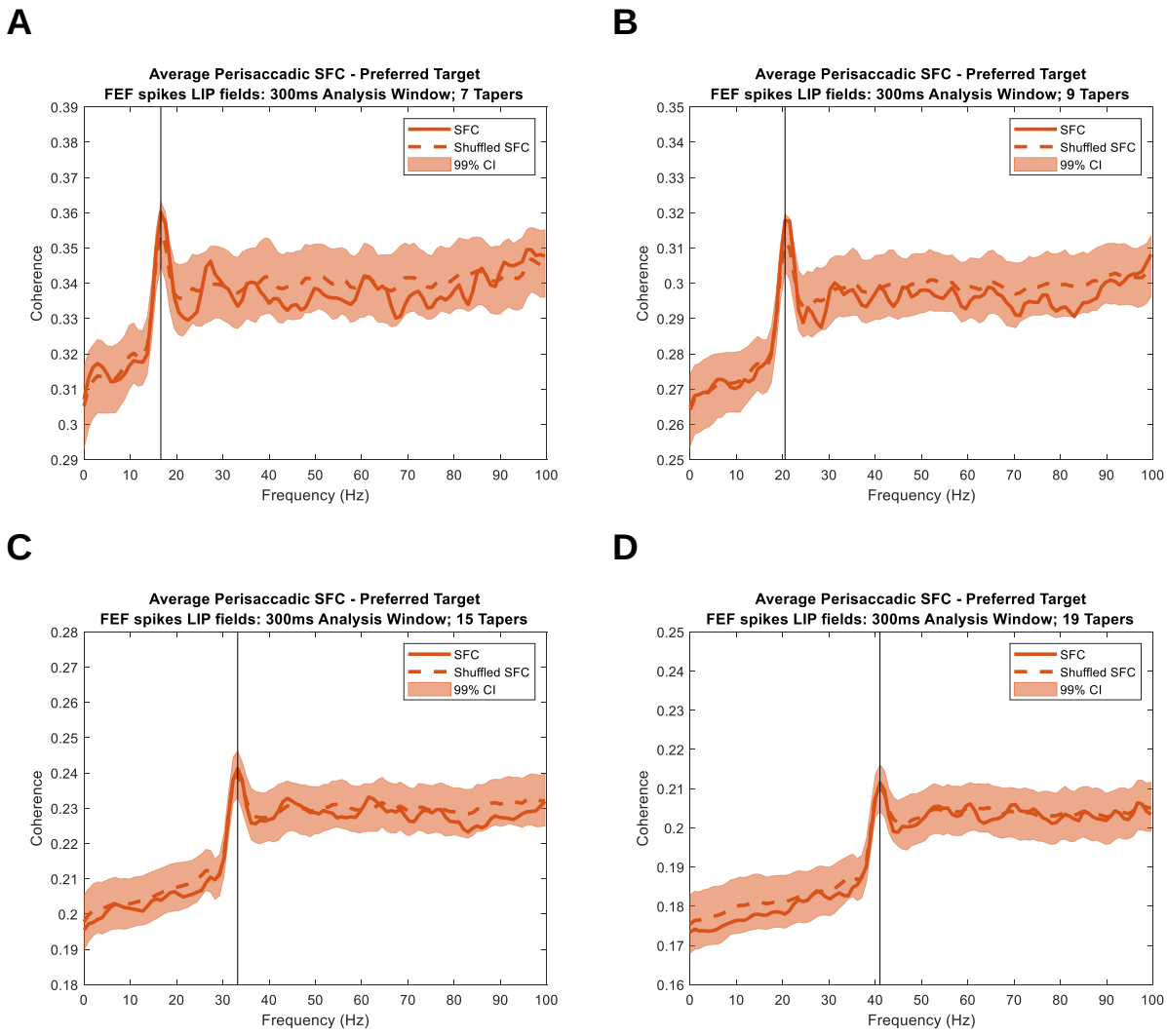

Figure 4-9. FEF spikes & LIP LFPs – Preferred Target: Effect of increasing tapers

Artifact in raw SFC calculation using multi-taper methods increases in frequency as number of tapers are increased. (A) Shows the artifact occurring at 16 Hz when 7 tapers are used. (B) Shows the artifact occurring at 20 HZ when 9 tapers are used. (C) Shows the artifact at 32 Hz with 15 tapers. Lastly, (D) shows the artifact at ~40 Hz with 19 tapers. All analyses used a time window of ± 150 ms around the saccade onset and show the results from the LIP spiking and FEF LFPs for the preferred target location. Conventions are the same as in Figure 3-18.

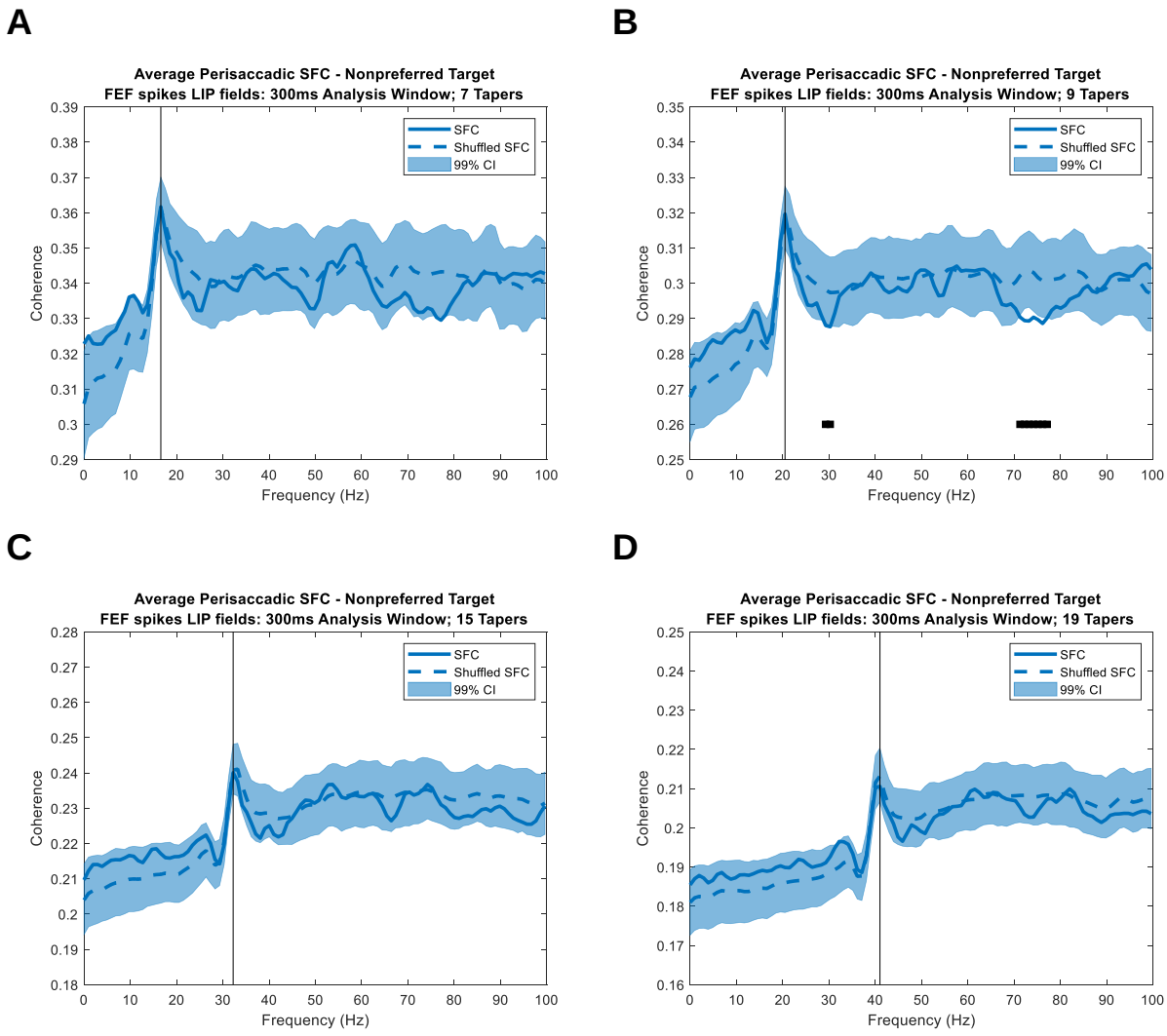

Figure 4-10. FEF spikes & LIP LFPs – Nonpreferred Target: Effect of increasing tapers

Artifact in raw SFC calculation using multi-taper methods increases in frequency as number of tapers are increased. (A) Shows the artifact occurring at 16 Hz when 7 tapers are used. (B) Shows the artifact occurring at 20 HZ when 9 tapers are used. As reported in Figure 3-1, the SFC falls below the lower 99th percentile bounds at 29-30 & 71-77 Hz. (C) Shows the artifact at 32 Hz with 15 tapers. Lastly, (D) shows the artifact at ~40 Hz with 19 tapers. All analyses used a time window of ± 150 ms around the saccade onset and show the results from the LIP spiking and FEF LFPs for the preferred target location. Conventions are the same as in Figure 3-18.

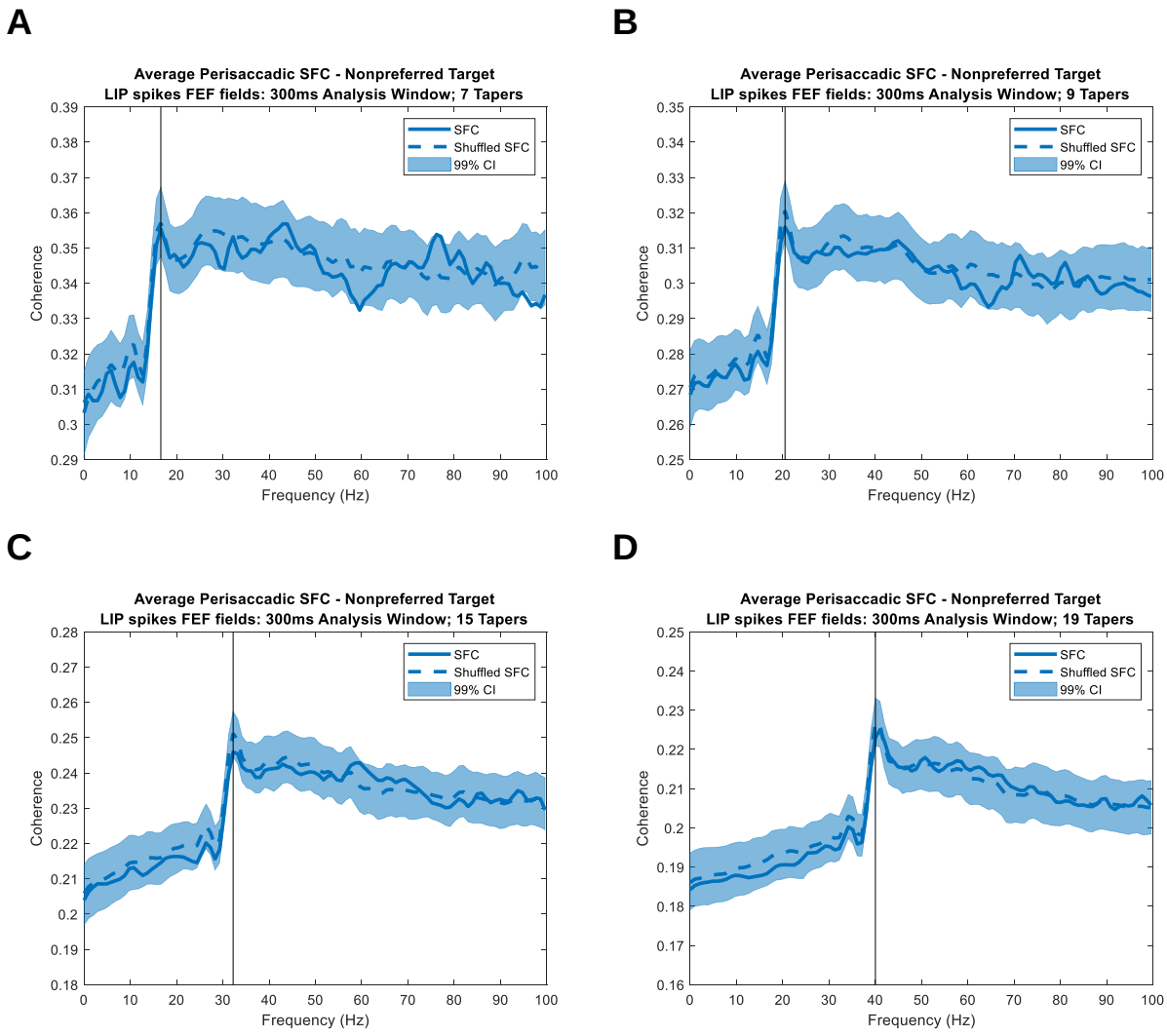

Figure 4-11. LIP spikes & FEF LFPs – Nonpreferred Target: Effect of increasing tapers

Artifact in raw SFC calculation using multi-taper methods increases in frequency as number of tapers are increased. (A) Shows the artifact occurring at 16 Hz when 7 tapers are used. (B) Shows the artifact occurring at 20 HZ when 9 tapers are used. (C) Shows the artifact at 32 Hz with 15 tapers. Lastly, (D) shows the artifact at ~40 Hz with 19 tapers. All analyses used a time window of ± 150 ms around the saccade onset and show the results from the LIP spiking and FEF LFPs for the preferred target location. Conventions are the same as in Figure 3-18.

Bibliography

Andersen, R. A., C. Asanuma, G. Essick and R. M. Siegel (1990). "Corticocortical connections of anatomically and physiologically defined subdivisions within the inferior parietal lobule." J Comp Neurol 296(1): 65-113.

Andersen, R. A., R. M. Bracewell, S. Barash, J. W. Gnadt and L. Fogassi (1990). "Eye position effects on visual, memory, and saccade-related activity in areas LIP and 7a of macaque." J Neurosci 10(4): 1176-1196.

Anderson, J. C., H. Kennedy and K. A. Martin (2011). "Pathways of attention: synaptic relationships of frontal eye field to V4, lateral intraparietal cortex, and area 46 in macaque monkey." J Neurosci 31(30): 10872-10881.

Armstrong, K. M., J. K. Fitzgerald and T. Moore (2006). "Changes in visual receptive fields with microstimulation of frontal cortex." Neuron 50(5): 791-798.

Baker, S. N. (2007). "Oscillatory interactions between sensorimotor cortex and the periphery." Curr Opin Neurobiol **17**(6): 649-655.

Barash, S., R. M. Bracewell, L. Fogassi, J. W. Gnadt and R. A. Andersen (1991). "Saccade-related activity in the lateral intraparietal area. II. Spatial properties." J Neurophysiol 66(3): 1109-1124.

Berens, P., G. A. Keliris, A. S. Ecker, N. K. Logothetis and A. S. Tolias (2008). "Feature selectivity of the gamma-band of the local field potential in primate primary visual cortex." Front Neurosci 2(2): 199-207.

Berger, H. (1929). Archiv f. Psychiatrie 87: 527.

Bisley, J. W. and M. E. Goldberg (2010). "Attention, intention, and priority in the parietal lobe." Annu Rev Neurosci 33: 1-21.

Blatt, G. J., R. A. Andersen and G. R. Stoner (1990). "Visual receptive field organization and cortico-cortical connections of the lateral intraparietal area (area LIP) in the macaque." J Comp Neurol 299(4): 421-445.

Bokil, H., P. Andrews, J. E. Kulkarni, S. Mehta and P. P. Mitra (2010). "Chronux: a platform for analyzing neural signals." J Neurosci Methods 192(1): 146-151.

Brosch, M., E. Budinger and H. Scheich (2002). "Stimulus-related gamma oscillations in primate auditory cortex." J Neurophysiol 87(6): 2715-2725.

Bruce, C. J. and M. E. Goldberg (1985). "Primate frontal eye fields. I. Single neurons discharging before saccades." J Neurophysiol 53(3): 603-635.

Bruce, C. J., M. E. Goldberg, M. C. Bushnell and G. B. Stanton (1985). "Primate frontal eye fields. II. Physiological and anatomical correlates of electrically evoked eye movements." J Neurophysiol 54(3): 714-734.

Buschman, T. J. and E. K. Miller (2007). "Top-down versus bottom-up control of attention in the prefrontal and posterior parietal cortices." Science 315(5820): 1860-1862.

Caton, R. (1875). "Electrical Currents of the Brain." British Medical Journal 2: 378-379.

Cavada, C. and P. S. Goldman-Rakic (1989). "Posterior parietal cortex in rhesus monkey: II. Evidence for segregated corticocortical networks linking sensory and limbic areas with the frontal lobe." J Comp Neurol 287(4): 422-445.

Cavanagh, P., A. R. Hunt, A. Afraz and M. Rolfs (2010). "Visual stability based on remapping of attention pointers." Trends Cogn Sci 14(4): 147-153.

Chafee, M. V. and P. S. Goldman-Rakic (1998). "Matching patterns of activity in primate prefrontal area 8a and parietal area 7ip neurons during a spatial working memory task." J Neurophysiol 79(6): 2919-2940.

Chafee, M. V. and P. S. Goldman-Rakic (2000). "Inactivation of parietal and prefrontal cortex reveals interdependence of neural activity during memory-guided saccades." J Neurophysiol 83(3): 1550-1566.

Colby, C. L., J. R. Duhamel and M. E. Goldberg (1996). "Visual, presaccadic, and cognitive activation of single neurons in monkey lateral intraparietal area." J Neurophysiol 76(5): 2841-2852.

Crowe, D. A., S. J. Goodwin, R. K. Blackman, S. Sakellaridi, S. R. Sponheim, A. W. MacDonald, 3rd and M. V. Chafee (2013). "Prefrontal neurons transmit signals to parietal neurons that reflect executive control of cognition." Nat Neurosci 16(10): 1484-1491.

Donoghue, J. P., J. N. Sanes, N. G. Hatsopoulos and G. Gaal (1998). "Neural discharge and local field potential oscillations in primate motor cortex during voluntary movements." J Neurophysiol **79**(1): 159-173.

Dias, E. C., M. Kiesau and M. A. Segraves (1995). "Acute activation and inactivation of macaque frontal eye field with GABA-related drugs." J Neurophysiol 74(6): 2744-2748.

Dias, E. C. and M. A. Segraves (1999). "Muscimol-induced inactivation of monkey frontal eye field: effects on visually and memory-guided saccades." J Neurophysiol 81(5): 2191-2214.

Engel, A. K., P. Fries and W. Singer (2001). "Dynamic predictions: oscillations and synchrony in top-down processing." Nat Rev Neurosci 2(10): 704-716.

Fanini, A. and J. A. Assad (2009). "Direction selectivity of neurons in the macaque lateral intraparietal area." J Neurophysiol 101(1): 289-305.

Fiebelkorn, I. C., M. A. Pinsk and S. Kastner (2018). "A Dynamic Interplay within the Frontoparietal Network Underlies Rhythmic Spatial Attention." Neuron 99(4): 842-853 e848.

Freedman, D. J. and J. A. Assad (2006). "Experience-dependent representation of visual categories in parietal cortex." Nature 443(7107): 85-88.

Fries, P. (2005). "A mechanism for cognitive dynamics: neuronal communication through neuronal coherence." Trends Cogn Sci **9**(10): 474-480.

Fries, P., P. R. Roelfsema, A. K. Engel, P. Konig and W. Singer (1997). "Synchronization of oscillatory responses in visual cortex correlates with perception in interocular rivalry." Proc Natl Acad Sci U S A **94**(23): 12699-12704.

Fuster, J. M. and G. E. Alexander (1971). "Neuron activity related to short-term memory." Science 173(3997): 652-654.

Gnadt, J. W. and R. A. Andersen (1988). "Memory related motor planning activity in posterior parietal cortex of macaque." Exp Brain Res 70(1): 216-220.

Gold, J. I. and M. N. Shadlen (2007). "The neural basis of decision making." Annu Rev Neurosci 30: 535-574.

Goodwin, S. J., R. K. Blackman, S. Sakellaridi and M. V. Chafee (2012). "Executive control over cognition: stronger and earlier rule-based modulation of spatial category signals in prefrontal cortex relative to parietal cortex." J Neurosci 32(10): 3499-3515.

Gregoriou, G. G., S. J. Gotts and R. Desimone (2012). "Cell-type-specific synchronization of neural activity in FEF with V4 during attention." Neuron 73(3): 581-594.

Gregoriou, G. G., S. J. Gotts, H. Zhou and R. Desimone (2009). "High-frequency, long-range coupling between prefrontal and visual cortex during attention." Science 324(5931): 1207-1210.

Hall, N. J. C., C.L.; Olson, C.O. (in review). "Push-Pull Interaction between Prefrontal and Parietal Cortex during Memory Guided Saccades."

Hamed, S., J. R. Duhamel, F. Bremmer and W. Graf (2001). "Representation of the visual field in the lateral intraparietal area of macaque monkeys: a quantitative receptive field analysis." Exp Brain Res **140**(2): 127-144.

Histed, M. H., V. Bonin and R. C. Reid (2009). "Direct activation of sparse, distributed populations of cortical neurons by electrical microstimulation." Neuron 63(4): 508-522.

Ibos, G., J. R. Duhamel and S. Ben Hamed (2013). "A functional hierarchy within the parietofrontal network in stimulus selection and attention control." J Neurosci 33(19): 8359-8369.

Itti, L. and C. Koch (2000). "A saliency-based search mechanism for overt and covert shifts of visual attention." Vision Res 40(10-12): 1489-1506.

Jia, X., M. A. Smith and A. Kohn (2011). "Stimulus selectivity and spatial coherence of gamma components of the local field potential." J Neurosci 31(25): 9390-9403.

Kiani, R. and M. N. Shadlen (2009). "Representation of confidence associated with a decision by neurons in the parietal cortex." Science 324(5928): 759-764.

Koch, C. and S. Ullman (1985). "Shifts in selective visual attention: towards the underlying neural circuitry." Hum Neurobiol 4(4): 219-227.

Kreiman, G., C. P. Hung, A. Kraskov, R. Q. Quiroga, T. Poggio and J. J. DiCarlo (2006). "Object selectivity of local field potentials and spikes in the macaque inferior temporal cortex." Neuron 49(3): 433-445.

Kurylo, D. D. and A. A. Skavenski (1991). "Eye movements elicited by electrical stimulation of area PG in the monkey." J Neurophysiol 65(6): 1243-1253.

Lawrence, B. M., R. L. White, 3rd and L. H. Snyder (2005). "Delay-period activity in visual, visuomovement, and movement neurons in the frontal eye field." J Neurophysiol 94(2): 1498-1508.

Li, C. S., P. Mazzoni and R. A. Andersen (1999). "Effect of reversible inactivation of macaque lateral intraparietal area on visual and memory saccades." J Neurophysiol 81(4): 1827-1838.

Liu, J. and W. T. Newsome (2006). "Local field potential in cortical area MT: stimulus tuning and behavioral correlations." J Neurosci 26(30): 7779-7790.

Lynch, J. C. (1992). "Saccade initiation and latency deficits after combined lesions of the frontal and posterior eye fields in monkeys." J Neurophysiol 68(5): 1913-1916.

Maris, E. and R. Oostenveld (2007). "Nonparametric statistical testing of EEG- and MEG-data." J Neurosci Methods 164(1): 177-190.

Mazzoni, P., R. M. Bracewell, S. Barash and R. A. Andersen (1996). "Motor intention activity in the macaque's lateral intraparietal area. I. Dissociation of motor plan from sensory memory." J Neurophysiol 76(3): 1439-1456.

McPeek, R. M. and E. L. Keller (2004). "Deficits in saccade target selection after inactivation of superior colliculus." Nat Neurosci 7(7): 757-763.

Medalla, M. and H. Barbas (2006). "Diversity of laminar connections linking periarcuate and lateral intraparietal areas depends on cortical structure." Eur J Neurosci 23(1): 161-179.

Mirpour, K. and J. W. Bisley (2016). "Remapping, Spatial Stability, and Temporal Continuity: From the Pre-Saccadic to Postsaccadic Representation of Visual Space in LIP." Cereb Cortex 26(7): 3183-3195.

Mitra, P. P. B., H. (2007). Observed Brain Dynamics, Oxford University Press.

Monosov, I. E., J. C. Trageser and K. G. Thompson (2008). "Measurements of simultaneously recorded spiking activity and local field potentials suggest that spatial selection emerges in the frontal eye field." Neuron 57(4): 614-625.

Moore, T. and K. M. Armstrong (2003). "Selective gating of visual signals by microstimulation of frontal cortex." Nature 421(6921): 370-373.

Perel, S., P. T. Sadtler, E. R. Oby, S. I. Ryu, E. C. Tyler-Kabara, A. P. Batista and S. M. Chase (2015). "Single-unit activity, threshold crossings, and local field potentials in motor cortex differentially encode reach kinematics." J Neurophysiol 114(3): 1500-1512.

Pesaran, B., M. J. Nelson and R. A. Andersen (2008). "Free choice activates a decision circuit between frontal and parietal cortex." Nature 453(7193): 406-409.

Pessoa, L., A. Rossi, S. Japee, R. Desimone and L. G. Ungerleider (2009). "Attentional control during the transient updating of cue information." Brain Res 1247: 149-158.

Petrides, M. and D. N. Pandya (1984). "Projections to the frontal cortex from the posterior parietal region in the rhesus monkey." J Comp Neurol 228(1): 105-116.

Premereur, E., W. Vanduffel and P. Janssen (2014). "The effect of FEF microstimulation on the responses of neurons in the lateral intraparietal area." J Cogn Neurosci 26(8): 1672-1684.

Premereur, E., W. Vanduffel, P. R. Roelfsema and P. Janssen (2012). "Frontal eye field microstimulation induces task-dependent gamma oscillations in the lateral intraparietal area." J Neurophysiol 108(5): 1392-1402.

Rossi, A. F., N. P. Bichot, R. Desimone and L. G. Ungerleider (2007). "Top down attentional deficits in macaques with lesions of lateral prefrontal cortex." J Neurosci 27(42): 11306-11314.

Rozzi, S., R. Calzavara, A. Belmalih, E. Borra, G. G. Gregoriou, M. Matelli and G. Luppino (2006). "Cortical connections of the inferior parietal cortical convexity of the macaque monkey." Cereb Cortex 16(10): 1389-1417.

Rubino, D., K. A. Robbins and N. G. Hatsopoulos (2006). "Propagating waves mediate information transfer in the motor cortex." Nat Neurosci **9**(12): 1549-1557.

Salazar, R. F., N. M. Dotson, S. L. Bressler and C. M. Gray (2012). "Content-specific fronto-parietal synchronization during visual working memory." Science 338(6110): 1097-1100.

Sapountzis, P., S. Paneri and G. G. Gregoriou (2018). "Distinct roles of prefrontal and parietal areas in the encoding of attentional priority." Proc Natl Acad Sci U S A 115(37): E8755-E8764.

Schall, J. D., A. Morel, D. J. King and J. Bullier (1995). "Topography of visual cortex connections with frontal eye field in macaque: convergence and segregation of processing streams." J Neurosci 15(6): 4464-4487.

Schiller, P. H. and I. H. Chou (1998). "The effects of frontal eye field and dorsomedial frontal cortex lesions on visually guided eye movements." Nat Neurosci 1(3): 248-253.

Schiller, P. H., J. H. Sandell and J. H. Maunsell (1987). "The effect of frontal eye field and superior colliculus lesions on saccadic latencies in the rhesus monkey." J Neurophysiol 57(4): 1033-1049.

Schiller, P. H., S. D. True and J. L. Conway (1980). "Deficits in eye movements following frontal eye-field and superior colliculus ablations." J Neurophysiol 44(6): 1175-1189.

Selemon, L. D. and P. S. Goldman-Rakic (1988). "Common cortical and subcortical targets of the dorsolateral prefrontal and posterior parietal cortices in the rhesus monkey: evidence for a distributed neural network subserving spatially guided behavior." J Neurosci 8(11): 4049-4068.

Sereno, A. B. and J. H. Maunsell (1998). "Shape selectivity in primate lateral intraparietal cortex." Nature 395(6701): 500-503.

Shirhatti, V., A. Borthakur and S. Ray (2016). "Effect of Reference Scheme on Power and Phase of the Local Field Potential." Neural Comput 28(5): 882-913.

Siegel, M., T. J. Buschman and E. K. Miller (2015). "Cortical information flow during flexible sensorimotor decisions." Science 348(6241): 1352-1355.

Snyder, A. C., D. Issar and M. A. Smith (2018). "What does scalp electroencephalogram coherence tell us about long-range cortical networks?" Eur J Neurosci 48(7): 2466-2481.

Sommer, M. A. and E. J. Tehovnik (1997). "Reversible inactivation of macaque frontal eye field." Exp Brain Res 116(2): 229-249.

Sommer, M. A. and R. H. Wurtz (2001). "Frontal eye field sends delay activity related to movement, memory, and vision to the superior colliculus." J Neurophysiol 85(4): 1673-1685.

Stanton, G. B., C. J. Bruce and M. E. Goldberg (1995). "Topography of projections to posterior cortical areas from the macaque frontal eye fields." J Comp Neurol 353(2): 291-305.

Tallon-Baudry, C. and O. Bertrand (1999). "Oscillatory gamma activity in humans and its role in object representation." Trends Cogn Sci 3(4): 151-162.

Thier, P. and R. A. Andersen (1998). "Electrical microstimulation distinguishes distinct saccade-related areas in the posterior parietal cortex." J Neurophysiol 80(4): 1713-1735.

Toth, L. J. and J. A. Assad (2002). "Dynamic coding of behaviourally relevant stimuli in parietal cortex." Nature 415(6868): 165-168.

Waldert, S., R. N. Lemon and A. Kraskov (2013). "Influence of spiking activity on cortical local field potentials." J Physiol 591(21): 5291-5303.

Walker, M. F., E. J. Fitzgibbon and M. E. Goldberg (1995). "Neurons in the monkey superior colliculus predict the visual result of impending saccadic eye movements." J Neurophysiol 73(5): 1988-2003.

Walther, D. and C. Koch (2006). "Modeling attention to salient proto-objects." Neural Netw 19(9): 1395-1407.